DESIGN OF PRINTED COPRIME ANTENNA ARRAYS FOR DIRECTION FINDING APPLICATIONS

BY

Ahmad I. Oweis

A Thesis Presented to the

DEANSHIP OF GRADUATE STUDIES

KING FAHD UNIVERSITY OF PETROLEUM & MINERALS

DHAHRAN, SAUDI ARABIA

In Partial Fulfillment of the
Requirements for the Degree of

MASTER OF SCIENCE

In

ELECTRICAL ENGINEERING

December 2018

KING FAHD UNIVERSITY OF PETROLEUM & MINERALS

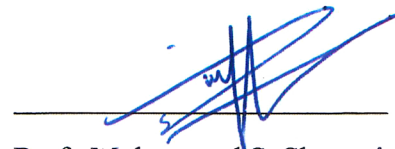DHAHRAN- 31261, SAUDI ARABIA

DEANSHIP OF GRADUATE STUDIES

This thesis, written by **Ahmad I. Oweis** under the direction of his thesis advisor and

approved by his thesis committee, has been presented and accepted by the Dean of

Graduate Studies, in partial fulfillment of the requirements for the degree of **MASTER**

OF SCIENCE IN ELECTRICAL ENGINEERING.

Prof. Mohammad S. Sharawi
(Advisor)

Dr. Ali Ahmad Al-Shaikhi
Department Chairman

Dr. Ali Muqaibel
(Member)
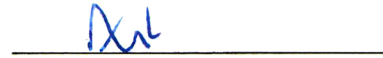
Prof. Salam A. Zummo
Dean of Graduate Studies

Dr. Ali Arshad Nasir
(Member)

23/12/17

Date

To my parents who were the first reason for me to exist in this world.

To my wife, Nada, who bore disproportionate load in looking after the family.

To my five wonderful children Mariam, Nour, Aisha, Ibrahim and Yahya who tolerated my never-ending absence.

To my colleagues at Halliburton who understood, motivated and supported me along the journey.

ACKNOWLEDGMENTS

TABLE OF CONTENTS

LIST OF TABLES

LIST OF FIGURES

x

xiii

LIST OF ABBREVIATIONS

AMSDL : Antennas and Microwave Structures Design Lab

CS : Compressed Sensing

DOA : Direction of arrival

DOF : Degree of Freedom

DUT : Device Under Test

EM : Electromagnetic

EXP : Experiment

LASSO : Least Absolute Shrinkage and Selection Operator

MUSIC : Multiple Signals Classification

MVG : Microwave Vision Group

RMSE : Root Mean Square Error

SDR : Software Defined Radio

SIM : Simulation

SLL : Side Lobe Level

ULA : Uniform linear array

USRP : Universal Software Radio Peripherals

VNA : Vector Network Analyzer

ABSTRACT

Full Name   : Ahmad I. Oweis

Thesis Title   : Design of Printed Coprime Antenna Arrays for Direction Finding Applications

Major Field   : Electrical Engineering

Date of Degree : December 2018

In fifth generation (5G) wireless communication systems, beamforming will play a major role in increasing the overall capacity by pointing individual beams from the base station to the users and vice versa. For such a system to work, both the base station and the mobile user need to have the capability to estimate the Direction of Arrival (DOA) of the incoming electromagnetic waves. Uniform linear antenna arrays (ULAs) are usually used for DOA estimation with the help of various algorithms. It was shown recently that nonuniform arrays can provide comparable DOA estimation performance with a smaller number of antennas.

Most of previous work on DOA estimation focused on improving the utilized algorithms and overlooked the effects of hardware parts, i.e. antennas, on the algorithm performance. Only few works incorporated basic antenna behavior in the algorithms while most of the remaining literature assumed the antennas to be isotropic radiators.

In this work, we highlight this gap in previous works and provide several additions to address such shortcoming. Microstrip antenna arrays are designed based on the coprime array (CPA) concept. The first array is a patch-based 4-element CPA operating in the 5.8 GHz band, intended to be used in handheld wireless devices. This array demonstrated the

ability to use CPAs in small form factor terminals, something that was not studied enough in the literature, as most of the work demonstrated the advantage of large sparse arrays over ULAs, leaving the question of "how applicable this is to small arrays" open. The second and third arrays target tablet-based devices and consist of four printed patch and monopole antennas respectively, arranged in a coprime configuration and operating in the 2.1 GHz band. The complex radiation patterns of the arrays are incorporated in the DOA estimation simulation and the results are compared with those obtained by using isotropic antennas to quantify the error introduced when using physical antennas. With the 5.8 GHz patches CPA, assuming 4 sources impinging the array from angles falling within -50° and 50°, the average error between the isotropic and physical cases was 0.51°. Beyond this range of angles, the error can be as high as 7.6° assuming only one source at an angle of -80°. In the 2.1 GHz band, the average error between isotropic and patch cases for four sources impinging the array within the -50° and 50° range was 0.34° only, rising to 14.89° with one source located at -70°. The monopole arrays were found to introduce higher error compared to the patch case. An average error of 0.62° was found with four sources located within the -50° and 50° range. With only one source located near -90°, the error was 5.25°. The possibility to reduce the inter-element spacing of the CPA is investigated in the 5.8 GHz band, where we obtained 2.6° estimation error in DOA using 0.31λ.

To study the benefits of coprime configuration over ULAs, 4-element and 5-element ULAs consisting of patch-based and monopole-based elements, operating in the 2.1 GHz band, are also designed, fabricated and used in DOA simulations. A typical 4-element ULA of patches can detect the DOA of three sources with a root mean square error (RMSE) of 0.79° at 20 dB SNR. However, by re-arranging the 4-elements according to the coprime

concept, four sources can be detected with 0.75° RMSE at the same SNR. To be able to detect 4 sources using ULAs, a 5-element ULA will be needed, and the RMSE will be 1.08°. A monopole-based 4-element ULA can detect 3 simultaneous sources with 7.87° RMSE at 20 dB SNR. A CPA of monopoles can detect 4 sources with an RMSE of 0.64°, while a 5-element ULA can detect 4 sources with 1.19° RMSE at 20 dB SNR.

DOA estimation experiments are conducted on the six arrays operating at 2.1 GHz using a software defined radio (SDR) setup in a laboratory environment and the results are compared with the simulation. With a single source located at varying DOA angles, the average difference in RMSE between simulation and experiments for the patch-based CPA was 2.87°, while for the monopole-based CPA, it was 1.23°. Experiments using two sources were also carried out, and the results were compared with those obtained by running equivalent simulations. For the patch-based CPAs, the difference in error between the simulation and the experiment was only 1.4°. However, due to multipath and lower polarization purity in monopole elements, the monopole experiments showed extra 2.63° error over the simulation predictions.

ملخص الرسالة

الاسم الكامل: أحمد إبراهيم عويس

عنوان الرسالة: تصميم مصفوفات هوائيات أولية نسبيا لأغراض تحديد الإتجاه

التخصص: هندسة كهربائية

تاريخ الدرجة العلمية: كانون الأول 2018

يعتبر تقدير الاتجاه الذي وصلت عن طريقه الموجة الكهرمغناطيسية من المكونات المهمة للجيل الخامس من الاتصالات اللاسلكية حيث ترسل المحطات الأرضية إشاراتها إلى كل مستخدم على حدة مما يزيد من السعة الكلية للنظام اللاسلكي. ويحتاج تقدير الاتجاه إلى مصفوفات من الهوائيات لاستقبال الإشارة وتحليلها لمعرفة الزاوية التي سقطت منها الأشعة الكهرومغناطيسية. في السابق كان الاعتماد على المصفوفات المنتظمة لهذا الغرض حيث تكون المسافة بين الهوائيات ثابتة. إلا أنه تبين أنه من الممكن الحصول على نتائج أفضل في تحديد الاتجاه عند استخدام مصفوفات غير منتظمة من الهوائيات حيث لا يشترط أن تكون المسافة بينها ثابتة. تحديدا، أثبتت الأبحاث أن استخدام مصفوفات غير منتظمة من الهوائيات يزيدعدد الإشارات التي يستطيع النظام تحديد اتجاهها في الوقت نفسه. من هذه المصفوفات ما يسمى بالمصفوفات الأولية نسبيا أو coprime arrays.

بعد مراجعة الدراسات التي بحثت في المصفوفات غير المنتظمة تبين أن معظمها اعتمد على هوائيات مثالية وركز دراسته وبحثه على الخوارزميات مع إهمال تأثير الهوائي. في بحثنا هذا، صممنا مجموعة من مصفوفات الهوائيات غير المنتظمة وأدخلناها في الخوارزميات لتقدير الاتجاه الذي تسقط منه الموجات الكهرومغناطيسية فاستطعنا دراسة تأثير خواصّ الهوائي على تحديد الاتجاه.

الهوائيات المصممة في هذا البحث اشتملت على نوعين يسميان ال patch antennas وال monopole antennas واستهدفت الأجهزة المحمولة وأجهزة الحاسوب اللوحي. استخدمت في هذا البحث برامج لمحاكاة خوارزميات تحديد الاتجاه بعد إدخال خواص الهوائيات المصنعة لأجل هذا الغرض، كما وأجريت تجارب عملية لإثبات النتائج التي وصلنا إليها عن طريق المحاكاة وفي النهاية حددنا مقدار الخطأ الناتج عن استخدام هوائيات فعلية بدل الهوائيات المثالية الموجودة في معظم الدراسات.

CHAPTER 1

INTRODUCTION

This chapter introduces the motivation behind the proposed work. It starts by the evolution of wireless communication systems and the importance of Direction of Arrival (DOA) estimation in wireless systems with a highlight on where the work will advance previous knowledge. The chapter concludes by listing the objectives of this work.

1.1   Wireless Systems Evolution

The IEEE fifth generation (5G) and beyond technology roadmap describes 5G as a system that will allow data rates of up to 100 Mb/s in metropolitan areas. Several users in an office floor will simultaneously have connections providing data rates up to 1 Gb/s. Significant increase in system capacity and coverage is expected with enhanced spectral efficiency compared to 4G systems [1].

One of the enabling technologies in 5G is beamforming. 5G will support individual links between each user and the base station via massive multiple-input-multiple-output (mMIMO) technology. As depicted in Figure 1, base stations will employ directional antennas with narrow beams steered towards the mobile users. Similarly, mobile users will steer their beams towards the base station. This implies that space is used as a new multiplexing dimension allowing greater system capacity and higher data rates.

For the 5G and beamforming system to operate properly, base stations and mobile users need to know and keep track of the direction of one another. This allows the base station and the mobile user to steer their beams in the right direction. This is where direction of arrival (DOA) estimation comes into play.
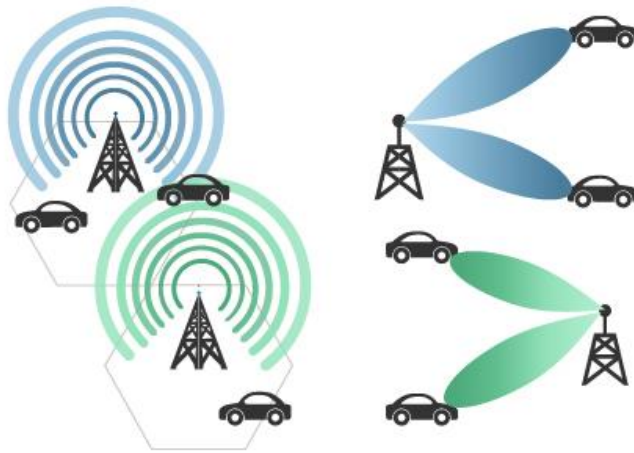
Figure 1 Conventional omnidirectional antennas versus smart beamforming.

1.2   Direction of Arrival (DOA) Estimation

The problem of DOA estimation in one dimension can be stated as the following. Given a number of sources that transmit electromagnetic (EM) waves located in the far field region of an array of antennas, it is required to estimate the angle θ formed between the direction of propagation of the EM waves and a reference direction usually taken as the normal to antenna array axis. This scenario is shown in Figure 2 where two sources are impinging waves on an linear array of antennas. In this figure, θ_j is the DOA of source j and d_i is the location of antenna i. The assumption about far field ensures that all array elements see the same angle of arrival for the same source.

Two main performance indicators are usually considered in this context. The first is the accuracy of the estimation measured by the root mean square error (RMSE) between the actual azimuth of the source and the estimated one, and the number of sources that can be resolved usually termed as the degrees of freedom (DOF).
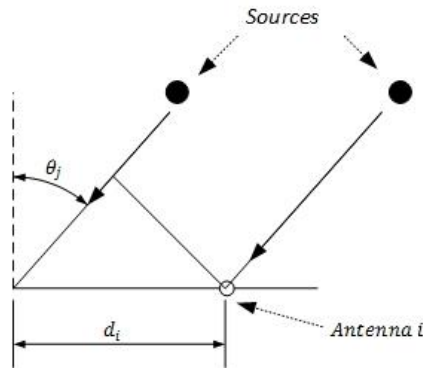
Figure 2 Direction of arrival estimation.

Numerous methods have been developed to estimate the DOA using antenna arrays. Some examples are; the maximum likelihood method (MLM) and maximum entropy (ME) [2]. The multiple signal classification (MUSIC) algorithm has been extensively mentioned in the literature and will therefore be presented in some details. Compressed Sensing (CS) methods were introduced recently to relax the processing complexity of both hardware and the algorithms. CS exploits the sparsity of the covariance matrix and is mainly used in sparse nonuniform arrays as it increases the DOF. CS will be discussed further Chapter 2.

1.3   Antenna Arrays for DOA Estimation

Most original works on DOA estimation methods focused on uniform linear arrays (ULA). These linear arrays consist of several equally spaced antennas. To avoid spatial aliasing, the spacing is set to $\lambda/2$ where λ is the wavelength of the impinging wave. The number of

antenna elements within an array needs to be increased to enhance its DOF and resolution. This means larger and more complex arrays to be developed. Recent work shows that accurate DOA estimation can be achieved using nonuniform arrays. Several new array configurations were introduced and will be discussed in details in the literature review chapter (i.e. Chapter 3). One of the most promising nonuniform array configurations is the coprime arrays (CPA) formed by interleaving a ULA with M antennas spaced by Nd and another ULA with N antennas spaced by Md where $M\ and\ N$ are coprime numbers and d is an arbitrary spacing factor. This configuration was shown to provide similar performance as an array with a larger number of antennas. A detailed explanation of CPAs is provided in the theoretical background (i.e. Chapter 2).

1.4   Work Objectives

As will be shown in the literature review chapter, most of the previous work in DOA estimation assumed isotropic antennas and focused on the signal processing algorithms. Isotropic antennas do not exist in real life. They are simple mathematical models which assume that an antenna radiates equally in all directions in space with constant phase. Real antennas have complex radiation patterns that affect both the magnitude and phase of the received waves. There is very limited number of published work that studied the effect of actual antennas on DOA estimation performance with omnidirectional radiation patterns; i.e., dipole or monopole-based antennas. No previous work studied the effect of directional based patterns on the performance of DOA estimation. The purpose of this work is to explore the impact of using physical antennas with directional complex radiation patterns

4

placed within small and medium size handheld devices (i.e. smart phones and table devices) on DOA estimation.

The objectives of this work are:

- Design, build and test a printed patch-based CPA ($M = 2, N = 3$) that operates in the 5.8 GHz band with a minimum bandwidth of 80 MHz suitable for use in mobile phones. Investigate the effect of interelement spacing on antenna behavior.

- Design, build and test a printed monopole-based CPA ($M = 2, N = 3$) that operates in the 2.1 GHz band with a minimum bandwidth of 150 MHz suitable for use in tablet devices along with a patch-based array operating at 2.1 GHz with at least 30 MHz bandwidth.

- Incorporate the complex radiation patterns of the above 3 arrays in the DOA estimation algorithm using CS and assess the effects of inter-element spacing, directivity and antenna type on the DOA estimation.

- Verify the DOA estimation of various antenna arrays in a laboratory setup and come up with a general conclusion of the effect of radiation pattern on the DOA estimation.

It is worth mentioning that this research is carried out under a joint project. The author of this thesis is responsible for the electromagnetic aspects of the project including designing the antennas and modeling them. The signal processing part is outside the scope of this thesis, although some relevant parts will be presented here for completeness.

CHAPTER 2

THEORITICAL BACKGROUND

In this chapter, we introduce the theoretical background behind DOA estimation using CPAs. First, we go through the basic principles of antennas and antenna arrays. More details are provided for the printed antennas and CPAs. We then introduce the MUSIC algorithm for estimating DOA with full details since it is one of the most popular algorithms in DOA estimation. We show how to apply MUSIC for CPAs and introduce a brief introduction about using CS in DOA estimation. Some other methods for DOA estimation are listed and then different methods to calculate the RMSE are presented. A summary then concludes the chapter.

2.1   Antennas and Antenna Arrays

A static electric charge has electric properties marked by the attraction of opposite charges and repulsion of similar charges but exhibits no magnetic properties (electrostatics). If the electric charge moves at a constant speed in a conductive wire forming an electric current, a static magnetic field surrounding the wire is formed (magnetostatics). If the electric charge starts to accelerate or decelerate, then Maxwell equations predict that a propagating EM field will be produced, and we will get radiation (electromagnetics) [3] [4].

The simplest antenna is the straight wire dipole antenna with a $\lambda/2$ height where λ is the wavelength of the transmitted (or received) EM wave. Numerous other forms of antennas exist like loop, aperture, and horn antennas [4]. One important class of antennas is the

planar or printed antennas. A printed antenna consists of a thin metallic layer placed on top of a substrate. These antennas are low profile, simple and inexpensive to manufacture using same technologies as printed circuit boards (PCB). They are usually printed on the same PCB used to mount the electronic components of the device. Two common printed antenna types are the rectangular patch and monopole antennas.

A rectangular patch is constructed by having a rectangle-shaped metallic layer on the top of the substrate while the ground plane covers the bottom face. Figure 3 depicts a probe fed $W \times L$ rectangular patch antenna mounted on a substrate with dielectric constant of ϵ_r.
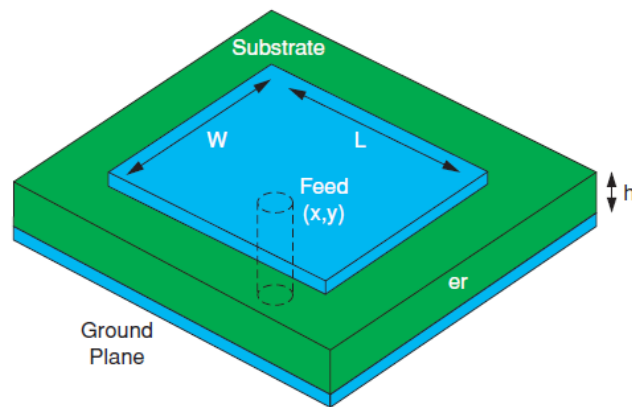
Figure 3 Rectangular patch antenna [5].

Another way to feed the patch antenna is by edge feeding where a microstrip transmission line feeds the patch as shown in Figure 4a. It has been shown that the input impedance of the patch antenna can be adjusted by using an inset feed as shown in Figure 4b. The length of the recess can be calculated to provide a specific input impedance. In practice, this calculation is used as a first approximation while the actual recess length is found by simulations. Due to the ground plane beneath the patch antenna that minimizes back radiation, the radiation pattern of a patch antenna is approximately a semi-ellipsoid directed normal to the patch plane as shown in Figure 4c. Patch antennas suffer from relatively

narrow bandwidth compared to other antennas. Additionally, due to losses in the dielectric and metallic parts, their efficiency is usually low [5].

(a)

(b)

(c)
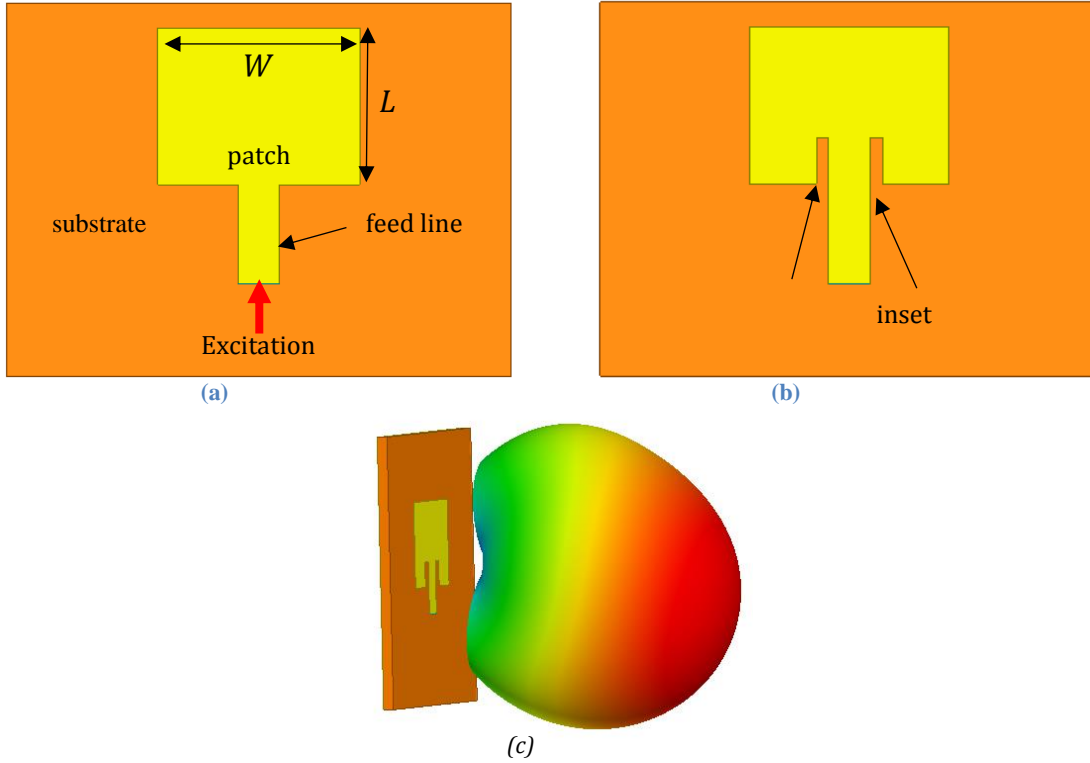
Figure 4 Edge fed patch antenna (a) without inset (b) with inset (c) 3D radiation pattern.

The dimensions of an efficient rectangular patch that radiates at frequency f_r are given by equations (1) to (4) [4].

$$W = \frac{1}{2f_r\sqrt{\mu_0\epsilon_0}}\sqrt{\frac{2}{\epsilon_r + 1}} \tag{1}$$

$$L = \frac{1}{2f_r\sqrt{\epsilon_{reff}}\sqrt{\mu_0\epsilon_0}} - 2\Delta L \tag{2}$$

$$\epsilon_{reff} = \frac{\epsilon_r + 1}{2} + \frac{\epsilon_r - 1}{2}\left[1 + 12\frac{h}{W}\right] \tag{3}$$

$$\frac{\Delta L}{h} = 0.412 \frac{(\epsilon_{reff} + .3)\left(\frac{W}{h} + 0.264\right)}{(\epsilon_{reff} - .258)\left(\frac{W}{h} + 0.8\right)} \qquad (4)$$

where W is the patch width, μ_0 is the permeability of free space, ϵ_0 is the permittivity of free space, ϵ_r is the relative permittivity of the substrate, L is the physical length of the patch, ΔL is the nonphysical extra patch length resulting from the field fringing, ϵ_{reff} is the effective relative permittivity of the substrate, and h is the substrate thickness.

A monopole wire antenna consists of a simple $\lambda/4$ long conductor above a ground plane. The ground plane produces a virtual image of a current carrying conductor of the same length of the monopole. When the effect of the main wire and image are combined, an omni-directional radiation pattern is formed.

Monopoles can be constructed on PCBs like the patch antennas. An example of a printed monopole is shown in Figure 5a. The major difference in the construction of a printed monopole versus a patch is the lack of ground plane beneath the monopole. In terms of radiation pattern, monopoles exhibit an omni-directional pattern which means that the antenna will radiate approximately equally around the monopole including the back side as depicted in Figure 5b.

The input impedance of a printed monopole is controlled by slightly varying its length or width or by introducing a matching network at the feed.
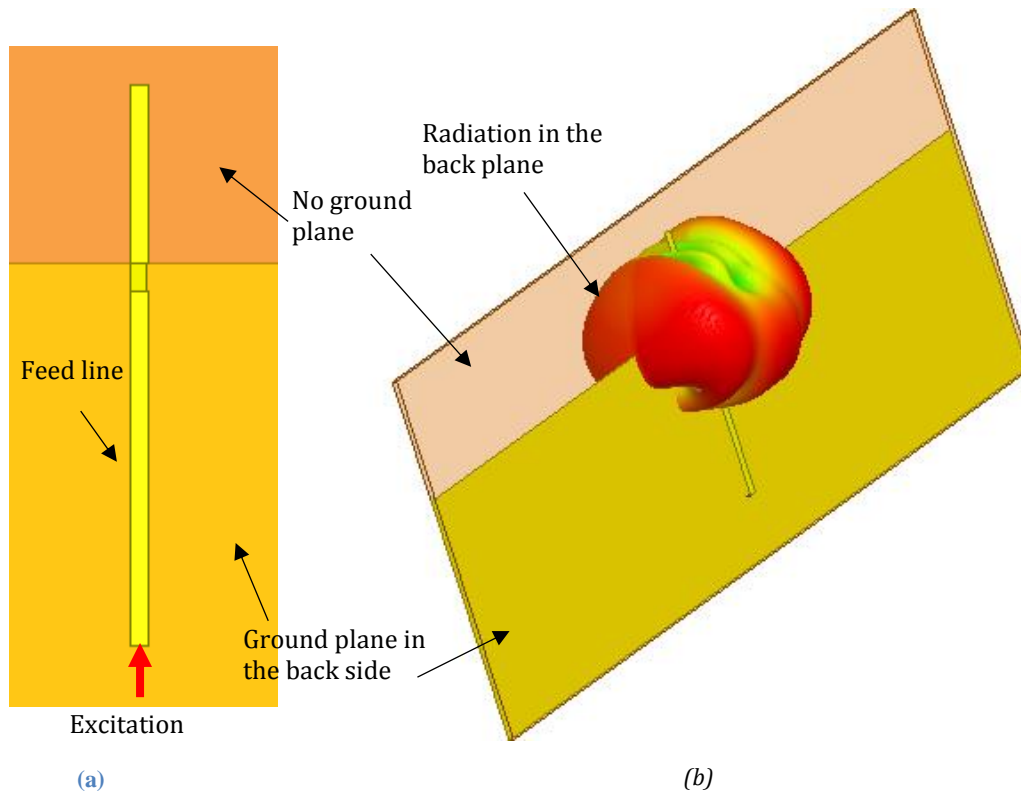
Figure 5 (a) Printed monopole antenna (b) 3D radiation pattern of a printed monopole.

It is often desired to design antennas with highly directive radiation pattern to meet the needs of long-distance communications. This is achieved by using antenna arrays. In addition to providing high gain and directivity, antenna arrays have several other applications. By controlling the inter-element spacing and excitation of each array element, the radiation pattern of an array can be steered towards the desired direction. Antenna arrays also play a major role in direction finding applications. In fact, one needs at least two properly spaced antennas, which is the simplest form of an antenna array, to detect the DOA of an EM wave.

The elements in an antenna array can be placed linearly forming a linear array. If the spacing among the elements is uniform, the array is called uniform linear array (ULA). Antennas can also be arranged in a 2D pattern creating 2D planar array. The overall far

10

field of an array of identical antenna elements was found to be equal to the product of the single element field and an array factor (AF) determined by the array geometry [4].

$$\mathbf{E}\,(total) = [\mathbf{E}(single\ element\ at\ reference\ point)] \times [array\ factor] \quad (5)$$

For an N-element ULA, the AF is given by:

$$AF = \sum_{n=1}^{N} e^{j(n-1)(kdcos\theta+\beta)} \quad (6)$$

where k is the wave number, d is the spacing between elements, θ is the angle in spherical coordinators at which the total array field is calculated and β is the progressive phase difference between elements. If all elements are fed with the same phase, then β will be zero.

2.2   Coprime Antenna Arrays

CPAs come in different configurations. In what we will refer as the prototype configuration used in [6], the array is constructed by interleaving two uniform linear subarrays of antennas. The first sub-array contains N elements (indexed from 0 to $N - 1$) and spaced by Md. The second sub-array contains M elements (indexed from 0 to $M - 1$) and spaced by Nd where d is an arbitrary distance usually taken as *λ/2* and N, M are coprime integers (i.e. their greatest common devisor is 1). Figure 6 depicts the subarrays of a general CPA.
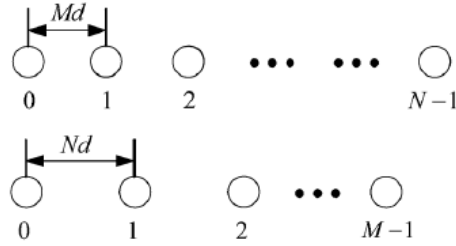
Figure 6 Coprime sub arrays as in [6].

For example, choosing $M = 6$ and $N = 7$, we have $(6 + 7 - 1 = 12)$ real sensors at the locations shown in Table 1. The first sub-array has $N = 7$ elements located at $\{0, 6, 12, \dots, 36\}d$ while the second sub-array shares the first element with sub-array 1 and has 5 other elements located at $\{7, 14, \dots, 35\}d$. Therefore, the CPA will have elements located at $\{0, 6, 7, 12, 14, 18, 21, 24, 28, 30, 35, 36\}d$.

Table 1 Location of real array elements with $M = 6, N = 7$ assuming $d = 1$.

Sub-array 1	Sub-array 2
0	
6	7
12	14
18	21
24	28
30	35
36	

The cross-difference matrix C_p is constructed by subtracting all possible locations in Table 1 from each other as show in Table 2. This results in a matrix containing all the possible spacings between the elements of the CPA. As will be shown, when estimating the DOA of the impinging signals using the CPA in Table 1, the correlation of the received signal can be calculated at all differences in C_p. In Table 2, there are 53 unique differences (also called lags) that can be exploited. Hence, the maximum theoretical DOF is 53.

12

Table 2 Cross difference matrix for $M = 6, N = 7 \ and \ d = 1$.

	0	6	7	12	14	18	21	24	28	30	35	36
0	0	6	7	12	14	18	21	24	28	30	35	36
6	-6	0	1	6	8	12	15	18	22	24	29	30
7	-7	-1	0	5	7	11	14	17	21	23	28	29
12	-12	-6	-5	0	2	6	9	12	16	18	23	24
14	-14	-8	-7	-2	0	4	7	10	14	16	21	22
18	-18	-12	-11	-6	-4	0	3	6	10	12	17	18
21	-21	-15	-14	-9	-7	-3	0	3	7	9	14	15
24	-24	-18	-17	-12	-10	-6	-3	0	4	6	11	12
28	-28	-22	-21	-16	-14	-10	-7	-4	0	2	7	8
30	-30	-24	-23	-18	-16	-12	-9	-6	-2	0	5	6
35	-35	-29	-28	-23	-21	-17	-14	-11	-7	-5	0	1
36	-36	-30	-29	-24	-22	-18	-15	-12	-8	-6	-1	0

Note that the term difference co-array is defined as the set that contains unique values of all differences (or lags) in C_p. Another term that is frequently used is the weight function $w(d)$ which is the number of occurrences of d in C_p. For example, in Table 2, $w(0) = 12$.

Another possible configuration appears in [7] and is shown in Figure 7. To avoid confusion, we will refer to it as *the conventional CPA*. It uses $2M - 1$ antennas for the second sub-array. As will be shown later, this configuration ensures that the cross-difference matrix contains all the integers from $-MN$ to MN, an essential property for spatial smoothing.

To have the minimum number of physical sensors for a certain number of lags, M and N should be as close to each other as possible. Typically, M and N are chosen such that $N = M + 1$ as proposed in [8].
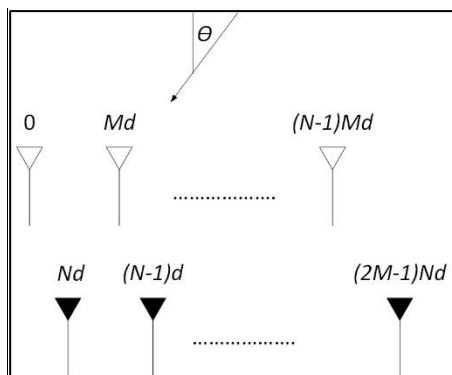
Figure 7 Coprime sub arrays as in [7].

The CPA with displaced subarrays (CADiS) structure was introduced in [9]. Instead of interleaving the two sub arrays, the subarrays were displaced from each other by a distance equal to Ld where $L \geq M$ as shown in Figure 8. With this configuration, the minimum interelement spacing becomes Md as opposed to d in the conventional and prototype configurations. This increased minimum spacing is desirable in some applications (e.g. when the dimensions of the antenna element are larger than d or $\lambda/2$).
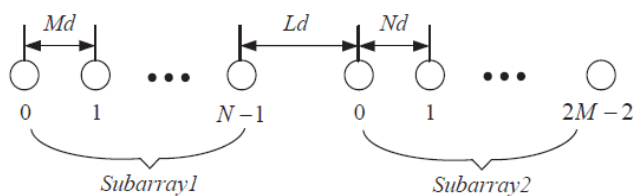
Figure 8 Proposed CADiS configuration in [9].

The new CADiS configuration gives $4MN + 2M - 1$ unique lags as opposed to $3MN + M - N$ lags using the conventional configuration. Among those lags, $MN + 2M + N - 1$ are consecutive when choosing $L = M + N$. The number of consecutive lags is less than

14

the that of the conventional algorithm. The useable DOF of the CADiS geometry is slightly larger than half of the conventional one.

The last coprime configuration is CPA with compressed inter-element spacing (CACIS) introduced in [6]. The CACiS configuration is like the prototype M, N configuration with a different spacing in the N-element subarray. Instead of Md, the elements of the N-subarray are spaced by $\breve{M}d$ where $M = \breve{M}p$ and p is a compression factor as shown in Figure 9.
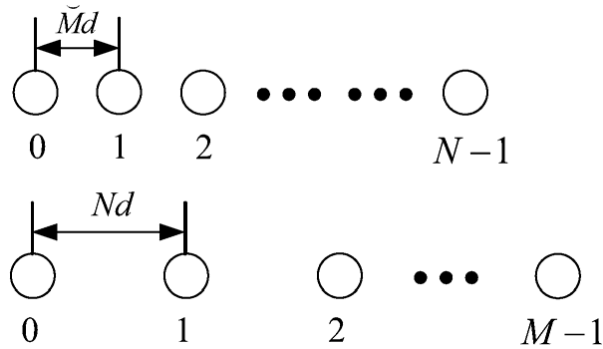
Figure 9 The CACIS configuration [6].

2.3 DOA Algorithms

Several algorithms have been developed to estimate the DOA of an incoming wave when it impinges upon an antenna array. We will provide full analysis of MUSIC since it is one of the most famous algorithms. We will also introduce spatial smoothing which is a method used to preprocess the received coherent signals before MUSIC can be applied. Spatial smoothing is required when using MUSIC on CPAs. Alternatively, CS can be used to estimate the DOA with CPAs without the need of spatial smoothing. Other DOA estimation algorithms are listed in Section 2.3.4.

2.3.1 MUSIC Algorithm with ULAs

MUSIC is a common method for estimating the DOA of narrow band signals impinging on an array of antennas. The method was first described in 1979 in a paper authored by Schmidt. The paper was then reprinted in 1986 [10]. This section provides an overview of the algorithm and discusses its strengths and weaknesses. An online tutorial [11] was used to explain the algorithm in addition to the main paper [10].

The MUSIC algorithm is capable of estimating the following:

- The number of impinging signals

- DOA of the impinging signals

- Strength and cross correlation of the signals

- Strength and cross correlation of the noise

The MUSIC algorithm requires the signals and noise to be uncorrelated. Theoretically speaking, the signals themselves need not be fully uncorrelated but they cannot be fully correlated either. However, in practice, difficulties are encountered when the signals are highly correlated as in multipath propagation or with smart jammers [12].

Let N be the number of antennas (sensors) in the array and q be the number of sources. Let K be the number of snapshots (samples) of the received signal. Then,

$$X = AF + W \tag{7}$$

where X is an $N \times K$ matrix representing the received signal, A is the $N \times q$ steering matrix, F is a $q \times K$ matrix representing the source signal and W is the $N \times K$ noise matrix.

Each impinging signal will be delayed (shifted) by a certain time (phase). This delay depends on the position of the receiver antenna and the angle of arrival. The delay is accounted for by introducing the matrix A. Each element in A adds the interaction between the impinging signal from a certain angle and an array element. Therefore, the size of A is $N \times q$.

Let a_{ij} be the element of A at row i and column j representing the delay when signal j with DOA of ϑ_j impinges on the array element i. Then from Figure 10,

$$a_{ij} = e^{-j\omega \frac{d \sin \vartheta_j}{c}} = e^{-j\frac{2\pi d_i \sin \vartheta_j}{\lambda}} \tag{8}$$

where c is speed of the EM wave, λ is the wavelength, and d_i is the distance from the origin to the array element i. Note that in most of the reviewed literature, a_{ij} has a constant magnitude of 1. This essentially means that the sensors are assumed to be ideal with an isotropic radiation pattern. In practice, a coefficient should be added as in equation (9).

$$a_{ij} = \alpha_i(\vartheta_j)e^{-j\frac{2\pi d_i \sin \vartheta_j}{\lambda}} \tag{9}$$

where $\alpha_i(\vartheta_i)$ represents the complex response (amplitude and phase) of antenna i when signal j impinges on it.

17
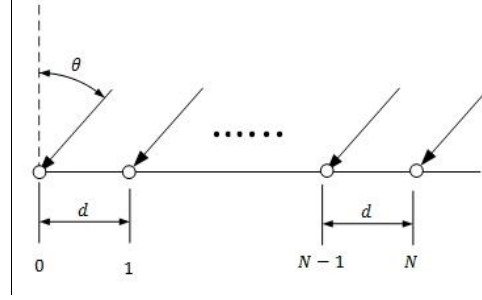
Figure 10 Phase shift of the impinging signals on a linear array from [11].

From (7), the correlation matrix can be calculated.

$$R_x = E\{X(t)X^H(t)\} = AR_sA^H + \sigma_0^2 I \tag{10}$$

where R_x is the covariance matrix, $E[.]$ Is the expectation operator, $(.)^H$ is the Hermitian operator, R_s is the covariance matrix of the source signal, σ_0^2 is the noise variance, and I is an $N \times N$ identity matrix.

When $N > q$ (number of sensors is greater than the number of sources), the matrix AR_sA^H will be singular and hence its determinant will be zero.

$$det(AR_sA^H) = det\ (R_x - \sigma_0^2 I) = 0 \tag{11}$$

Equation (11) implies that σ_0^2 is an eigenvalue for the matrix R_x. The number of these eigenvalues is $N - q$. Since R_x and AR_sA^H are non-negative definite then there are other q eigenvalues (σ_i^2) such that

$$\sigma_i^2 > \sigma_0^2 > 0 \tag{12}$$

Let u_i be the eigen vector corresponding to σ_i^2. Then,

$$R_x u_i = \sigma_i^2 u_i \tag{13}$$

$$[AR_sA^H + \sigma_0^2 I\ ]u_i = \sigma_i^2 u_i \tag{14}$$

18

Therefore,

$$AR_s A^H u_i = (\sigma_i^2 - \sigma_0^2)u_i = \begin{cases} (\sigma_i^2 - \sigma_0^2)u_i & i = 1,2,\dots,q \\ 0 & i = q+1,\dots,N \end{cases} \tag{15}$$

where u_i is partitioned into $[u_s \quad u_n]$. $a(\vartheta_i)$ is one vector in the steering matrix A. Since $a(\vartheta_i)$ is in the signal subspace and since the signal subspace is orthogonal to the noise subspace, then

$$a(\vartheta_i)u_n = 0 \tag{16}$$

Now, define the spatial spectrum as:

$$P(\vartheta_i) = \frac{1}{a^H(\vartheta_i)u_n} \tag{17}$$

The MUSIC algorithm works by splitting the entire range of ϑ (e.g. from -90° to 90°) into small steps and evaluating the spatial spectrum at each ϑ. If there is a signal impinging at the given ϑ, then the spectrum will exhibit a peak as in Figure 11. Three peaks are identified indicating the presence of 3 sources at 10°, 20°, and 30°.
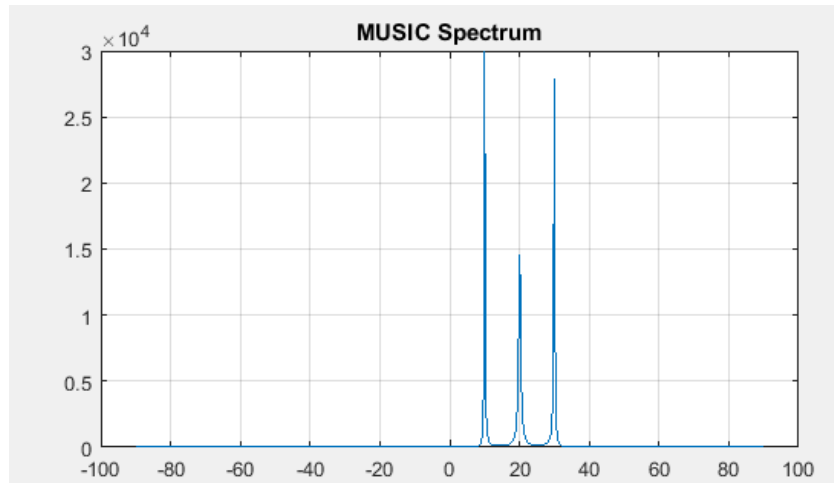
Figure 11 MUSIC Spectrum of three impinging signals at 10°, 20° and 30° generated by applying the MUSIC algorithm using MATLAB.

19

The original MUSIC method described in the previous section requires the covariance matrix of the sources R_s to be non-singular [12]. This is the case when the source signals are uncorrelated. If some signals are correlated, spatial smoothing, as explained in [12], can be applied on the received signals prior to processing them. It works by dividing the antenna array into overlapping sub arrays of length p. The number of sub arrays M becomes

$$M = N - p + 1 \tag{18}$$

To apply the MUSIC algorithm correctly on q coherent sources, M must always be greater than q and the size of each sub-array p must be at least $q + 1$. Therefore, N should be at least $2q$. Thus, the increased robustness of the method comes at the cost of increased hardware.

One disadvantage of the MUSIC algorithm is that it requires heavy processing power since it searches through all possible ϑ's. Additionally, the algorithm requires significant memory size for storing the array response.

2.3.2 MUSIC Algorithm with CPAs

The discussion presented so far assumes a ULA at the receiver. Recently, it was shown that using CPAs provide several advantages over ULAs.

The data model introduced in the MUSIC algorithm can be applied to CPAs. By vectorizing both sides of equation (10), we get [6]:

$$z = vec(R_x) = \tilde{A}\left(\vartheta_1, \dots, \vartheta_q\right)b + \sigma_n^2 \tilde{I}_n = Br \tag{19}$$

$$\tilde{A}\left(\vartheta_1, \dots, \vartheta_q\right) = [a^*(\vartheta_1)\otimes a(\vartheta_1) \dots a^*\left(\vartheta_q\right)\otimes a\left(\vartheta_q\right)] \tag{20}$$

$$b = [\sigma_1^2, \dots, \sigma_q^2]^T \tag{21}$$

$$\tilde{I} = vec(I_{M+N-1}) \tag{22}$$

$$B = \left[\tilde{A}, \tilde{I}\right] \tag{23}$$

$$r = [b^T, \sigma_n^2]^T = [\sigma_1^2, \dots, \sigma_q^2, \sigma_n^2] \tag{24}$$

where $a(\vartheta_i)$ is the steering vector for the signal $i, \otimes$ denotes the kronecker product, q is the number of sources, vec is an operation that converts a matrix into a column vector by stacking all columns on top of each other and I_k is the $k \times k$ identity matrix.

Equation (19) has the same form as the data model in equation (7) with z replacing the received signal, $\tilde{A}$ is the steering matrix for an array of virtual sensors located in the set of cross differences C_p and b is the modified source vector. To see this clearly, consider for example the element $\tilde{a}_{21}$ in $\tilde{A}$

$$\tilde{A} = \left[a^*(\vartheta_1)\otimes a(\vartheta_1) \dots a^*(\vartheta_q)\otimes a(\vartheta_q)\right] = \begin{bmatrix} a_{11}^* a_{11} & a_{12}^* a_{12} & \dots \\ a_{11}^* a_{21} & a_{12}^* a_{22} & \dots \\ \dots & \dots & \dots \end{bmatrix} \tag{25}$$

$$\tilde{a}_{21} = a_{11}^* a_{21} = e^{+j\frac{2\pi d_1 sin\vartheta_1}{\lambda}} * e^{-j\frac{2\pi d_2 sin\vartheta_1}{\lambda}} = e^{-j\frac{2\pi (d_2 - d_1)sin\vartheta_1}{\lambda}} \tag{26}$$

Equation (26) shows that $\tilde{a}_{21}$ represents the phase shift suffered by a signal with DOA ϑ_1 impinging on an array element located at $(d_2 - d_1)$. The same applies for the other elements of $\tilde{A}$. Another thing to notice in the equation is that the modified source matrix b consists of the incoming signal power as opposed to the incoming data in the original equation. Therefore, b becomes a source matrix of fully coherent signals.

We should be able to apply the MUSIC algorithm on equation (19) to estimate the DOAs. However, because the virtual sources are now coherent, the rank of the covariance matrix

R_{zz} is one, and we cannot apply the MUSIC algorithm directly. Instead, one can use spatial smoothing as the authors of [7] did.

Using spatial smoothing requires the location of the sensors (or the virtual locations in the coprime case) to be consecutive integers of the primary distance d. This is why the authors of [7] used $2M - 1$ sensors in the second subarray as opposed to the simpler option of M. This $2M - 1$ configuration guarantees continuous integers from $-MN$ to MN. Spatial smoothing reduces the DOF by half so that a maximum of MN sources can be detected using $N + 2M - 1$ physical sensors.

2.3.3 Compressed Sensing

Alternatively, Compressed Sensing (CS) can be applied directly as shown in [6]. This allows the exploitation of the full aperture of the array. Using $M + N - 1$ sources, the maximum DOF will be MN. This is significantly larger than the DOF in the spatial smoothing algorithm. CS works as follows.

- B° matrix is calculated like B in equation (23). It consists of the steering vectors for the cross differences of the entire search grid $\vartheta_1^g, \dots, \vartheta_G^g$ where $G \gg q$ to ensure sparsity.

- r° is obtained from the solution of the following minimization problem. Several techniques can be used such as Least Absolute Shrinkage and Selection Operator (Lasso), Orthogonal Matching Pursuit (OMP), and Compressive Sampling Matched Pursuit (CoSaMP). The Lasso technique may induce erroneous peaks

when the SNR is low. This can be worked around empirically when the number of

sources is less than the number of physical sensors [13].

$$r^{\circ} = \arg\min_{r^{\circ}} \left[\frac{1}{2} \| z - B^{\circ} r^{\circ} \|_2 + \lambda_t \| r^{\circ} \|_1 \right] \tag{27}$$

Where λ_t is a penalty parameter.

- The last element in the vector r° corresponds to the noise variance whereas the

  peaks in r° denote received signals. Therefore, DOAs are the ϑ^g's that have

  corresponding peaks in r°.

The advantage of the CS algorithm is that it does not need spatial smoothing and hence the

location of the sensors need not to be consecutive which, in turn, means higher DOF.

2.3.4 Other DOA Estimation Algorithms

ESPRIT stands for estimation of signal parameters via rotational invariance techniques

[14]. It is based on "doublets" of sensors. Doublets are pairs of identical antennas aligned

in the same direction **Δ**. That is, the first element of each doublet is identical to the other

element in the doublet but doublet 1 can have different elements from doublet 2. Also, the

displacement vector **Δ** between the two elements of the doublet must be the same for all

doublets while the location of the doublets is arbitrary. See Figure 12 for clarification.
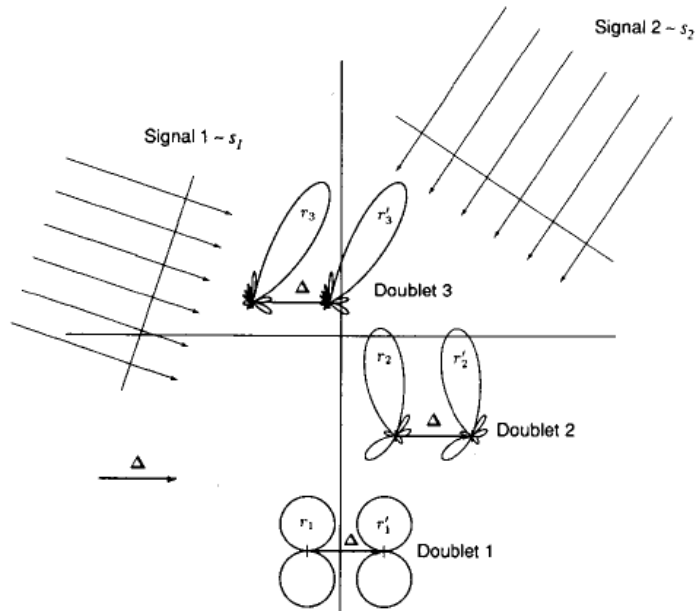
Figure 12 Sensors array in ESPRIT algorithm [14].

This additional constraint on the antenna arrays reduces the required computations in estimating DOA. Therefore, ESPRIT reduces the required computational power at the cost of doubling the number of sensors compared to MUSIC.

Other methods also exist for estimating DOA like the maximum likelihood method (MLM) and maximum entropy (ME) [2] and will not be discussed further.

2.4   Root Mean Square Error (RMSE)

The RMSE is used to quantify the accuracy of the DOA estimation. It is a measure of the error between the actual and estimated DOA. There are two formulas in the literature to calculate the DOA: equation (28) that appeared in [6] and equation (29) that appeared in [15].

24

$$RMSE = \sqrt{\frac{\sum_{i=1}^{L} \sum_{q=1}^{Q} (\widehat{\Phi}_q(i) - \Phi_q)^2}{LQ}} \tag{28}$$

$$RMSE = \begin{cases} \sqrt{\dfrac{\sum_{l=1}^{\hat{L}} \sum_{q=1}^{Q} |\Phi_l - \widehat{\Phi}_l|^2 + |L - \hat{L}|(\Delta\Phi_{max})^2}{L}} & ,\hat{L} \leq L \\[4mm] \sqrt{\dfrac{\sum_{l=1}^{\hat{L}} \sum_{q=1}^{Q} |\Phi_l - \widehat{\Phi}_l|^2 + \sum_{j=L+1}^{\hat{L}} |\widehat{\Phi}_l - \bar{\Phi}_l|^2}{LQ}} & \hat{L} > L \end{cases} \tag{29}$$

Where L is the number of actual sources, $\hat{L}$ is the estimated number of sources, Q is the number of iterations, Φ is the actual DOA angle and $\widehat{\Phi}$ is the estimated DOA angle, $\Delta\Phi_{max}$ is the maximum localization error (e.g. 180°) and $\bar{\Phi}_l$ is the closest actual DOA to the estimation.

The MUSIC spectrum will have several peaks representing the estimated DOAs and their locations and possibly some other spurious peaks for wrong estimations. The two RMSE formulas represent two different methods of extracting DOAs from the MUSIC spectrum. The first method assumes that the number of impinging signals L is known a priori, so it selects the L highest peaks as the estimated DOAs. For this method, formula (28) is used to calculate the error in DOA estimation.

The other method sets a threshold in the MUSIC spectrum and considers all peaks that exceed the threshold. This method does not require a prior knowledge of the number of impinging signals. However, the number of peaks exceeding the threshold need not to be equal to the number of impinging signals which results in possibly missed or erroneous DOAs. In this case, formula (29) can be used to calculate the RMSE. If the number of detected signals is less than the actual impinging signals, i.e. some DOAs were missed, a

penalty term equals the maximum possible error is added to the RMSE for each missed signal. In the case of extra erroneous signals, the formula adds an error term for each extra signal that is equal to the difference between the wrong DOA and the closest correct one.

A third method was mentioned in [16]. The method works by setting a certain range of DOA. For each actual DOA, the algorithm would look for estimated DOAs within that specified range and select the highest peak. This takes care of the spurious peaks. As for the missed sources, the method simply ignores them in the RMSE calculation. This method does not need prior knowledge of the number of actual DOAs and can use the simpler RMSE formula (28).

To demonstrate the difference between the three methods, consider the situation with two sources located at 50° and 10°. Consider also the following three scenarios:

- Two peaks were detected. One large peak at 51° and another small peak at 13°.

- Three large peaks were detected at 51°, 20° and 13°. The peak at 20° is spurious and does not relate to any of the original sources.

- Two peaks were detected around the 50° original source: one at 51° and one spurious at 47°. The source originally located at 10° is missed.

The three scenarios are shown in Figure 13 and the resulting RMSE values are shown in Table 3. In scenario (a), the first method will try to find 2 peaks due to the a priori knowledge of the number of sources. Therefore, it considers both peaks although the peak at 13° is low. The RMSE will be 2.2°. The second method will only consider the peaks above the threshold and hence will count a missed peak for the source at 10°. This adds a

penalty of 180° to the RMSE which becomes 127.3°. The third method also ignores the peak at 13° since it is below the threshold but will just report it as missed and ignore it in the RMSE calculation which results in RMSE of 0.7°.

In scenario (b), the first method will consider the highest peaks which are 20° and 13° as the estimated DOA ignoring the smaller peak at 51°. The resulting RMSE is 21.3°. The second method will map the estimated peak at 51° to the actual source at 50° and the peak at 13° to the actual source at 10° but will add a penalty for the spurious peak at 20°. The penalty is equal to the distance to the closest actual peak to the spurious one which is 10°. The resulting RMSE is 7.4°. The third method does the same without considering the spurious peak at 20° because it falls outside the detectable range of the both DOAs. It calculates the RMSE as 2.2°.

In scenario (c), the first method detects both peaks around the 50° DOA and maps one to the source at 50° and the other to the source at 10° giving a high RMSE value of 26.2°. The second method performs the same since both peaks exceed the threshold. The third method will only take one peak near the 50° signal which is 51°. The other signal at 10° is declared missed and does not count in the RMSE value. The calculated RMSE is as low as 0.7°. Table 3 shows the calculated RMSE for each scenario and method.
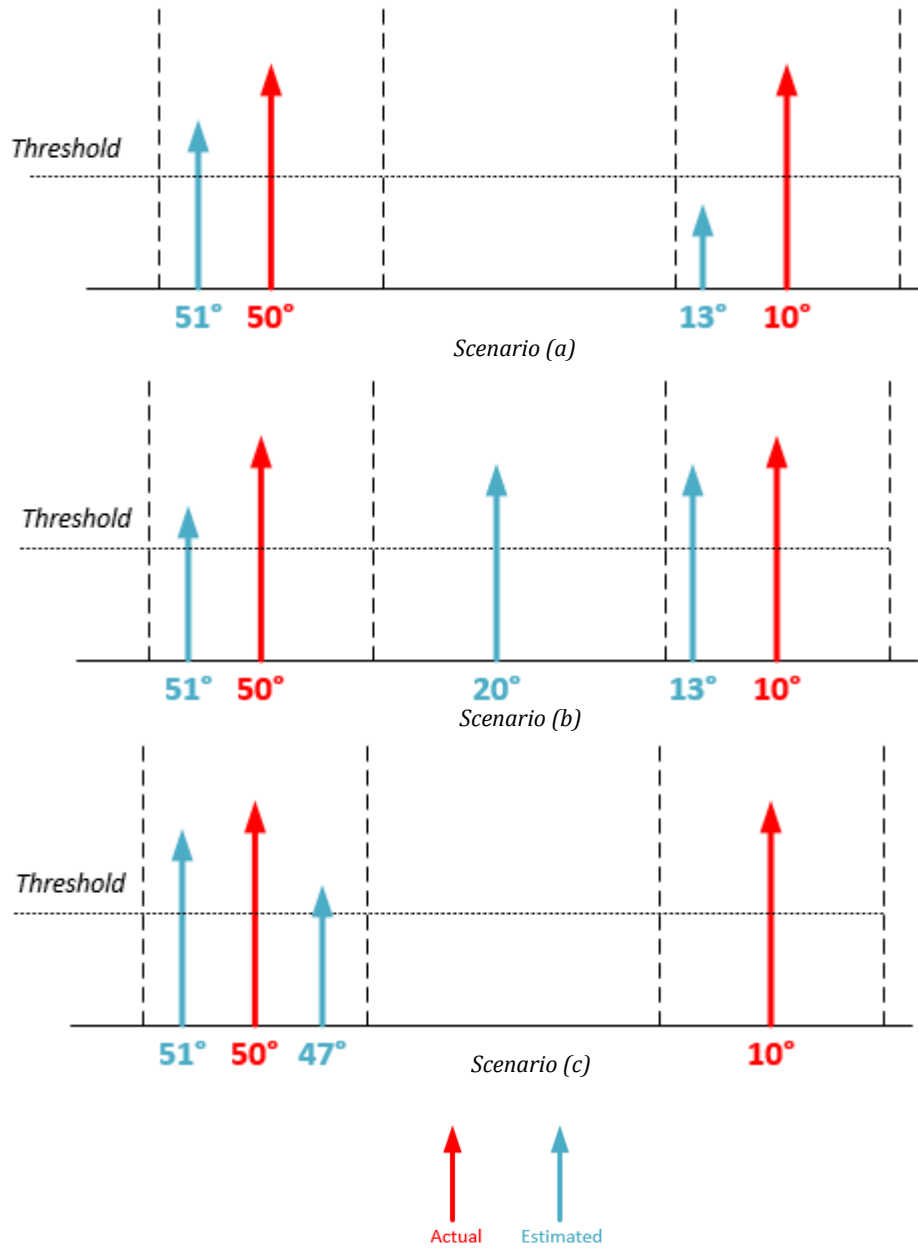
Figure 13 Demonstration of different RMSE methods.

Scenario	Method 1	Method 2	Method 3
(a)	$\sqrt{\dfrac{(50-51)^2+(10-13)^2)}{2}}=2.2°$	$\sqrt{\dfrac{(50-51)^2+180^2}{2}}=127.3°$	$\sqrt{\dfrac{(50-51)^2}{2}}=0.7°$
(b)	$\sqrt{\dfrac{(50-20)^2+(10-13)^2)}{2}}=21.3°$	$\sqrt{\dfrac{(50-51)^2+(10-13)^2+(10-20)^2}{2}}$ $=7.4°$	$\sqrt{\dfrac{(50-51)^2+(10-13)^2}{2}}$ $=2.2°$
(c)	$\sqrt{\dfrac{(50-51)^2+(10-47)^2)}{2}}=26.2°$	$\sqrt{\dfrac{(50-51)^2+(10-47)^2)}{2}}=26.2°$	$\sqrt{\dfrac{(50-51)^2}{2}}=0.7°$

Table 3 shows that different RMSE methods can give different measures for the same scenario. It is therefore important to specify the definition of the RMSE being utilized before the analysis is conducted. If missed or spurious peaks are ignored in the RMSE calculation, they can be provided as a separate accuracy measure.

2.5   Summary

In this chapter, we gave a brief background about antennas and focused on printed patch and monopole antennas along with their design equations. We then introduced antenna arrays and explained how different CPAs are constructed. We then presented a detailed derivation of the MUSIC algorithm used to estimate DOA and showed how to apply it to CPAs. The use of CS for DOA estimation was presented and a detailed analysis of the different RMSE calculation methods is introduced.

CHAPTER 3

LITERATURE REVIEW

This chapter provides a detailed literature review of previous works on DOA estimation using various types of arrays.

3.1   DOA Estimation Using ULA

In [17], the authors studied the effect of the processing algorithm and the number and spacing of sensors on a ULA performance in estimating DOA. The performance was measured by the RMSE and beam width. Four processing methods were discussed: Beamforming, Capon, MUSIC and l_1-SVD. With $\lambda/2$ spacing, one impinging signal and two array elements, RMSE versus SNR graphs of the four algorithms were close. Best RMSE was achieved when the antenna interelement spacing was $\lambda/3$. This result was true for all four algorithms considering one impinging signal on an array of 2,4 or 8 elements with SNR=20 dB. The paper assumed isotropic antennas and ignored the effect of the radiation pattern on the results.

The authors in [18] analyzed via simulations the difference between estimating the DOA using an 8-element isotropic ULA versus ULA of directional antennas with the same number of elements. The elements of the isotropic ULA were separated by 0.6λ. For the directional antenna, the authors used circular patches operating at 2.45 GHz separated by 0.2λ. Simulations with patches and isotropic arrays using 3 sources located at -50°, 0°, 60° were conducted. The isotropic antenna was able to detect all the sources. For the directional

array, the algorithm was only able to detect one source at time. When the main beam was directed at $\theta = 0°$, the algorithm could only detect the signal impinging at $\theta = 0°$. The main beam was then shifted to -50° and 60° to detect the other two signals.

Although the idea of the paper was new as little work has been done in this area, there were several flaws identified in this paper. First, having two different separations between the isotropic and directional arrays adds a second variable in the comparison so the comparison is not fair. Besides, the authors did not explain how they shifted the directional beam to detect the other two signals. Finally, the authors did not quantify the error introduced due to the directional radiation pattern.

In [19], the authors used two types of antennas in a uniform linear array to improve the spectrum efficiency of their MIMO system in determining the DOA. The first antenna type was a short-circuited ring patch antenna which produced an omni-directional radiation pattern while the second antenna was a circular patch which had a broadside radiation pattern. The array operated at 2.4 GHz. The purpose of the paper was to improve the spectral efficiency and did not analyze the effect of the radiation pattern on DOA estimation.

A new algorithm was introduced in [15] to estimate the DOA using a single snap shot of the received signal and without the need to calculate the difference covariance. Their method is based on Bayesian Compressive Sensing (BCS). It exploits the degree of reliability of the DOA estimation to implement an iterative approach to improve the accuracy of the estimation. The authors used a uniform linear array of half wave dipoles to test their approach. They relied on an equation that relates the induced current in a dipole

with the incident electric field. The voltage at the antenna terminals is then calculated by doing a matrix multiplication of the calculated antenna current and the impedance matrix of the antenna array.

To validate their method, they simulated a system of 3 BPSK signals with DOAs of (-22°, -3° and 8°) and SNR equals 10 dB impinging on a linear array of 10 half wave dipole antennas separated by $\lambda/2$. The method was able to accurately estimate the DOAs with zero RMSE. Note that this was only one simulation run as opposed to Monte Carlo simulations where many simulation runs are performed and then the RMSE is calculated for all the runs. The authors performed more than one iteration, but they did not show the RMSE. Instead, they presented the minimum, maximum and average error.

Another set of simulations were performed using 2, 4 and 6 sources impinging on a uniform array of 20 dipoles. They performed 100 simulations and the average RMSE was 0.32°. The paper assumed ideal dipole radiation patterns derived from analytical equations rather than simulated or measured radiation patterns.

3.2 DOA Estimation Using non-ULA

In [20], the authors introduced random arrays. A certain number of physical sensors is selected from ULA with a uniform random distribution. The motivation was to allow the spacing between the physical sensors to exceed $\lambda/2$ which is important in some applications like when the antenna aperture is large. The authors used CS to extract the DOA and waveform of the impinging signals. They simulated a random array consisting of 30 locations randomly chosen from a ULA with 41 sensors. Three sources located at DOA (17°, 21°, and 49°) were used. Notice that the difference in DOA between the first

two sources is only 4°. Source 1 was an up-chirp source with bandwidth of 200 MHz, source 2 was a down-chirp with 100 MHz bandwidth and source 3 had a sinusoidal waveform with fc=50MHz. SNR was 5 dB and was then lowered to -1.5 dB. The simulation showed that their proposed method could resolve all the DOAs at both SNRs. In contrast, standard MUSIC algorithm failed to distinguish the first two close sources at SNR=-1.5 dB. Another simulation assumed two sources of identical wave forms (up-chirp with 200 MHz bandwidth) impinging from DOA of 17° and 27°. The MUSIC algorithm failed to distinguish the two sources while the proposed CS based spectrum showed two peaks at the correct DOA. The presented random array had 30 isotropic sensors used to detect only 3 sources which does not tell what the true DOF is.

A new array concept called nested arrays that allow detecting $O(N^2)$ signals using N antennas was introduced in [21]. The array is formed by concatenating two uniform linear sub arrays called inner and outer subarrays. The inner sub-array has N_1 elements with d_1 spacing and the outer has N_2 elements with d_2 spacing such that $d_2 = (N_1 + 1)d_1$. Figure 14 illustrates a 2-level nested array geometry. Higher levels of nesting are also possible. This array configuration gives $2N_2(N_1 + 1) - 1$ degrees of freedom using $N_1 + N_2$ elements.

Figure 14 Nested array geometry with $N_1 = N_2 = 3$ from [21].

The authors used spatial smoothing MUSIC and compared it with Khatri-Rao (KR) product based MUSIC for DOA estimation. Their simulation considered a 6-sensor array with 8 narrow band sources impinging from different directions of arrival between -60° and 60°.

The spatial smoothing method could resolve up to $\frac{N^2}{4} + \frac{N}{2} - 1 = 11$ sources. Where the KR-product based method could resolve $\frac{N^2-2}{2} + N - 1 = 22$ sources but requires the sources to be quasi-stationary with a larger number of snapshots. The simulation showed that both methods could resolve the 8 sources with 4800 snapshots and SNR = 0 dB. However, when the number of snapshots was reduced to 480, the KR method missed one source at -60°.

The spatial smoothing method was also better in terms of RMSE. A major disadvantage in this array configuration is the closely spaced sensors of the inner array. This close spacing increases the mutual coupling of the array elements which degrades the array's ability to resolve the DOAs. Additionally, the authors focused on the performance of the array geometry and did not consider the effects of using physical antennas instead of isotropic radiators.

In [22], the authors took the path of reducing the mutual coupling in the array rather than trying to correct for it. Their simulations showed that reliable DOA estimation is possible without correcting for mutual coupling if the mutual coupling level is low enough. Hence, they proposed a new array configuration that reduces the mutual coupling called *super nested* array. This linear array has the advantages of the nested array in terms of DOF with significantly less mutual coupling. A closed-form expression was introduced to give the

location of each sensor. Several orders of nesting can be achieved. The details of the array construction can be checked in the reference.

The authors ran several simulations using MUSIC to compare the performance of the new array with that of ULA, Minimum Redundancy Array (MRA) and CPAs. All arrays had 14 isotropic sensors. The authors incorporated the mutual coupling between the array elements by assuming that the antennas have the same mutual coupling as the dipoles. However, they did not include the radiation pattern of the dipole in the system model.

Their results are listed in Table 4. With 20 sources, the MRA showed better performance (lower RMSE). As the authors explained, at large number of sources the main contributor to RMSE became the DOF of the array rather than the mutual coupling. MRAs have higher DOF and hence perform better with many sources. The authors used a coprime configuration that guarantees continuous lags so they can implement spatial smoothing. As discussed in the background chapter, spatial smoothing cuts the DOF of CPAs by half.

Table 4 RMSE for different array configurations using D=10 and D-20 sources with 0 dB SNR and 500 snap shots [22].

Array Configuration	Maximum DOF	RMSE D=10	RMSE D=20
ULA	13	0.17445	N/A
MRA	65	0.00060	0.00070
Nested	55	0.01216	0.01503
Coprime	31	0.12509	0.12749
2nd order super nested	55	0.00042	0.00082
3rd order super nested	55	0.00024	0.00071

New 2D planar arrays were proposed in [23]. They offered several generalizations of open box arrays (OBA) including partially OBA (POBA), half OBA (HOBA), HOBA with two layers (HOBA-2), partially open box with L layers (POBA-L), and the hourglass array. The new arrays, which all have closed form sensor locations, can resolve $O(N^2)$ sources with N sensors and offer reduced mutual coupling compared to OBA. Additionally, the new arrays have hole free difference co-array; i.e. the difference co-array is fully populated. The arrays were used for 2D DOA estimation where the azimuth and elevation of the impinging signal is estimated.

Numerical simulations were carried out to test the performance of these configurations. The number of elements in each array was fixed at 81 physical sensors. Nine uncorrelated equal-power sources with 0 SNR were impinged on the arrays from uniformly distributed azimuths and elevations. The DOA was estimated using the 2D unitary ESPRIT algorithm which does not correct for mutual coupling. Hence, these simulations illustrate the effect of mutual coupling on different array configurations. Simulations showed that the hourglass configuration has the lowest error and hence lowest mutual coupling. The paper assumed the elements as isotropic and only considered the effect of mutual coupling. The radiation pattern of the array elements was not considered.

3.3   CPAs

In [24], the authors compared the performance of CPAs with sparse ruler arrays. The authors used the conventional CPA configuration with $2M + N - 1$ elements. MUSIC algorithm with spatial smoothing was applied to estimate the DOA of both array types and compare the results. Simulations were run to compare DOA performance of both arrays

when they fix the array aperture at $9d$ where d is the minimum inter-element distance. The CPA had 6 elements with $M = 2, N = 3$ and the sparse array had 5 elements. With 0 dB SNR and 6 sources, the sparse array gave less error in DOA estimation. The authors took real measurements for comparison with the simulation results. The experiment showed that the 6-element CPA had a larger error than the 5-element sparse array. The paper did not explain the experiment setup and the type of antennas that were utilized.

A conventional CPA consisting of two sub arrays: N sensors spaced by Md and $2M - 1$ sensors spaced by Nd was used in [7]. This configuration gives continuous differences from $-MN$ to MN. That is, the maximum theoretical DOF is $2MN + 1$. The authors used MUSIC with spatial smoothing which cut the DOF to MN. A simulation was run with $N = 7, M = 5$ (i.e. 16 physical sensors). Theoretically, this should allow detecting 35 sources. However, the simulation was run with 20 impinging signals only. The paper used an isotropic model for the antennas.

The authors of [13] introduced the prototype array geometry with $N + M - 1$ sensors and used CS to compare their results with those of [7]. They did 6 different simulations all using 10 physical sensors with the following setup:

- The prototype $M = 5$, $N = 6$ array configuration with CS at $SNR = -10\,dB$, $0\,dB$

- The conventional $2M - 1, N$ $(where\ M = 3, N = 5)$ array configuration with CS at $SNR = -10\,dB, 0\,dB$

- The conventional $2M - 1, N$ $(where\ M = 3, N = 5)$ array configuration with MUSIC algorithm same as [7]

The simulations showed that they could detect 17 sources using the prototype configuration at both SNR levels. However, there were two spurious peaks at -9° and 9°. Using CS with the conventional CPA (N and $2M - 1$ sources) they could also resolve the 17 sources without any spurious peaks. The conventional configuration with MUSIC failed to resolve the 17 sources specially at low SNR. This work introduced the use of CS for CPAs. As demonstrated, CS exploits all elements of the difference co-array; they do not need to be continuous. This allowed the authors to introduce another form of CPA with less number of elements but same DOF. The paper assumed isotropic antennas with ideally spherical radiation pattern and no phase difference introduced by the antennas.

In [9], the authors propose the CADiS coprime structure mentioned in the theoretical background. They compared the CADiS structure with the conventional one by running three sets of simulation using isotropic radiators. They showed that using CS the DOF is increased.

Simulation 1: 26 sources using MUSIC algorithm. The conventional structure could resolve all 26 signals because of its higher DOF. The CADiS configuration was unable to resolve all the signals although they are lower than the maximum DOF due to its imperfect covariance matrix as explained in the paper.

Simulation 2: using 41 sensors with MUSIC and CS algorithms. Both MUSIC and CS techniques were able to resolve all the signals in the conventional configuration. While for

the CADiS configuration, only CS was able to resolve the signals since the number of impinging signals exceed its maximum DOF when using MUSIC.

Simulation 3: using 51 impinging signals which exceeds the maximum DOF for both configurations using MUSIC. The simulation showed that CS is more effective in detecting the signals since it exploits all the available lags and not only the consecutive ones.

In [6], the authors introduced the CACIS CPA configuration, and they compared it with the CADiS configuration. Using these two generalized configurations (CADiS and CACIS), the nested configuration can be represented either by CADiS or CACIS with $p = M$. Also, the prototype configuration can be represented by a CACIS with $p = 2$. They ran their simulations with $M = 6, N = 7$ to explore the differences between both configurations. With CACIS, the maximum DOF is achieved when $p = M$ which is the nested configuration. Smaller separation between the physical antennas means higher mutual coupling and hence degradation of the DOA estimation capability.

The authors simulated 33 noise free impinging signals. The DOAs of the impinging signals were equally distributed between -60 ° and 60 °. The covariance matrix was estimated using 2000 snap shots. For CS, the authors used the LASSO algorithm with $\vartheta_i^g = 0.25°$ and the penalty parameter $\lambda_t = 0.25°$. They compared the results with the MUSIC algorithm.

The MUSIC algorithm failed to resolve the 33 signals with p=2,3. Only with p=6 (i.e. the nested configuration) could the MUSIC algorithm resolve all the signals since this is the only configuration with DOF > 33 for MUSIC for both CADiS and CACIS. Another set of simulations were carried out to explore the effect of noise on the two methods using the

generalized array configurations. The same number of signals (33) now with SNR=0 dB was simulated. The covariance matrix was estimated using 500 snapshots. Simulations showed better performance of the CS algorithm as compared to MUSIC. As expected, the DOA estimation performance increased with improved SNR and number of snapshots. In general, the simulations showed that CS outperforms MUSIC and that when CS is used, the CADiS structure outperforms the CACIS. The authors focused on the algorithms and the array configuration and ignored the effect of the antennas by using ideal isotropic radiators.

The mutual coupling in a conventional CPA was characterized and incorporated in the data model in [25]. The authors used an optimization algorithm to estimate the elements of the mutual coupling matrix along with the direction of arrivals. The method is called Receiving Mutual Impedance Method (RMIM) and requires the array to be in receiving mode and the antenna elements to be terminated with a known load Z_L. Equations (30) to (33) summarize their work.

$$\boldsymbol{Z} = \begin{bmatrix} 1 & -\dfrac{Z_{1,2}}{Z_L} & \cdots & -\dfrac{Z_{1,N-1}}{Z_L} & -\dfrac{Z_{1,N}}{Z_L} \\ -\dfrac{Z_{2,1}}{Z_L} & 1 & \cdots & -\dfrac{Z_{2,N-1}}{Z_L} & -\dfrac{Z_{2,N}}{Z_L} \\ \vdots & \vdots & \ddots & \vdots & \vdots \\ -\dfrac{Z_{N-1,1}}{Z_L} & \dfrac{Z_{N-1,2}}{Z_L} & \cdots & 1 & -\dfrac{Z_{N-1,N}}{Z_L} \\ -\dfrac{Z_{N,1}}{Z_L} & -\dfrac{Z_{N,2}}{Z_L} & \cdots & \dfrac{Z_{N,N-1}}{Z_L} & 1 \end{bmatrix} \tag{30}$$

Where $Z_{m,n}$ is the mutual coupling impedance between the mth and nth elements, N is the number of elements, Z_L is the load impedance of the antenna elements.

$$C = Z^{-1} \tag{31}$$

Where C is the mutual coupling matrix. The received signal $x(t)$ can now be modeled as below.

$$x(t) = CAs(t) + n(t) \tag{32}$$

And the covariance matrix R_{xx} becomes:

$$R_{xx} = E[x(t)x(t)^H] = CAR_{ss}A^H C^H + \sigma_n^2 I \tag{33}$$

The authors ran three simulations using $(M = 2, N = 3)$ conventional CPA with six physical antennas. Seven sources with 10 dB SNR and different DOAs between -64° and 64° were simulated. The first simulation used the MUSIC algorithm with spatial smoothing which could resolve all the 7 sources. Next, the authors calculated the mutual coupling matrix C of the CPA using RMIM and incorporated it into the received signal. It is unclear in the paper what impedance matrix they used and what type of antennas the elements were. They used the MUSIC algorithm without compensating for the mutual coupling. As a result, two sources were missed from the spectrum and the detected DOAs were slightly inaccurate.

Finally, they ran a third simulation that implemented their method to compensate for the mutual coupling. All seven sources were accurately estimated. This work demonstrated the effect of mutual coupling on DOA estimation. However, the authors did not mention what array elements they used for the impedance matrix.

In [26], the authors investigated the effect of mutual coupling on DOA estimation. They used three array configurations: Minimum Redundancy Array (MRA), CPA and nested

arrays. Mutual coupling was found by simulation for two types of antenna elements: dipoles and patches. They also considered different number of elements for each array configuration. The arrays were all tuned at 3 GHz and the fundamental interelement spacing was $\lambda/2$ and the DOA was estimated using MUSIC with spatial smoothing.

The authors characterized the effect of mutual coupling using a mutual coupling matrix (MCM) that is added to the data model as they did in [25]. The MCM was calculated using the receiving mutual impedance method (RMIM). FEKO simulation software was used to get the voltages at the antenna terminals. They also introduced two methods to account for mutual coupling. The first method is iterative and assumes some perturbation occurred to an already known MCM. The second method uses nested optimization to estimate the DOA together with the unknown MCM. The use of directional antennas was for mutual coupling estimation only. Neither the radiation pattern of the patches nor the dipoles was used in the data model. The elements of the steering vector all had unity magnitude and a phase that only depends on the location of the element. The only considered physical effect was the mutual coupling.

The work in [8], [27], [28] discussed the side lobe level (SLL) of CPAs. Although this topic is not directly related to DOA estimation, CPAs can still serve other applications that require low SLL (e.g. beam forming).

The work in [8] studied the optimum M, N factors that reduce the total number of elements in a CPA that has the same spatial resolution of a fully populated ULA, and presented ways to reduce the SLL of the CPA.

The optimum M, N numbers were found using an optimization problem. This resulted in $M = N = \sqrt{L}$ which does not satisfy the coprimality requirement. However, the closer M and N are to each other, the closer they are to the optimum values. For the rest of the paper, the authors always used $N = M + 1$.

The SLL of the CPAs was studied analytically in [8] as well. The array factor, assuming it is the product of the array factors of the two sub arrays, was introduced. Then, it was shown that increasing the number of elements of each subarray in the CPA reduces the peak SLL.

In [27], the authors introduced a new CPA structure. Compared to the prototype M, N structure where N is taken as $M + 1$, the proposed configuration has cN and $cN - 1$ elements spaced by M and N respectively, where c is an extension factor. The authors calculated the value of c which reduces the peak side lobe to match that of a corresponding ULA with $M \times N$ sensors. They used an array processor that multiplies each subarray by a weight function and then multiplies one output by the conjugate of the other. They referred to the new array configuration as Extended Coprime Sensor Array (ECSA).

The extension factor c is derived for uniform, hamming, Hann and Dolph-Chebyshev shadings. For the Hann shading with configurations $(M = 2, N = 3)$, $(M = 3, N = 4)$ and $(M = 4, N = 5)$, it is not possible to achieve a SLL below that of the ULA. It was found that uniform shading requires the least number of sensors to achieve a peak side lobe lower than the ULA and that for a given peak side lobe, Dolph-Chebyshev shading requires the least number of sensors.

A new array processor for CPAs was proposed in [28]. Instead of the conjugate and product processor [29], they proposed a minimum processor that achieves lower peak SLL than the product processor. They showed that for an $(M = 4, N = 5)$ CPA with extension factor $\alpha = 3$, the product processor achieved around -10 dB peak side lobe while the peak SLL of the min processor was -13 dB which is almost equal to that of an equivalent ULA with MN elements.

3.4   Experimental Work in DOA Estimation

In [30], a DOA system using a ULA with four quarter wave monopoles placed above a metallic ground was experimentally tested. The antennas were tuned to receive 2.4 GHz incoming signals and were spaced by $\lambda/2$. Two wide band horn antennas were used to impinge the array with two coherent signals coming from an azimuth angle of 76° and 124° at $\theta = 90°$ in experiment 1, and 63° and 111° in experiment 2. Figure 15 shows a picture of the antenna array. Figure 16 displays the experiment setup.

Figure 15 The four element monopoles array [30].
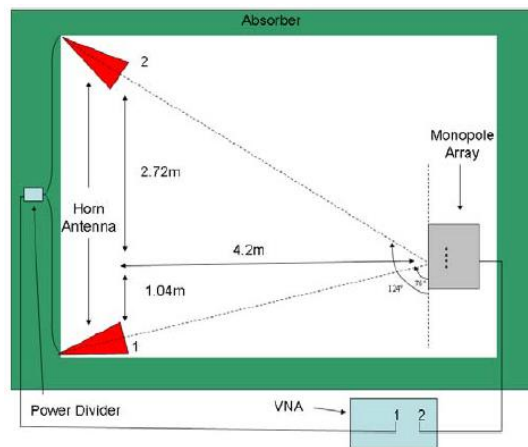
Figure 16 The DOA setup [30].

Both MUSIC and Matrix Pencil Method (MPM) were used for DOA estimation. Mutual coupling was modeled using the RMIM and the conventional mutual impedances method (CMIM) and was also measured. Both methods were compared experimentally, and it was shown that the RMIM is far better in compensating for the mutual coupling the CMIM. Another interesting finding made is that the effect of mutual coupling increases when the number of impinging signals increases. When one of the antennas is covered with an absorber so that only one signal is impinging on the array, DOA without mutual coupling compensation was close to the actual one.

45

Figure 16 presents the results of the one experiment. Applying MUSIC or MPM algorithms without accounting for mutual coupling missed one source (blue lines). Compensation for mutual coupling using either measured or theoretical values gave good results. This work provided an experimental validation for the MUSICM and MPM methods for ULAs. The effect of the omni-directional radiation pattern of the monopole antennas was imbedded in the experiment but the results were not compared with isotropic antennas. Additionally, the methods were validated at 4 DOAs only so the effect of the radiation pattern was not fully assessed. Finally, the paper used ULAs which have limited DOF compared to CPAs.

In [31], the authors used a 4×4 MIMO system of horn antennas to study the effect of the bandwidth on (Direction of Departure) DOD and DOA estimation in UWB MIMO RADARs. Two array configurations were used: a ULA and non-uniform linear array. The RADAR targets were two metallic spheres with RADAR cross section (RCS) of $-10 \, dBm^2$. Figure 18 depicts the structure of both arrays and Figure 19 shows the experimental setup. They used 2D MUSIC to estimate both DOD and DOA at different transmitted frequencies. The estimations at different frequencies are then combined to obtain the final DOD and DOA. Simulations and experimental measurements confirmed that increasing the bandwidth of the transmitted signal reduces the DOA and DOD estimation error. They also showed less RMSE with the non-ULA compared to the ULA. Since the RMSE was not compared with that of an isotropic source, the effect of the antennas radiation patterns was not clear. The used horn antennas might be appropriate for a RADAR setup but cannot be used for mobile phones or tablet devices.

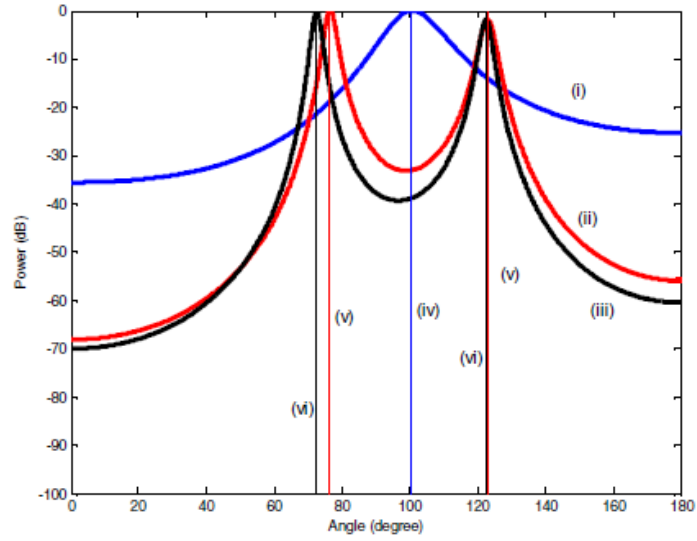**Figure 17 Results of experiment 1 in [30]. (i) MUSIC spectrum without compensation for MC (ii) with RMIM (measured) compensation (iii) with RMIM (simulated) compensation (iv) MPM (not compensated) (v) MPM with measured RMIM compensation (vi) MPM with theoretical RMIM compensation.**
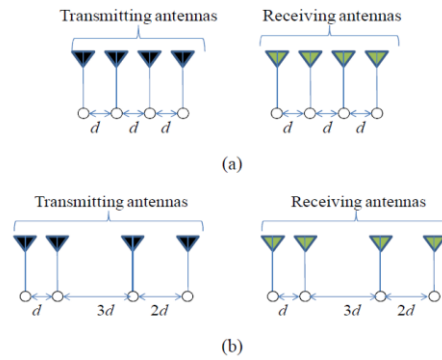

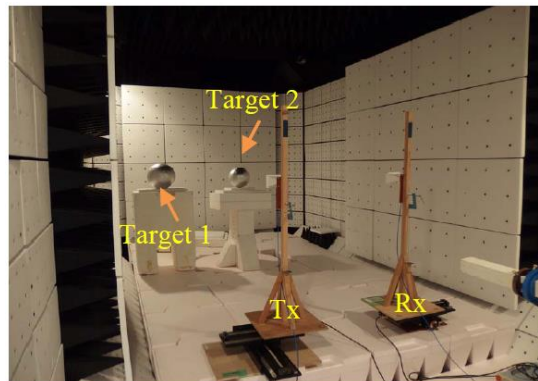**Figure 18 Array configurations used in [31] (a) ULA (b) non-uniform linear array.**

Figure 19 Experiment setup in [31].

47

The work in [32] investigated the estimation of DOA of signals with unknown polarization using MUSIC algorithm with a 2×2 planar array of printed Multibeam Antenna (MBA). The array is composed of four circularly polarized elements and a beam-forming network which provides a switchable set of radiation patterns. Circular polarization ensures that the DOA estimation accuracy is insensitive to the polarization of the source. The authors suggested a method to estimate the DOA and the source polarization of the impinging signal. They backed up their analytical derivations with experimental data. The experiments showed that at DOA=-5°, DOA can be estimated with 5° resolution while the source inclination can be coarsely found. However, for DOA=50°, DOA can be estimated with 7° resolution and source inclination can be estimated with 19° resolution. Using printed antennas incorporated the effect of the direction pattern but like the previous references, the results were not compared against isotropic antennas. Therefore, the effect of antenna radiation patterns was not clear.

In [33], the authors used two-port Leaky-Wave Antennas (LWA) operating in the 2.4 GHz band for DOA estimation. The antenna is 156 mm in length and 38mm in width. The advantages of using LWA are the reduced hardware requirements, compact size, and lower DC power consumption. Unlike conventional antenna arrays where different signals can be observed on array elements at one point of time, LWA allows only one sample at a time. Different samples are collected with different radiation patterns from the same LWA. Figure 20 shows a picture of the LWA.
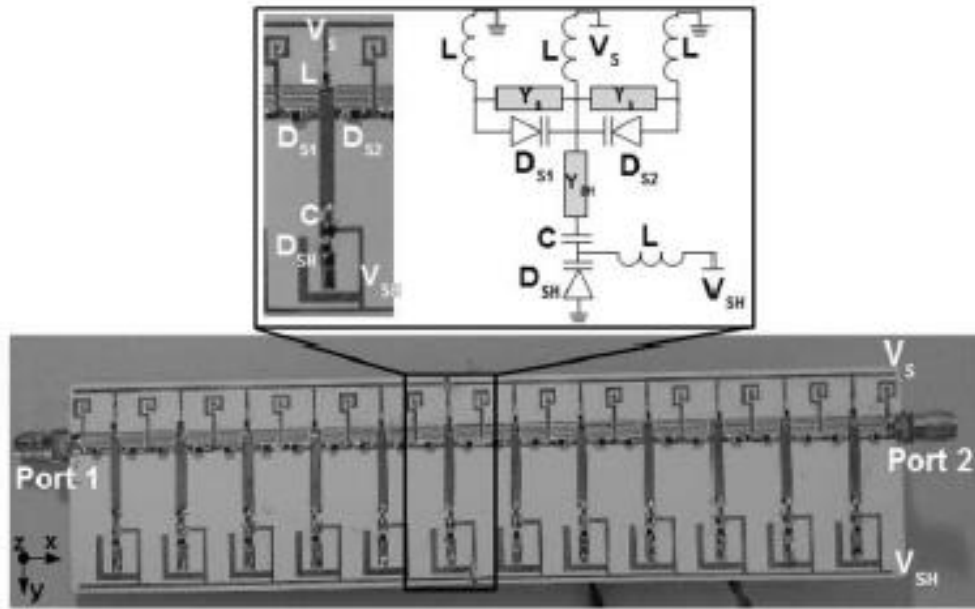
(a)
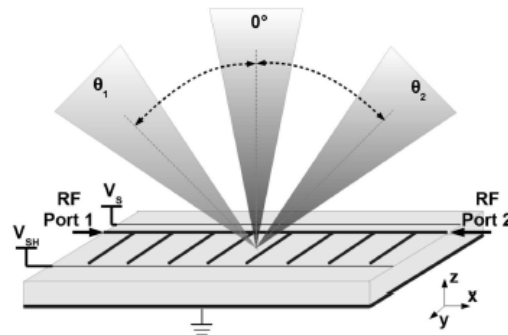
(b)

Figure 20 (a) picture of the fabricated LWA with the equivalent circuit of one cell. (b) example of the beam steering capability of the LWA [33].

By applying certain voltages at the two ports of the LWA, different radiation patterns can be realized. Figure 21 shows examples of the generated radiation patterns by applying different voltages at the two ports. Several DOA estimation algorithms were tested including a variant of the MUSIC algorithm modified for two-port LWA. They also carried out experiments to confirm their results in an indoor environment with severe multipath effect. Their results show that it is possible to use LWA for DOA estimation. While using

conventional antenna arrays occupying the same physical space provide better DOA accuracy, the LWA requires less hardware since one analog to digital converter (ADC) and radio frequency (RF) chain is required. The RMSE in the experimental setup using MUSIC was 11.2°.
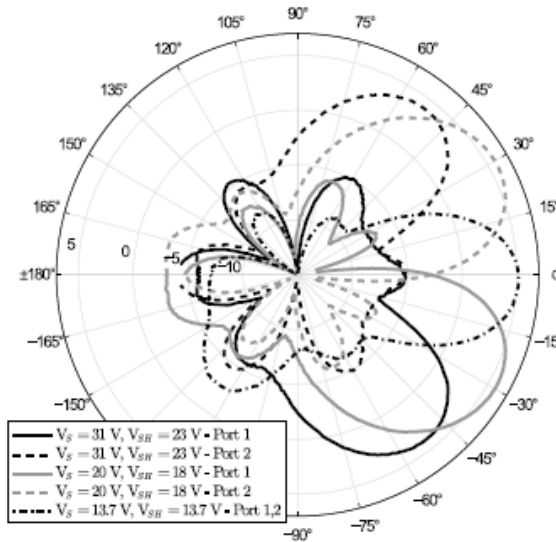
Figure 21 Measured radiation patterns at 2.46 GHz with different input voltages [33].

In [34], the authors built a system to measure the DOA using a ULA with MUSIC in one setup and a coprime with CS in another. Instead of building an array of sensors, they used one wide band horn antenna and moved it linearly to take samples at specific points corresponding to the locations of the array elements. The antenna was radiating a stepped frequency continuous wave signal from 30 KHz to 10 GHz. The unit spacing of the antenna arrays was adjusted to $d = \frac{\lambda_{min}}{2} = 0.015\ m$. The transmitter was placed at three distinct locations that gave DOA of -7.5°, 3.7°, and 23°. Two coprime prototype array configurations were tested: $(M = 2, N = 3)$ and $(M = 4, N = 5)$. The ULA configuration had 4 elements like the first coprime configuration.

The results were plotted in a rectangular graph where the x-axis represents θ and the y-axis represents the frequency of the received signal. The power of the signal was color coded. It was shown that the CPA $(M = 2, N = 3)$ with CS outperformed the ULA with MUSIC. As expected, the $(M = 3, N = 4)$ CPA with its more sensors has better DOA estimation capability than the (2,3) one. This experiment demonstrated the capabilities of CPAs in comparison to ULA. However, having one receiver that moves from one element location to the other eliminates the mutual coupling between the elements. In most of the real-world applications of DOA estimation, there will be an antenna at each array location which was not tested in this setup.

A low complexity method to estimate the DOA of wide band signals was proposed in [35]. The method was tested by building a conventional CPA of 8 microphones with $M = 2, N = 5$. The acoustic signals were sampled at 20 KHz and the frequency band of interest was 5 Khz to 10 KHz. The unit spacing was $\frac{\lambda}{2} = 1.7\ cm$ with speed of $340\ m/s$. Ten acoustic signals were impinged on the array with DOA between -40 ° and 50 °. Figure 22 shows the experiment setup and the resulting spectrum. The used setup is suitable for validating the new wide band DOA estimation method. However, practical antennas that radiate and receive EM waves behave in a different way which is not studied in this work.
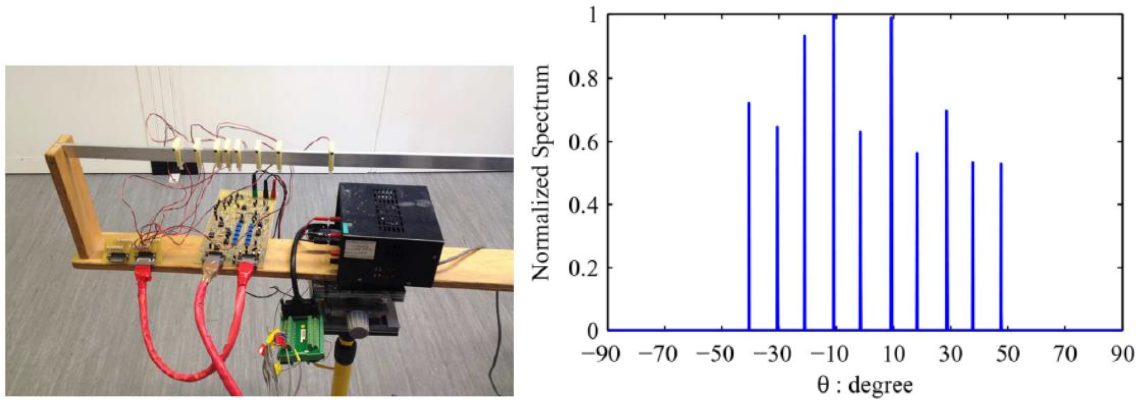
Figure 22 Experiment setup in [35] and the resulting spectrum.

In [36], the authors experimentally demonstrated the ability to use sparse arrays for DOA estimation. They built two arrays of quarter wave wire monopoles. The first array was a ULA with 4 elements while the second was a 4-element coprime with $M = 2, N = 3$. They used a Software Define Radio (SDR) system that transmits a wave at 1.2 GHz using a horn antenna. The SDR system is then used to decode the signals received by the monopole antennas and a LabView program processes the received signal and calculates the DOA. The authors tested DOA estimation using MUSIC, Capon and Lasso algorithms. Their results show that Lasso provides the best accuracy in DOA estimation. Figure 23 depicts the system setup. The effect of the omnidirectional radiation pattern was imbedded in the experiment. However, it was not compared against isotropic radiators to isolate the effect of the antenna. Additionally, future systems that rely on DOA estimation will most likely require low profile printed antennas rather than wire monopoles.
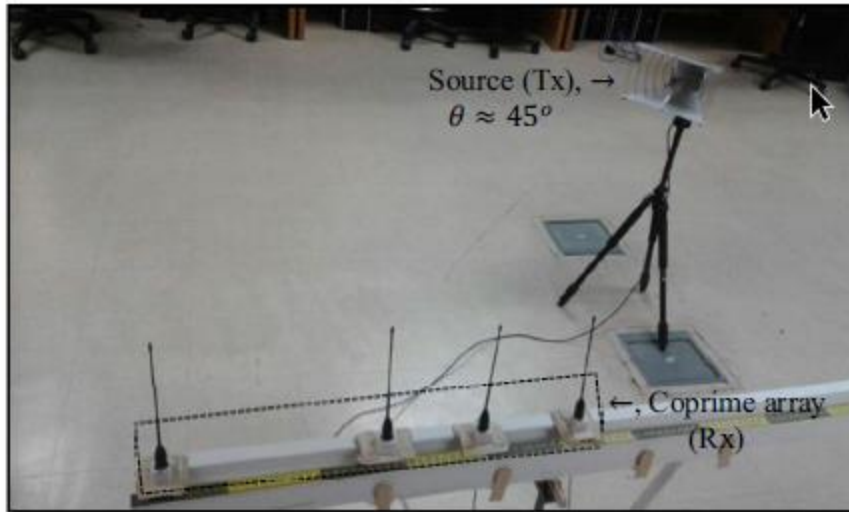
3.5   Summary Table of Reviewed Literature

Table 5 compares the main features in the reviewed literature. Most of previous works focused on the DOA estimation algorithm without paying much attention to the effects introduced by the antenna itself except for mutual coupling. Also, few papers considered small form factor low profile antennas that can be used in a real application. Furthermore, none of the reviewed papers compared the DOA estimation results between isotropic and real antennas. This comparison is important to eliminate the effect of the algorithm, so the impact of the antenna alone on DOA estimation can be isolated and analyzed separately. The number of papers with experimental work is limited and most of the experiments only considered few angles and sources.

Our work tries to fill the gap by identifying the effect of directional (patch) and omnidirectional (monopoles) antennas on DOA estimation in CPAs. The effect of the antenna will be isolated by comparing the DOA estimation performance with isotropic and physical antennas. Our work will cover the 5.8 GHz band which was not considered in the

reviewed work. Additionally, our work will use measured radiation magnitude and phase patterns and the results will be compared against isotropic radiators and ULAs.

Figure 24 displays a tree representing a summary of the antenna types in the reviewed literature. Only few papers used low profile microstrip antennas. Figure 25 shows a comparison of how the radiation pattern of the antennas was dealt with. Apparently, most of the papers totally ignored the effect of the antenna radiation pattern and considered isotropic antennas. Only one paper analyzed the effect of the radiation pattern.

Table 5 Summary of reviewed literature.

| Ref	Frequency	Array Type	Antennas	Simulation (S) / Experimental (E)	Effect of radiation pattern?	Printed antennas (y/n)	Small Form Factor
[6]	NA	CPA	Isotropic	S	N	N	N
[7]	NA	CPA	Isotropic	S	N	N	N
[8]	NA	CPA	Isotropic	S	N	N	N
[9]	NA	CPA	Isotropic	S	N	N	N
[13]	NA	CPA	Isotropic	S	N	N	N
[15]	2.4 GHz	ULA	Patches	S	N	Y	Y
[17]	NA	ULA	Isotropic	S	N	N	N
[18]	2.45 GHz	ULA	Circular Patches	S	Y	Y	Y
[19]	NA	ULA	Dipole	S	N	N	N
[20]	NA	Random	Isotropic	S	N	N	N
[21]	NA	Nested	Isotropic	S	N	N	N
[22]	NA	Super Nested	Isotropic	S	N	N	N
[23]	NA	2D Sparse	Isotropic	S	N	N	N
[24]	NA	CPA	Isotropic	S and E	N	N	N
[25]	NA	CPA	Isotropic with Mutual Coupling	S	N	N	N
[26]	3 GHz	MRA, CPA, nested	Dipoles / patches	S	N	Y	Y
[27]	NA	CPA	Isotropic	S	N	N	N
[28]	NA	CPA	Isotropic	S	N	N	N
[30]	2.4 GHz	ULA	Monopoles	E	N	N	N
[31]	3.1 GHz to 10.6 GHz and 3.6 GHz	ULA	Horn	S and E	N	N	N
[32]	900 MHz	ULA	Microstrip	E	N	Y	N
[33]	2.4 GHz	ULA	LWA	S and E	N	Y	Y
[34]	30 KHz - 10 GHz	CPA	Horn	E	N	N	N
[35]	5 KHz to 10 KHz	CPA	Acoustic	E	N	N	N
[36]	1.2 GHz	ULA and CPA	Monopoles	E	N	N	N
Proposed	2.1 / 5.8 GHz	CPA / ULA	Microstrip (patch and monopoles)	S and E	Y	Y	Y
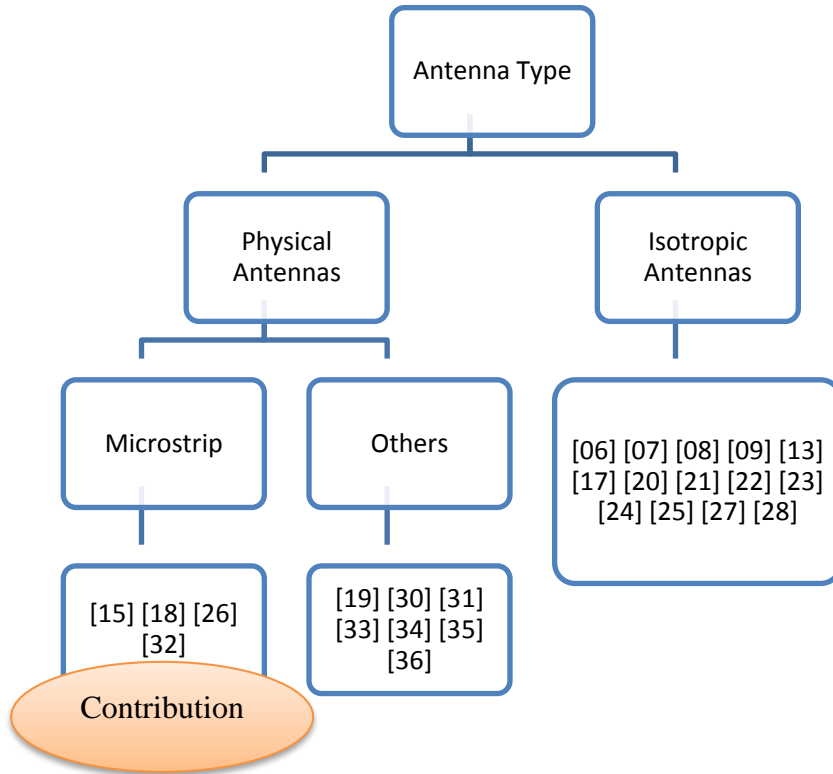
Figure 24 Overview of antenna types in literature about DOA estimation.

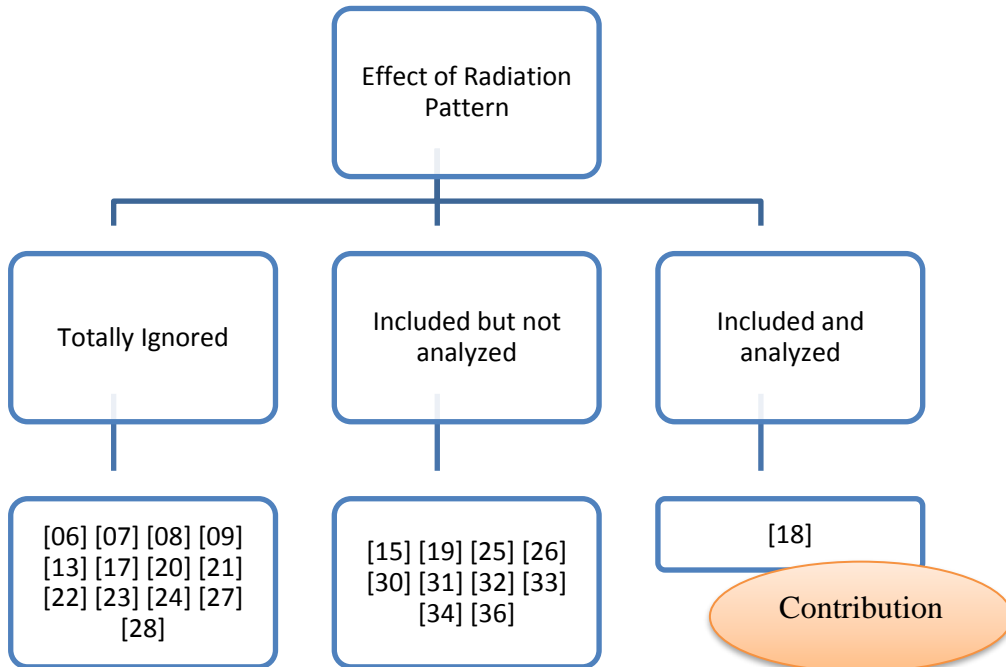**Figure 25 Overview of how different papers dealt with the effect of physical antenna's radiation pattern.**

3.6   Summary

In this chapter, we reviewed the published literature on DOA estimation and the use of CPAs. The review showed that most of the published work only focused on the estimation algorithms rather than the effect of the antennas. Some papers discussed the effect of mutual coupling and suggested some countermeasures. Some experimental work has been performed but it did not reveal the effect of using actual antennas on the DOA estimation. The impact of the complex radiation patterns of real antennas that will be used in the future for DOA estimation was not analyzed. This work tries to fill the gap in the literature by building real antennas, measuring their radiation patterns, and incorporate the measured patterns in the DOA estimation. The experimental work aims at confirming the simulation results and providing solid evidence on the effect of antennas on DOA estimation in CPAs.

CHAPTER 4

Antenna Arrays Design

This chapter presents the design of the antenna arrays used in this work. The first array is a CPA of patch antennas operating in the 5.8 GHz band. Next, coprime and ULAs of patch elements designed for the 2.1 GHz band are presented. Finally, coprime and ULAs of monopole elements operating in the 2.1 GHz band are introduced. The arrays geometry is presented, followed by the reflection coefficients and input impedance curves. Simulated and measured radiation patterns are shown as well.

4.1   Coprime Patch-based Array at 5.8 GHz

A CPA of microstrip patch antennas with $M = 2, N = 3$ and $d = 0.5\lambda$ was designed and fabricated using a 1.5 mm thick FR-4 board with dielectric constant of 4.0. Initially, a single patch, excited from the edge using a microstrip line, was designed and optimized to operate at 5.8 GHz. Equations (1) to (4) were used to calculate the length and width of the patch as 12.4 mm and 16.4 mm respectively. This size would give an input impedance of 225 Ω at the edge of the patch. To have good matching with the RF front end, the patch input impedance needs to be as close as possible to 50Ω. This was achieved using inset feeding. Theoretically, the recess depth was calculated using the formula in [4] to be 4.6 mm. However, multiple simulations and optimizations showed better results when the patch size is 12.6 mm × 16.0 mm and the recess depth is 3.7 mm. Figure 26 shows how the real and imaginary components of the simulated input impedance change with the recess depth.

Best matching occurs when the imaginary is zero and the real is 50 Ω. A parameter sweep was performed from 3.0 mm to 4.0 mm and the best matching occurred at recess depth of 3.7 mm.
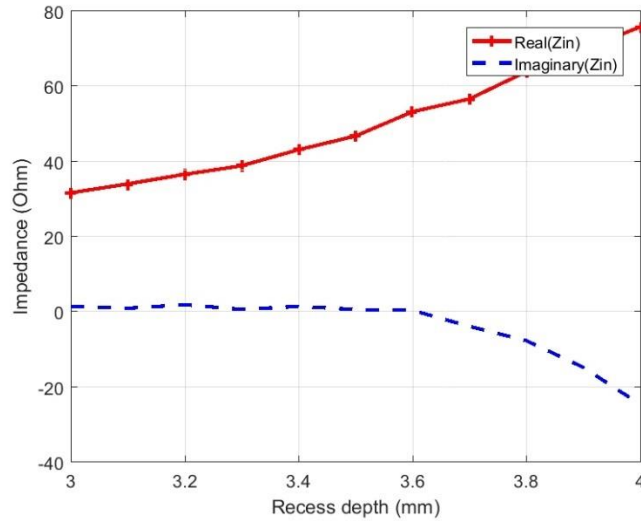

Figure 26 Patch input impedance versus recess depth at 5.8 GHz.

After optimizing the antenna parameters for one patch, the CPA was designed. It consists of four printed rectangular patches horizontally centered on a 125 mm × 60 mm board made from 1.5 mm thick FR-4 substrate. The first subarray includes three elements 1,2, and 4 spaced by $2d$ or λ. The second subarray consists of two elements 1 and 3 spaced by $3d$ or 1.5λ. The array is placed in the upper portion of the PCB occupying 18.60 mm of its width and leaving an area of 41.4 mm ×125 mm for other electronic components to be mounted on the board, making the array suitable for a mobile device. The array was fabricated in the Antenna and Microwave Structure Design Laboratory (AMSDL) at KFUPM. The complex S parameters were measured using an Agilent N9918A vector network analyzer (VNA). The array is depicted in Figure 27 along with its fabricated prototype.

The design initially targeted 5.8 GHz frequency with $\lambda_0 = 51.7\ mm$. S parameters measurements showed that the antennas were resonating at 5.7 GHz with $\lambda_0 = 52.6\ mm$. This difference is due to the inaccuracy of the dielectric constant (ϵ_r) of the FR4 material. The simulations were repeated with $\epsilon_r = 4.1$ which gave the closest match in S parameters to the measurements. In subsequent DOA simulations, the interelement spacing was left as $0.5\lambda_0$ using the original $\lambda_0 = 51.7\ mm$. In practice, the incoming signal will not be at single frequency. Rather, it will have a frequency bandwidth with a range of wavelengths. Therefore, small variations in wavelengths should not affect the overall system performance.

Figure 28a depicts the simulated input impedance of the four elements in the array while Figure 28b shows the simulated mutual coupling ($S_{12}, S_{13}, S_{14}, S_{23}, S_{24}$, and S_{34}) which give a measure of the isolation between the elements. Approximately, there is a minimum isolation of 20 dB between the elements. Figure 29 shows the simulated and measured reflection coefficients of the array. A minimum 10-dB bandwidth of 100 MHz was achieved.
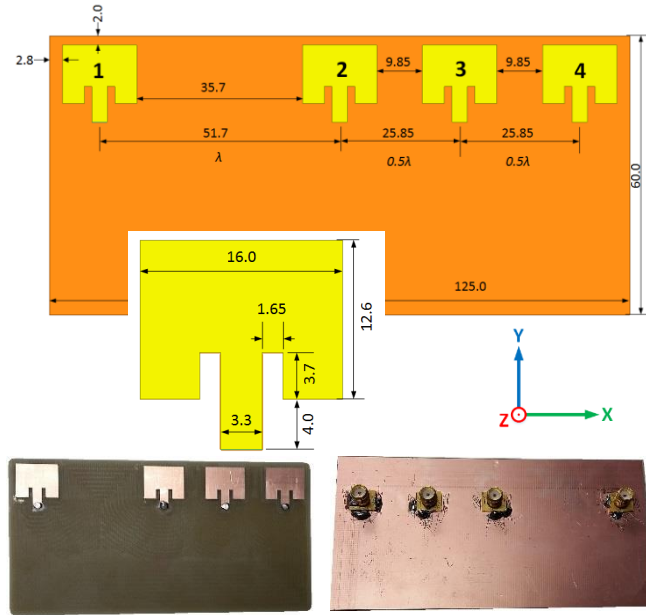
Figure 27 CPA of microstrip patch antennas for the 5.8 GHz band, all dimensions are in (mm).
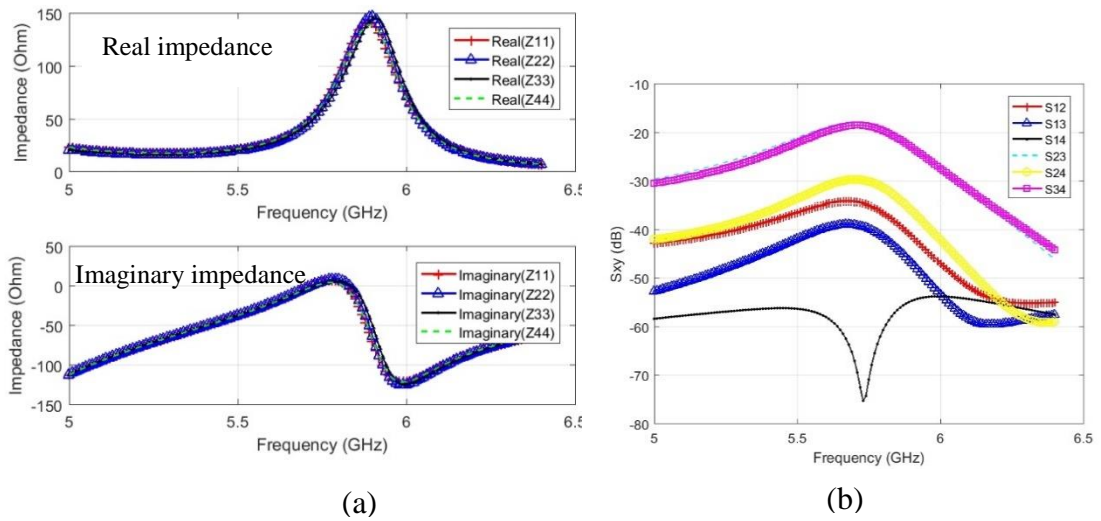

(a)

(b)

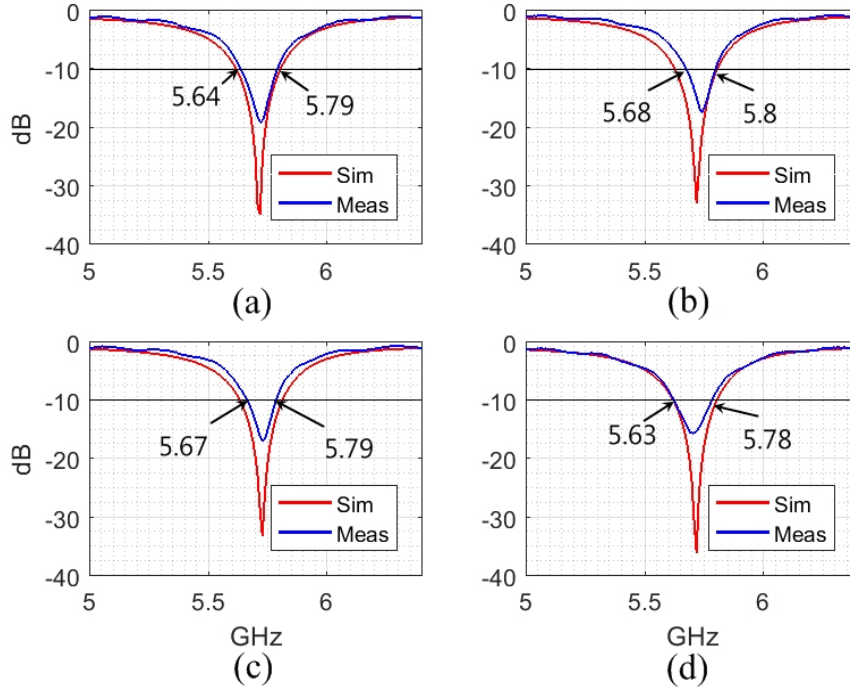**Figure 28 Patch-based CPA (a) Real and imaginary input impedance versus frequency (b) Interelement isolation.**

Figure 29 Simulated and meaured reflection coefficients for the patch-based CPA (a) S_{11}, (b) S_{22}, (c) S_{33}, (d) S_{44}.

The array was sent to Microwave Vision Group (MVG) in Italy to measure its radiation patterns. The magnitude and phase of the radiated $\vec{E}$ fields were measured at two different polarizations (namely E_θ and E_ϕ) for each antenna. The array was placed in the center of the measurement chamber. Each antenna was excited by a reference voltage at its port and then the two polarizations of the radiated electric field were measured in the far field region at each θ and ϕ where θ was varied from 0 to 180° in 2° increments and ϕ was varied from 0 to 360° in 2° increments. Figure 30 shows the coordinate system definitions in the measurement setup. Figure 31 shows a picture of the array in the measurement chamber at MVG. Figure 32 shows the measured and simulated magnitude of E_ϕ in the ZX plane for the four antennas in the array. There is an excellent match between simulations and measurements.
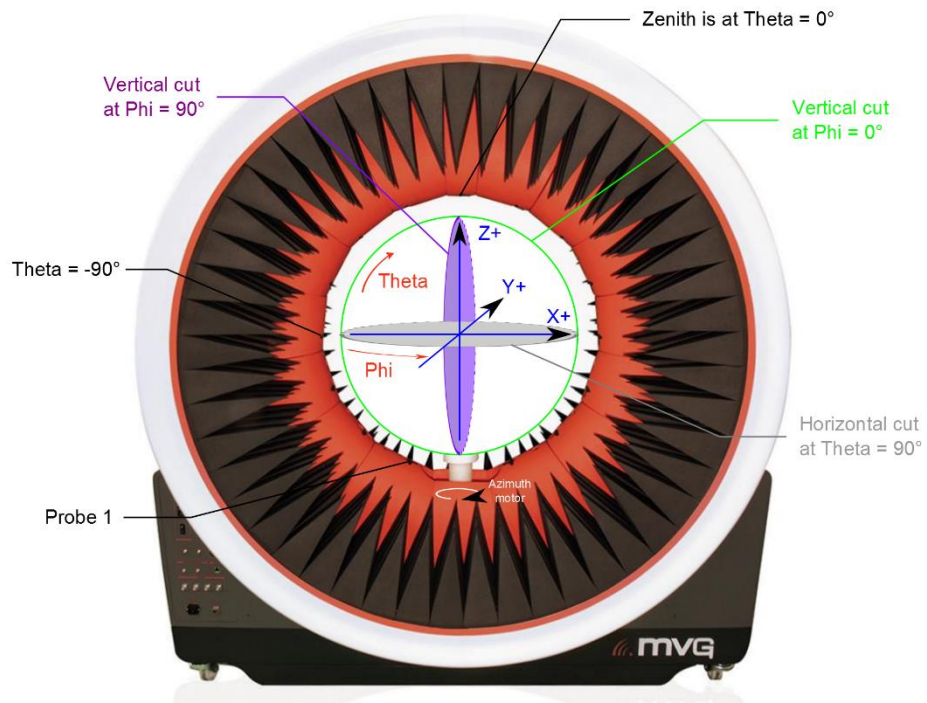
Figure 30 Radiation pattern measurement angle definitions as defined by MVG [37].
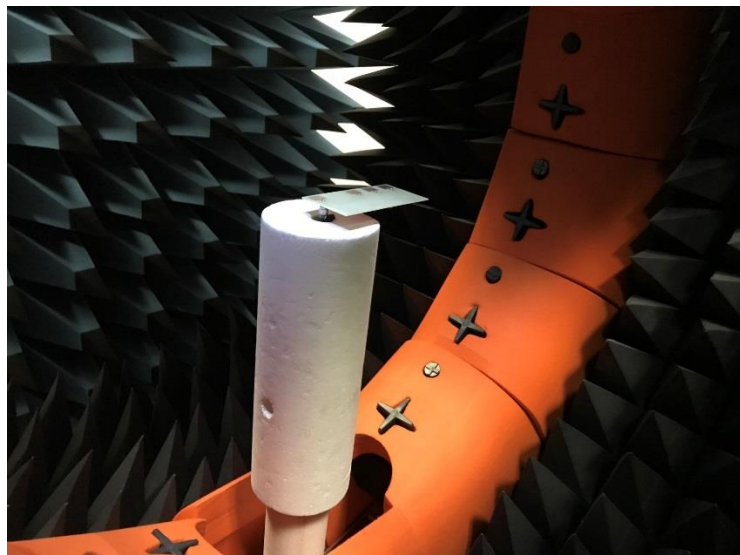

Figure 31 Picture of the patch-based CPA in the measurement chamber in MVG Ital.
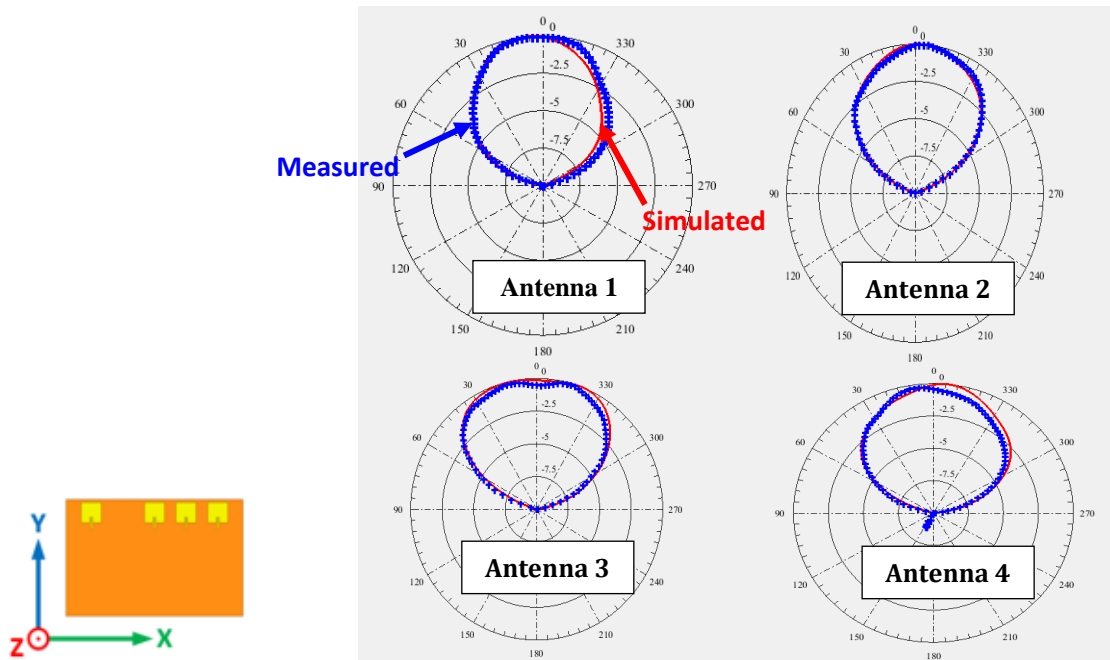
Figure 32 Measured and simulated radiation pattern of E_ϕ in the ZX plane for the four antennas at 5.7 GHz.

Conversely, the measured phase of the radiated field did not provide the same match with the simulations. There are several factors behind this difference. First, the simulated phase was referenced to the patch center while the measurements were referenced to the feeding point. Second, at 5.7 GHz, very small misalignments in the measurement setup produce large variations in the measured phase. In fact, at 5.7 GHz, a 1 mm shift translates to 6.8° error in phase. Ideally, the device under test (DUT) is placed at the center of a circle with measurement probes located at the perimeter of the circle at the same distance from the DUT. When the DUT is not exactly at the center of the chamber, the measurement probes will be at different distances from the DUT. Therefore, the phase error will not be constant for all angles. A third source of error is the accuracy of the measurement system in the time domain (i.e. stability of the clock, nonlinearities in the measurement electronics, etc.).

An attempt was made to correct for the phase difference between measured and simulated values. The correction versus angle was assumed to be a straight line with an arbitrary slope. The measured phase was corrected based on that line. The slope of the line was chosen to minimize the error between simulated and measured fields. Figure 33 shows the originally measured and corrected phase in addition to the simulated values.
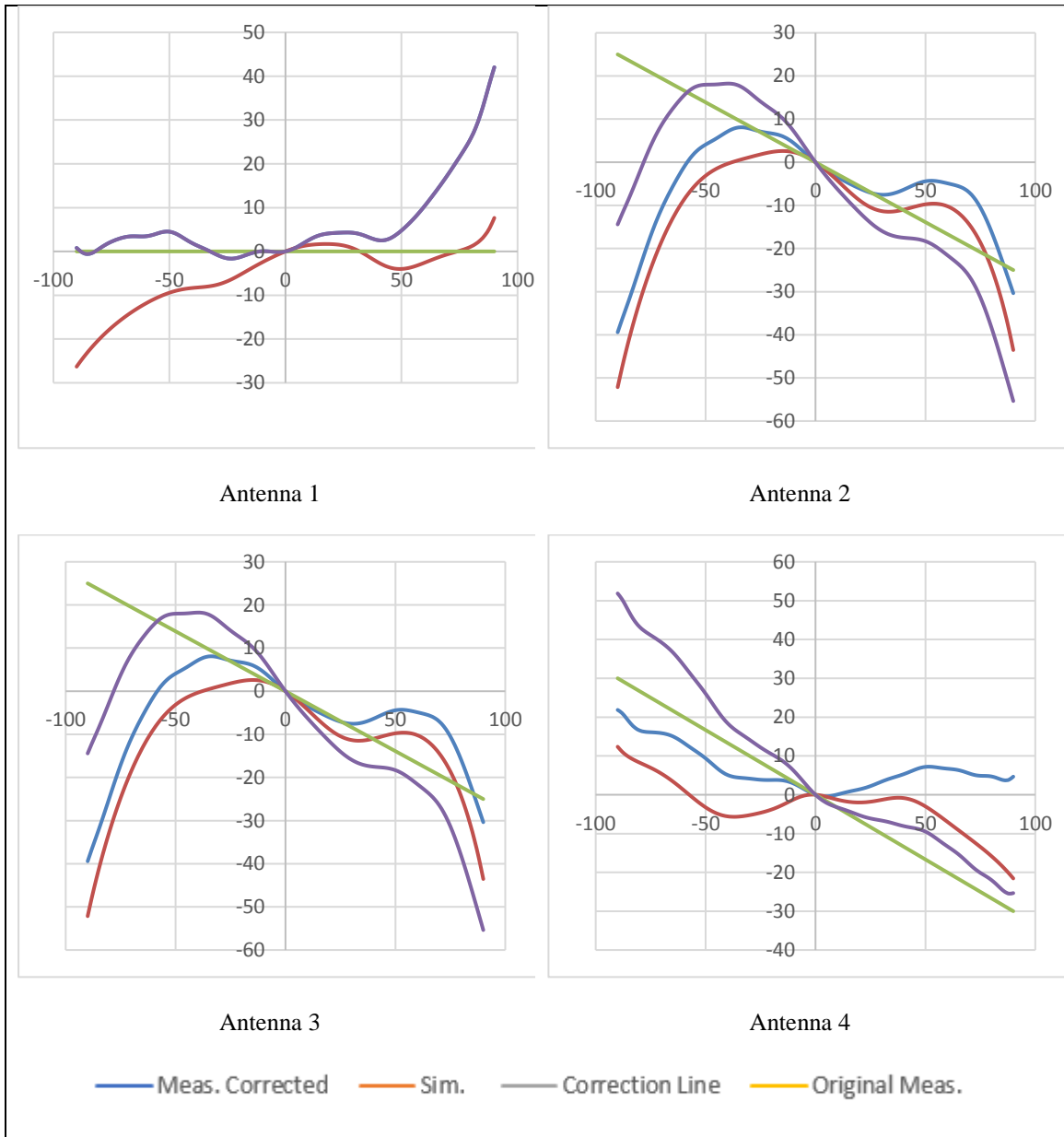

Figure 33 Measured and corrected phase of the coprime radiation pattern.

To test the effect of inter-element spacing on the DOA estimation performance, 20 different patch-based arrays, similar to the discussed one, were designed and modelled. With all design parameters kept the same, the inter-element spacing of the array was varied from 0.31λ to 0.5λ. At each spacing, the complex radiation pattern was exported to be used in the DOA simulation.

4.2   Patch-Based Coprime and ULA Arrays at 2.1 GHz

A patch-based coprime ($M = 2, N = 3$) array was designed to operate at 2.1 GHz. To analyze the advantage of using CPAs over ULAs, two patch-based ULAs were also built. The first ULA had 4 elements which was the same number of elements as the coprime and the other has 5 elements with a similar aperture as the CPA. This allowed comparing DOA estimation performance of a CPA with an equivalent ULA where equivalence can be defined in two ways: same number of elements and same array aperture.

The design process started by optimizing the dimensions of one patch and then forming the arrays. The optimized patch was 44.7 mm wide and 34.3 mm long with a 9.5 mm recess for impedance matching. The array was designed on a 200 mm $\times$ 400 mm $\times$ 1.6 mm FR-4 board. The arrays were fabricated at a local PCB manufacturer located in Jeddah and the S-parameters were measured at AMSDL.

Figure 34 shows the dimensions of the single patch and the three arrays in addition to pictures of the fabricated arrays. Figure 35, Figure 36, and Figure 37 show the measured and simulated S parameters for the coprime, 4-element ULA and 5-element ULA, respectively. A minimum bandwidth of 40 MHz was achieved for all antennas in all arrays.
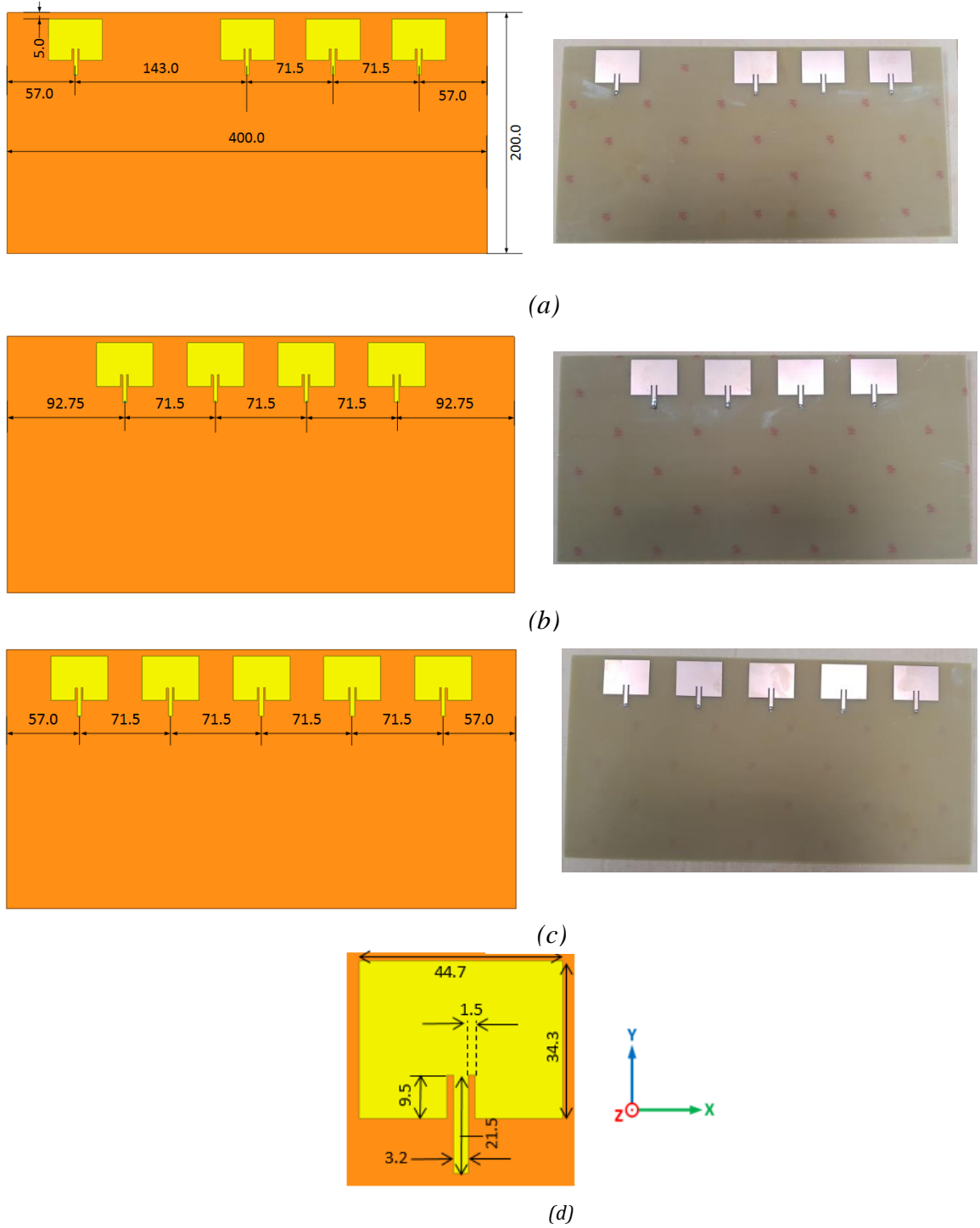
66

(a)

(b)

(c)

(d)

Figure 34 Array geometeries and the fabricated patch-based arrays operating at 2.1 GHz. (a) coprime (b) 4-element ULA (c) 5-element ULA (d) Single patch element, all dimensions are in (mm).
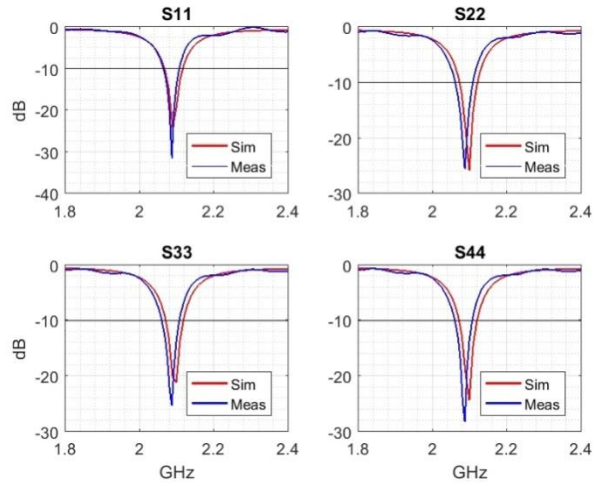
Figure 35 Simulated and measured S parameters for the patch-based CPA at 2.1 GHz.
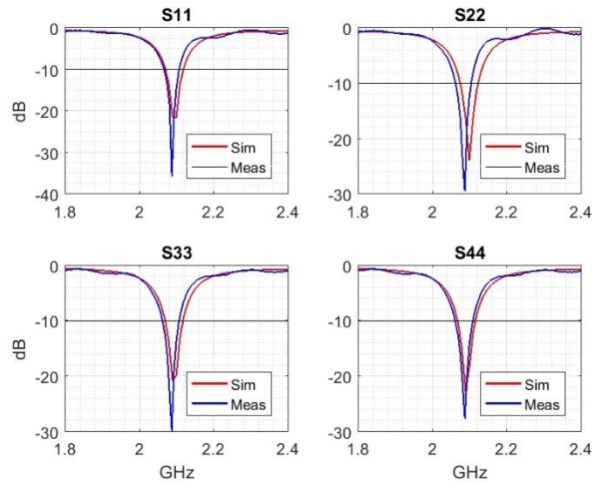

Figure 36 Simulated and measured S parameters for the patch-based 4-element ULA at 2.1 GHz.
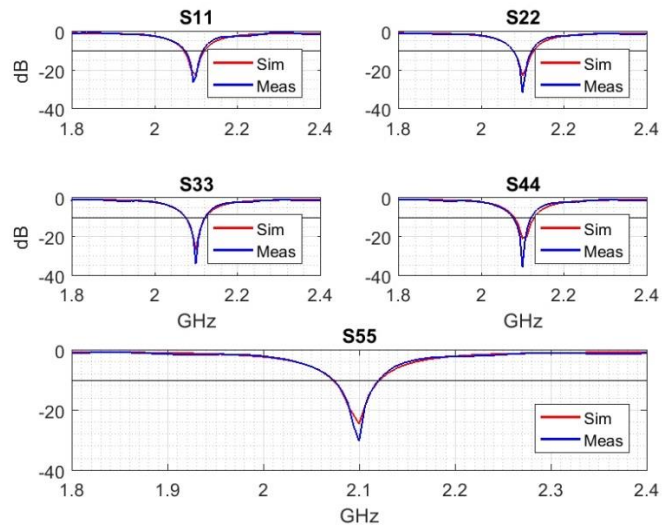
Figure 37 Simulated and measured S parameters for the patch-based 5-element ULA at 2.1 GHz.

The radiation pattern of the antennas in the three arrays resembles the normal patch-based antenna pattern. Figure 38, Figure 39, and Figure 40 show the radiation pattern of the E_ϕ component in the three arrays in the ZX plane.
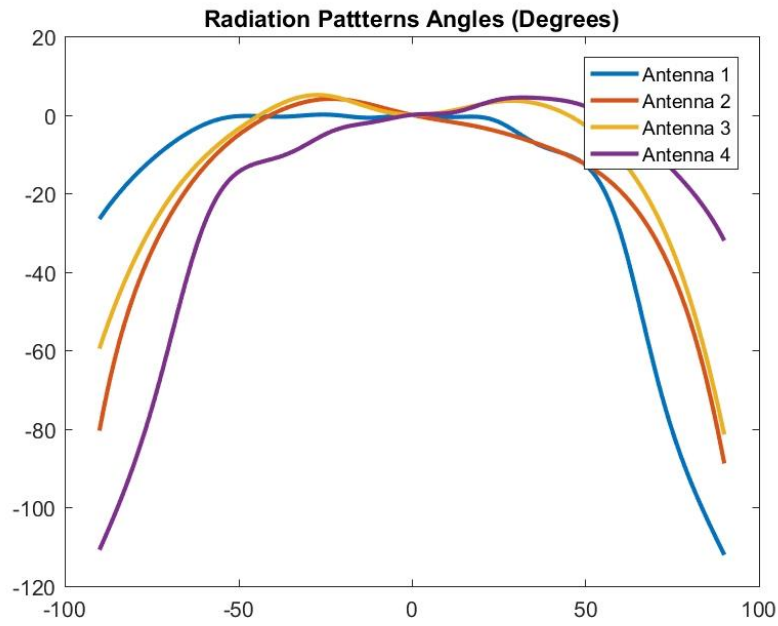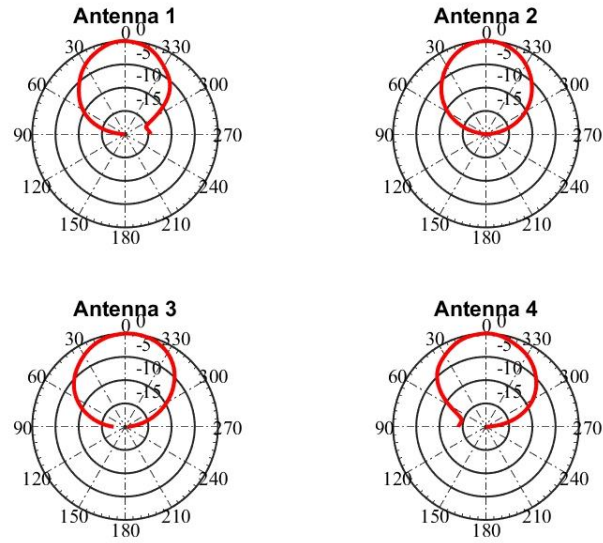
Figure 38 Magnitude and phase of the simulated E_ϕ pattern in ZX plane for the patch-based CPA at 2.1 GHz.
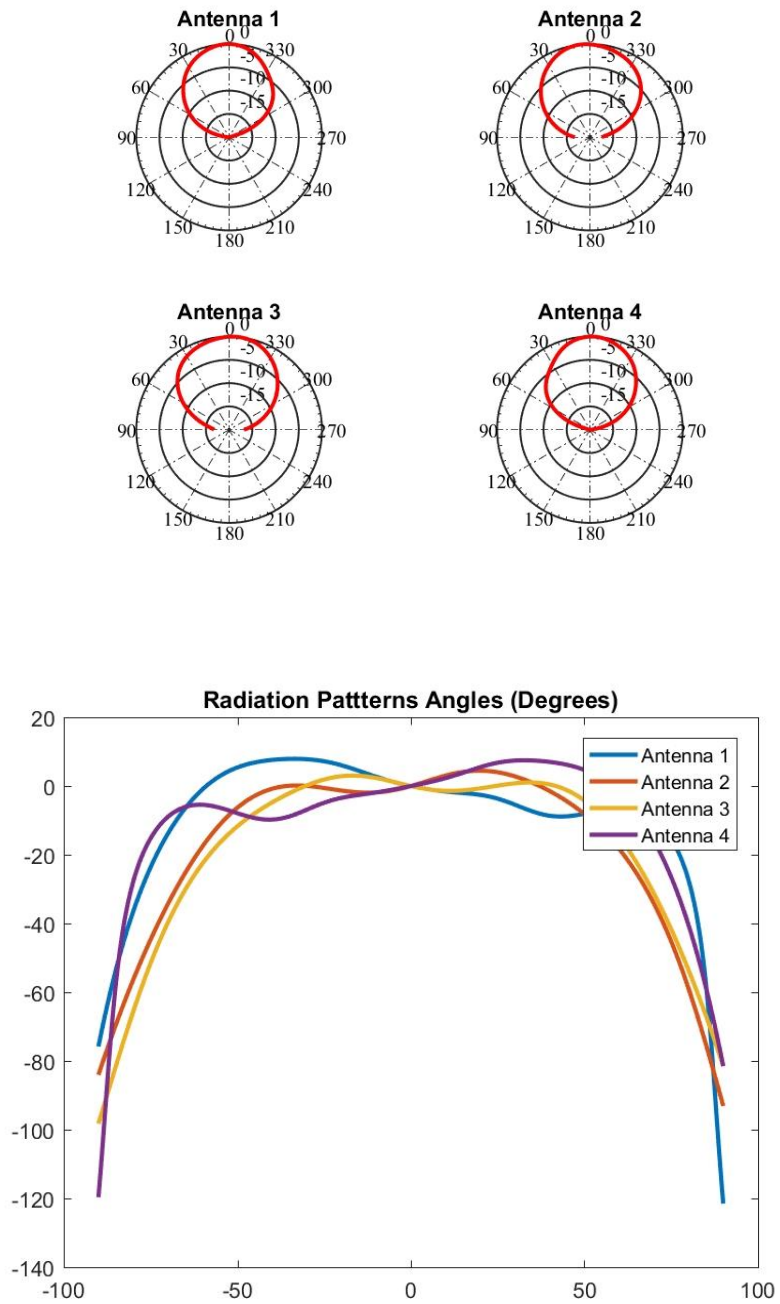
Figure 39 Magnitude and phase of the simulated E_ϕ pattern in ZX plane for the patch-based 4-element ULA at 2.1 GHz.
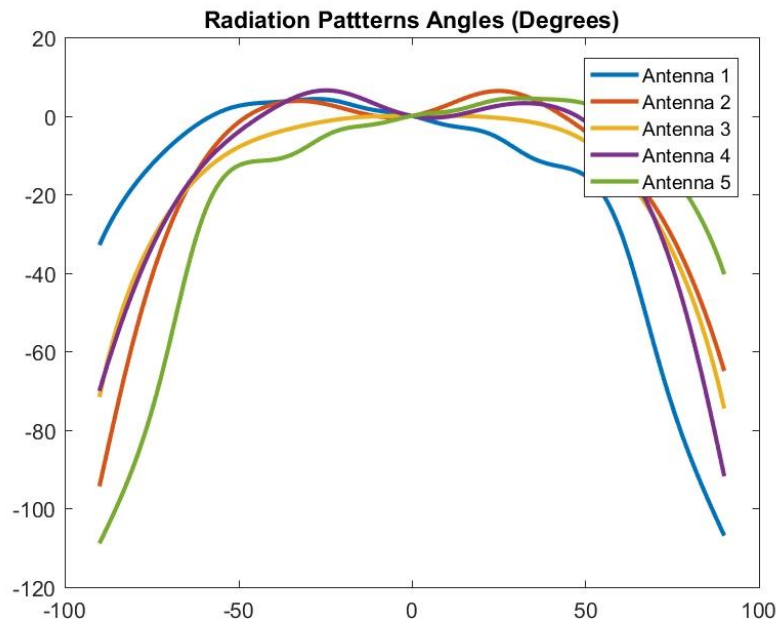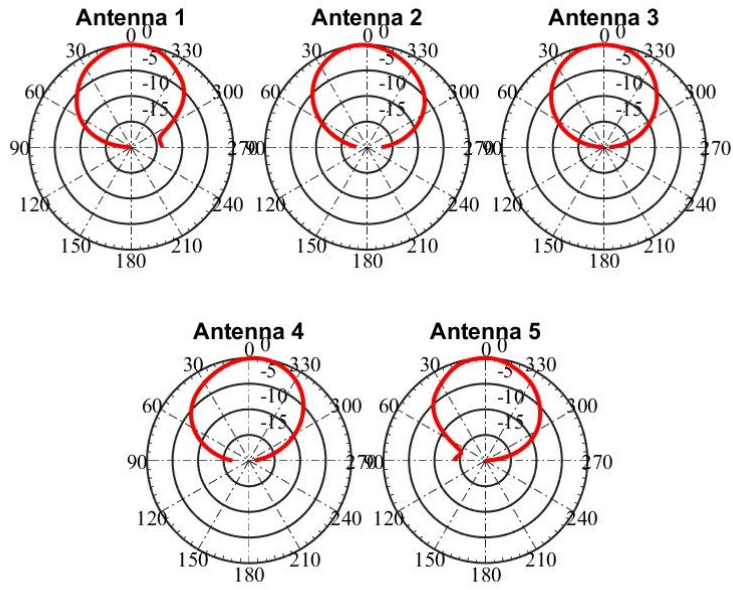
Figure 40 Magnitude and phase of the simulated E_ϕ pattern in ZX plane for the patch-based e-element array at 2.1 GHz.

4.3 Monopole-Based Coprime and ULA Arrays at 2.1 GHz

To fully understand the effect of radiation patterns on DOA estimation, it was required to design antennas with different radiation patterns than the patch. As discussed in the theoretical background, monopoles have omnidirectional patterns and provide a different insight to the effect of the radiation pattern.

Three arrays of printed monopoles were designed to operate at 2.1 GHz like the patch arrays discussed in the previous section. The first array was a CPA with $M = 2, N = 3$, the second was a 4-element ULA and the third was a 5-element ULA. Also, like the patch-based array design process, a single monopole was first designed and optimized and then the arrays were constructed. The optimized monopole length was 28 mm with 3 mm width. Unlike patches, monopoles should not have the ground plane extended beneath them. Therefore, 40 mm of the board width was left without ground. Each monopole was fed through a microstrip line with a certain width and height that transformed the monopole impedance to 50 Ω on its other end. This transformer is then followed by a standard 50 Ω transmission line to the SMA connector. The width and length of the transformer differs from one element to another and from one array to another depending on the mutual coupling. The transformer dimensions were all found via simulations. The three arrays were constructed on 330 mm × 120 mm × 1.6 mm FR-4 boards assuming the dielectric constant to be 4.1. Figure 41 shows detailed dimensions of the arrays. Table 6 lists the dimensions of the transformer elements for all antennas and Figure 42 shows pictures of the three fabricated monopole arrays.

Table 6 Transformer element dimensions for the three monopole arrays.

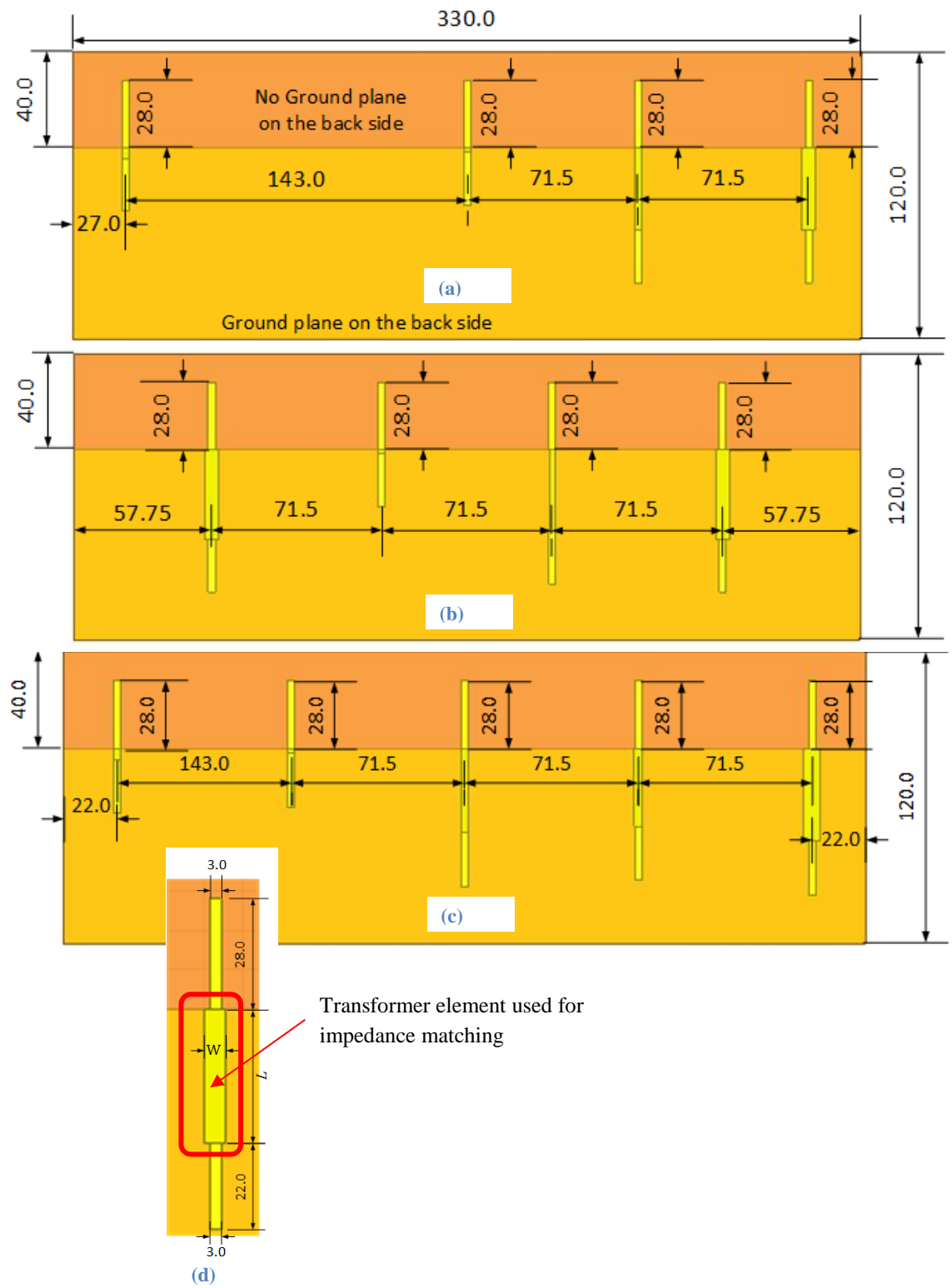|	Antenna Number	W (mm)	L (mm)
Coprime	Antenna 1	2.5	4.5
	Antenna 2	3	2
	Antenna 3	3	34.5
	Antenna 4	5.5	34.5
4-element ULA	Antenna 1	5.5	38
	Antenna 2	3	2
	Antenna 3	2.5	34.5
	Antenna 4	5.5	38
5-element ULA	Antenna 1	2.5	4.5
	Antenna 2	3	2
	Antenna 3	2.5	34.5
	Antenna 4	3.5	32
	Antenna 5	7	38

Figure 41 Design of the monopole arrays (a) coprime (b) 4-element ULA (c) 5-element ULA (d) single monopole element, all dimensions are in (mm).

75
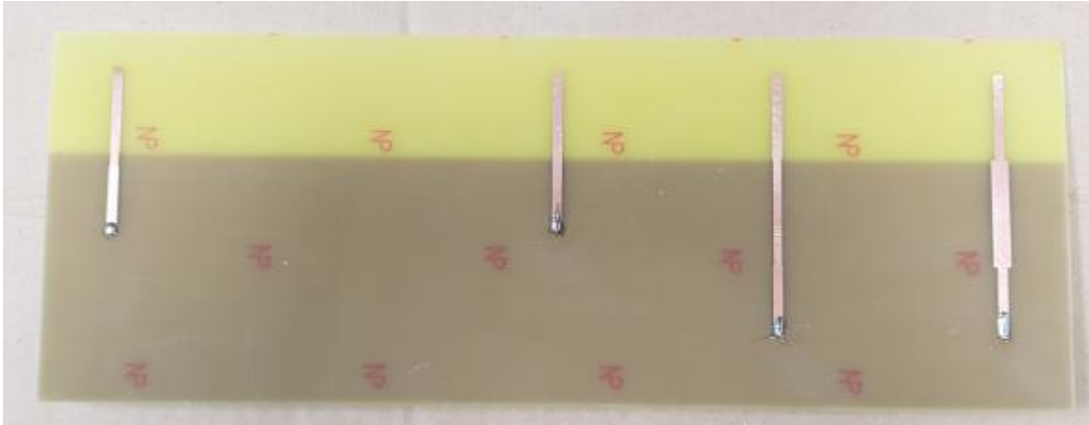
(a)
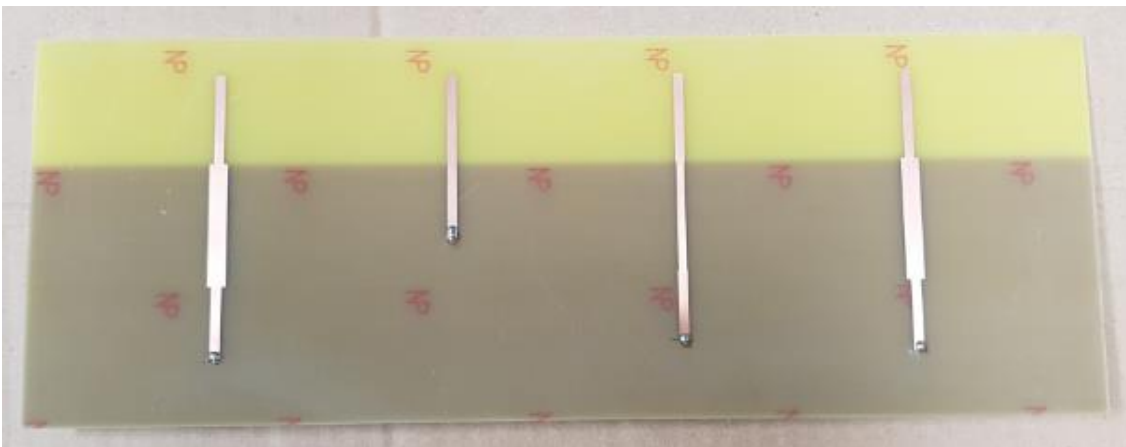
(b)
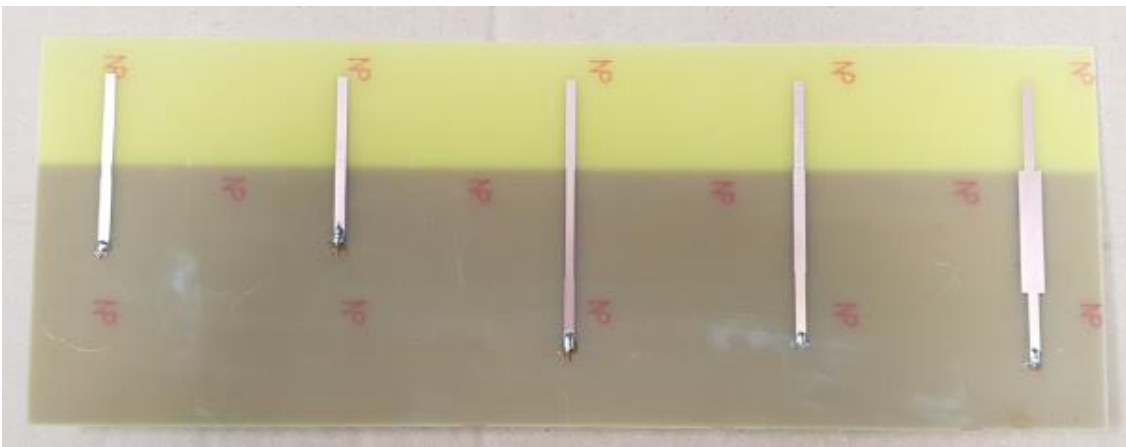
(c)

Figure 42 Pictures of the fabricated monopole arrays (a) coprime (b) 4-element ULA (c) 5-element ULA.

The S-parameters were measured at AMSDL at KFUPM using an Agilent N9918A VNA. Figure 43, Figure 44, and Figure 45 show comparisons between the measured and simulated S-parameters of the coprime, 4-element ULA and 5-element ULA respectively. All antennas had a minimum bandwidth of 180 MHz. The difference between the measured and simulated curves in the figure is most likely due to the fabrication tolerances, as monopoles are more sensitive compared to patches as the current distribution is different. The radiation patterns of E_ϕ for the antennas in the three arrays are shown in Figure 46, Figure 47, and Figure 48. It is noticed that the phase response of E_ϕ is fluctuating unlike that of the previous patch-based arrays. This will have a clear impact on the DOA estimation as will be shown in the next chapter.

Figure 43 Measured and simulated S parameters for the monopole CPA.

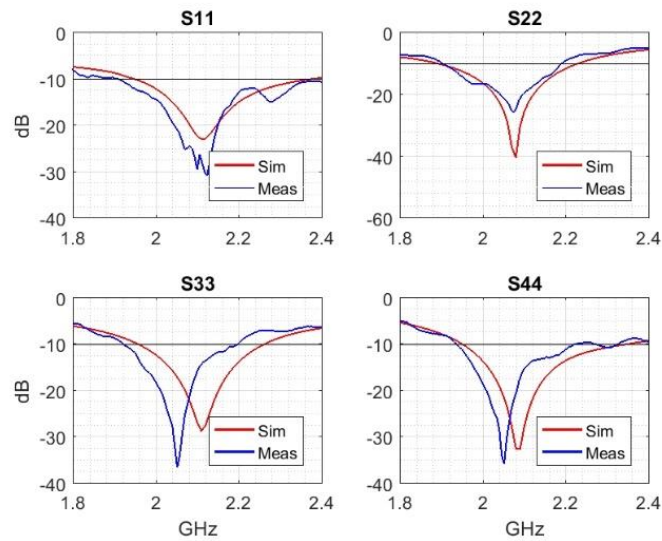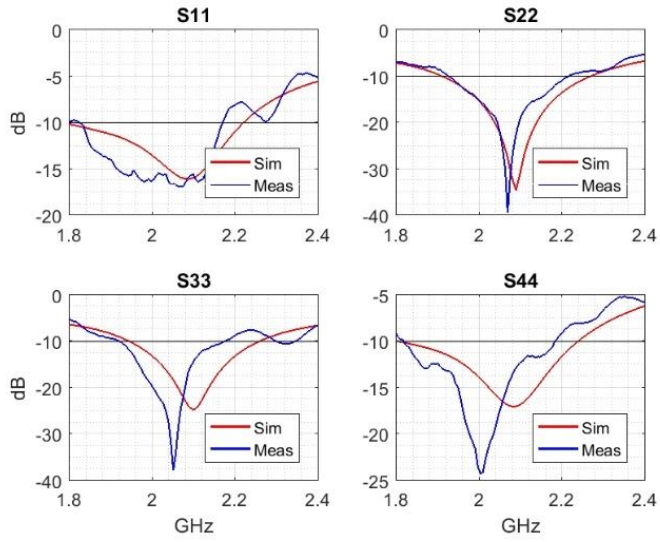**Figure 44 Measured and simulated S parameters for the monopole 4-element ULA.**
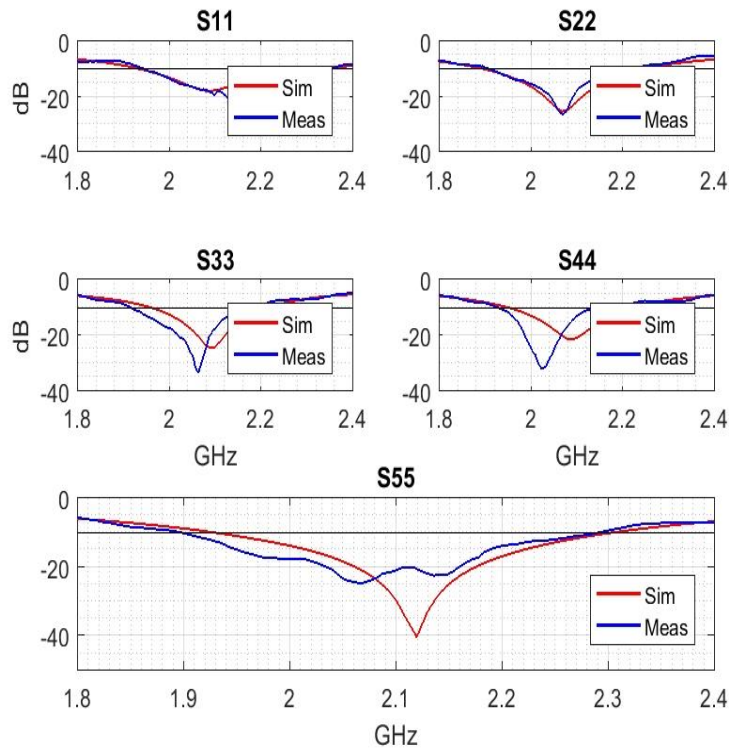
Figure 45 Measured and simulated S parameters for the monopole 5-element ULA.

78
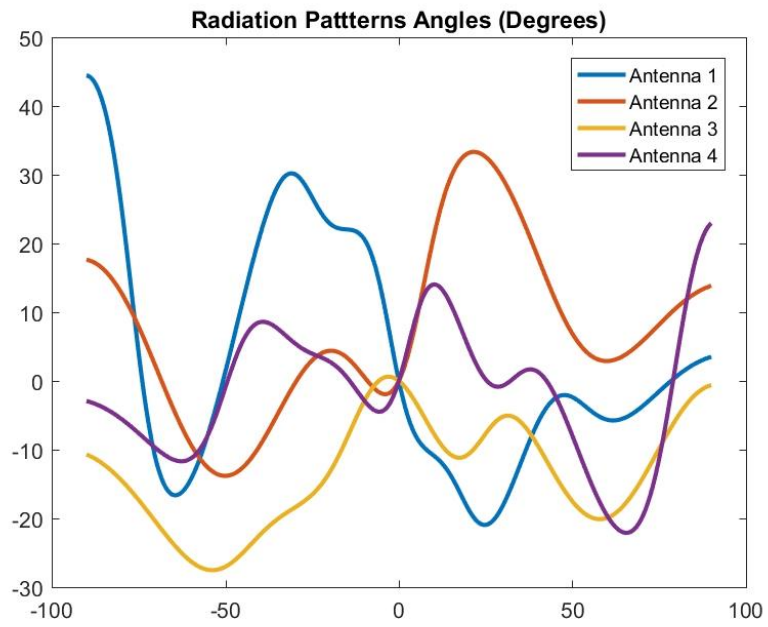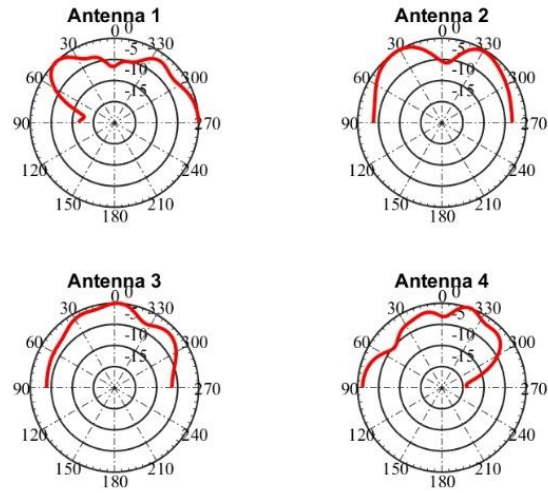
Figure 46 Magnitude and phase of the radiation patterns of E_ϕ for the coprime monopole array in the ZX plane.

Figure 47 Magnitude and phase of the radiation patterns of E_ϕ for the monopole 4-element ULA in the ZX plane.

80
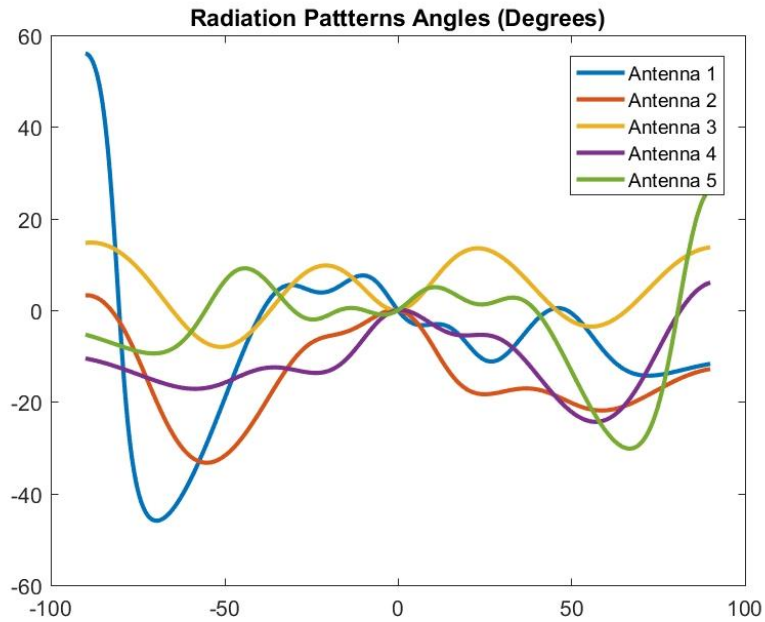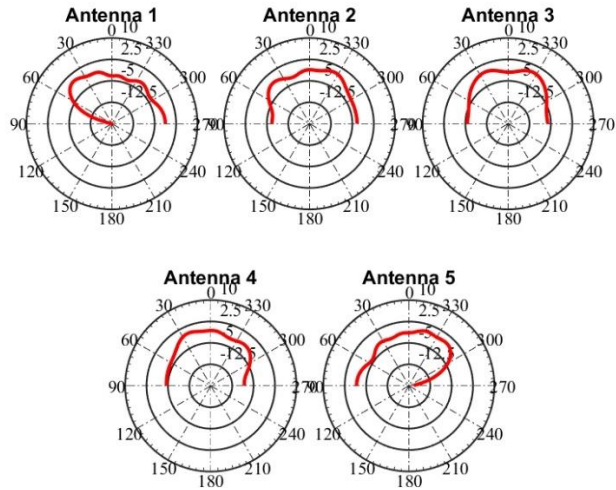
Figure 48 Magnitude and phase of the radiation patterns of E_ϕ for the monopole 5-element ULA in the ZX plane.

4.4   Antennas Polarization

When an EM wave impinges on an antenna, the voltage induced at the antenna terminals depends on the antenna complex radiation response. Therefore, for DOA applications,

when exporting the antenna radiation pattern, it is important to export both magnitude and phase of the radiated electric field $\boldsymbol{E}$.

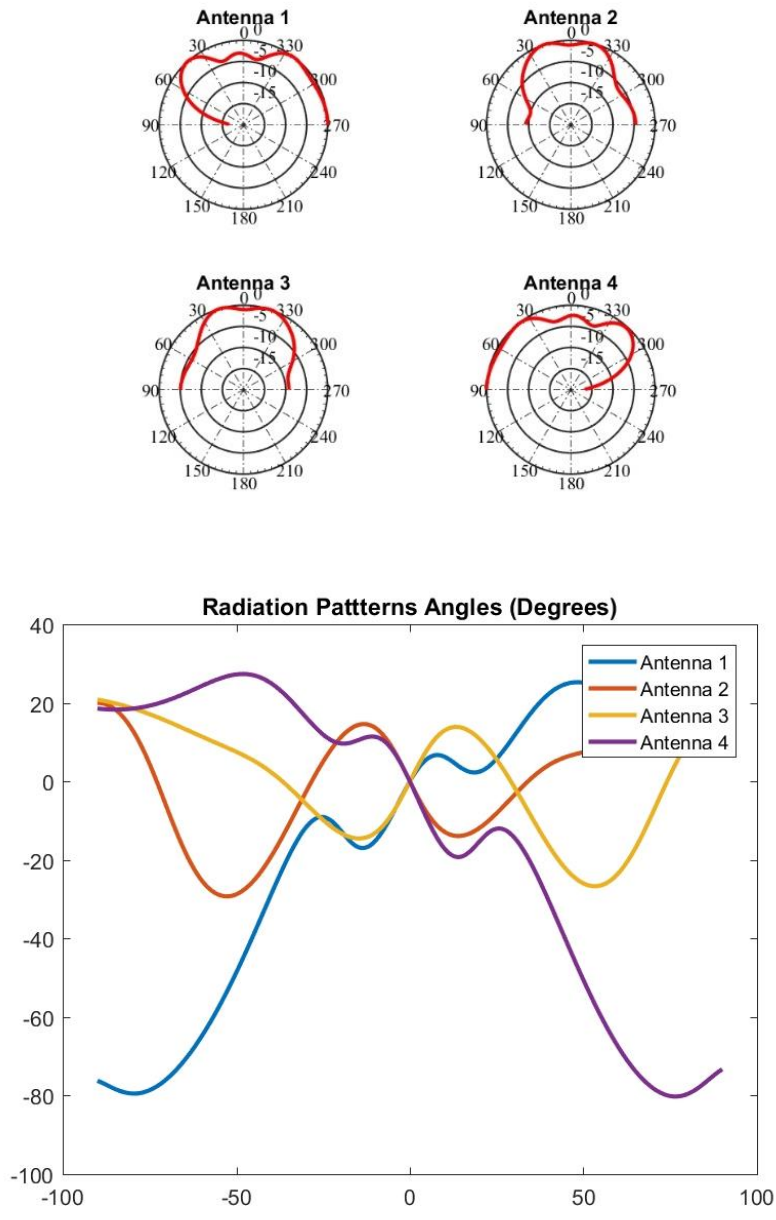When the antenna has a dominant component of the electric field in a certain direction (ϕ or θ), we can use that component of the electric field for DOA simulations. This is true for patch-based antennas. Figure 49 shows E_ϕ and E_θ patterns for antenna 1 in the patch-based CPA shown in Figure 34a. Notice how E_θ is very small compared to E_ϕ, justifying ignoring E_θ and only considering E_ϕ. This is true for all patch antennas in the designed arrays.
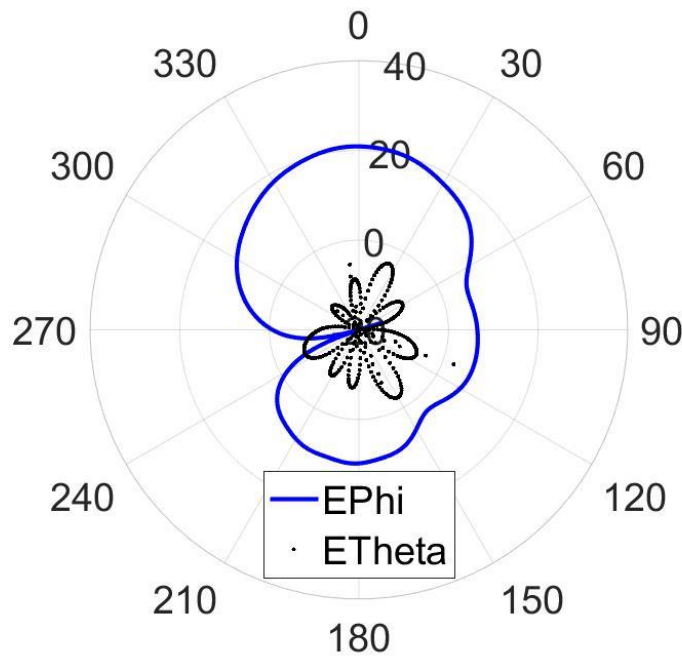
Figure 49 Co-polarization and cross-polarization of patch antenna 1 in the CPA in ZX plane (dB).

The situation for monopole antennas is different. As shown in Figure 50, none of the electric field polarizations (E_ϕ and E_θ) is negligible. We can find the magnitude of the total electric field consisting of E_ϕ and E_θ but not the phase. To solve this problem, we assume that the transmitter antenna, and hence the wave impinging on the array, have a linear

82

polarization in a certain direction and then consider the complex radiation pattern of the electric field in that polarization. Therefore, we assume that the impinging wave is polarized in ϕ direction, consequently, we consider the magnitude and phase of E_ϕ. If the impinging wave has a polarization component in other directions, we expect to have errors in the DOA estimation. As will be shown in the next chapter, this was indeed the case with the monopole-based arrays. Due to the polarization impurity, the separation between experimental and simulated DOA using monopole arrays was higher than the patch-based arrays. Note that this effect only appears in the experiments and not in simulations because simulations assume linearly polarized waves matching the receiver antennas; in practice this might not be the case.
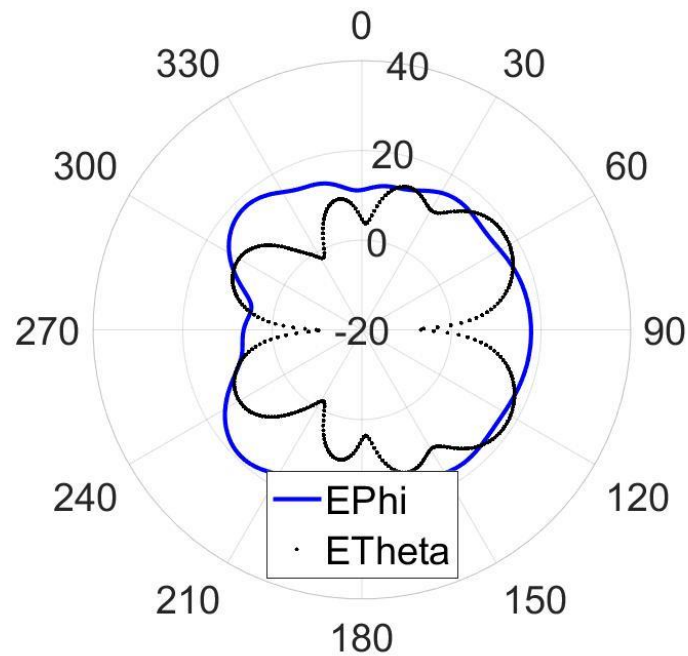
Figure 50 Co-polarization and cross-polarization of monopole antenna 1 in the CPA in ZX plane.

4.5 Summary

In this chapter we presented the design of the antenna arrays that will be used for DOA estimation. A CPA of patches operating at 5.8 GHz was designed, fabricated and measured. Measurements of the S parameters and the radiation patterns were compared with the simulated values and found matching.

Six more arrays were designed to operate at 2.1 GHz. Three arrays were patch-based and three were monopole based allowing testing the impact of different radiation patterns. For each element type (monopole and patch), three arrays were fabricated: coprime with $M = 2, N = 3$, 4-element ULA and 5-element ULA. This enabled us to compare the CPA with a ULA that is either equivalent by the number of antennas or array aperture. The S parameters were measured and found matching the simulated values.

To assess the effect of interelement spacing in a CPA on the DOA estimation performance, 20 patch-based CPAs were modeled and simulated at 5.8 GHz. Each array had a different interelement spacing. The radiation patterns of the arrays were used in the DOA estimation algorithm using CS. The next chapter presents the DOA performance of the fabricated and modeled arrays.

CHAPTER 5

DOA Estimation Results

The previous chapter showed the design details of the different arrays to be used for DOA estimation. The radiation patterns of these arrays were exported from HFSS or obtained from measurements and incorporated in a MATLAB based Monte Carlo simulator. Additionally, laboratory experiments using SDR to measure the DOA performance were carried out using the 2.1 GHz patch and monopole-based arrays. This chapter introduces the simulation and experimental results of the DOA estimation.

Monte Carlo Simulations are run to find the behavior of the RMSE versus SNR and DOA for different array types. For each value of SNR and DOA, 500 independent iterations are run. For the RMSE vs SNR curves, four sources with independent signals are assumed to impinge on the arrays from equally spaced DOA angles between -50° and 50°. RMSE versus DOA curves assume only one source with 20 dB SNR and a DOA angle that varies from -90° to 90°. Two thousand snap shots are used to calculate covariance matrix in each iteration. Estimation using CPAs utilized a CS algorithm using Lasso with 0.85 penalty parameter. Estimation for the ULAs used the standard MUSIC algorithm.

5.1 DOA Simulation for Coprime Patch-based Array at 5.8 GHz

Three sets of simulations were run: one assuming isotropic receivers, another using the simulated radiation patterns and a third using the measured radiation pattern.

Figure 51 shows the comparison of the simulated RMSE versus SNR for the patches (simulated and measured patterns) and isotropic cases. Since the used RMSE formula ignores the missed DOAs, another plot showing the missed DOA is also provided to fully characterize the estimation error. The first observation is, unsurprisingly, the RMSE decreases monotonically with increased SNR and so does the number of missed pluses. In general, the DOA estimation error using the measured radiation pattern is higher than the simulated one, but the difference is less than a degree.

The difference between the RMSE with isotropic arrays and that of patch-based arrays represents the extra error added due to the physical antennas. At low SNR, this error is masked by the high estimation error due to the noise. Therefore, it is more pronounced at high SNR. With the simulated radiation pattern, the maximum isotropic to patch error is $0.59°$ at -7 dB SNR, and the average is $0.27°$. With the measured radiation pattern, the maximum is $0.98°$ at 4 dB SNR and the average is $0.51°$.

Figure 51 shows that DOA estimation using the simulated and measured radiation patterns was more accurate than the isotropic case around zero SNR which is counterintuitive. The search matrix employed by the algorithm used a DOA increment of $2°$ which is the resolution of the measured radiation pattern. It is believed that at this relatively high step size, the difference in DOA performance between the isotropic and the simulated radiation pattern is not clear enough.

(a)   (b)
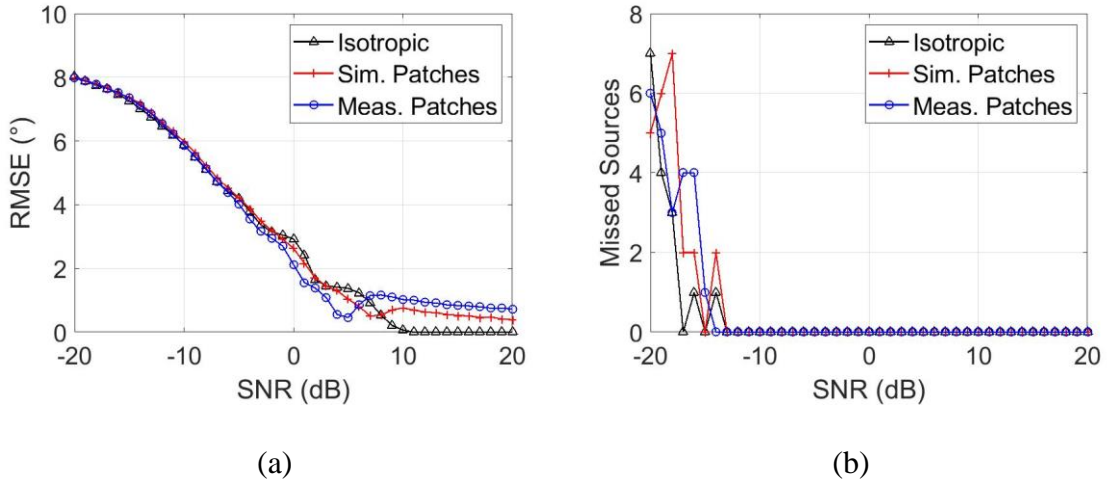
Figure 51 (a) RMSE (°) and (b) number of missed DOAs versus SNR (dB) for the isotropic antennas and patches considering both simulated and measured patterns with 2° step size in the DOA search matrix.

The radiation pattern of the patch antennas suggests that waves impinging the array from angles beyond -60° to 60° suffer high attenuation. To study the effect of this on DOA estimation, another set of simulations were carried out at fixed SNR=20 dB and varying DOA. This time, one source was assumed with DOA angle varying from -90° to 90°. The results are shown in Figure 52. Note that between DOA angles of -80° and 80°, the number of missed sources is zero and DOA estimation is possible albeit with high error. Depending on the error tolerance in the application, the range of DOAs that can be detected by this patch-based array can be as large as -80° to 80°. Excellent quality estimation can be achieved between -50° and 50°. The maximum error introduced by utilizing patch antennas versus isotropic is 5.72° and 7.64° using the simulated and measured radiation patterns, respectively.
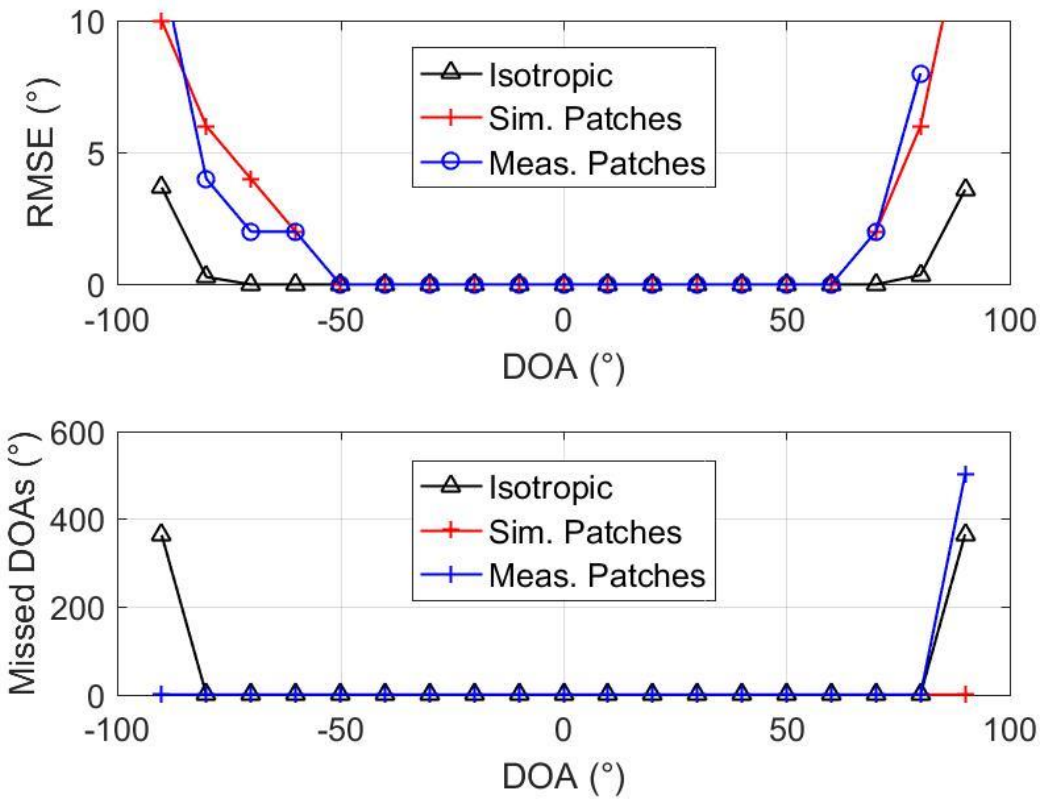
Figure 52 RMSE (°) **versus DOA** (°) **for one source using isotropic and patch antennas with the simulated radiation pattern and patch antennas with the measured radiation pattern.**

So far, the fundamental spacing in the designed CPA was 0.5λ. This is the maximum possible spacing that prevents spatial aliasing. It might be desirable in some applications to reduce the total size of the array. One way to achieve this is by reducing the interelement spacing of the array. To test the effect of this spacing on the performance of the DOA estimation, the radiation patterns of 20 CPAs were extracted from HFSS in the same way the previous pattern was extracted. The arrays were designed to work at 5.8 GHz and are like the array introduced in the first section of the chapter. Each array had a different fundamental spacing. The analyzed spacings ranged from 0.31λ to 0.5λ. MATLAB was then used to simulate the performance of DOA estimation for each array and the results are shown in Figure 53.

The first observation is that reasonable DOA estimation accuracy can be achieved with RMSE of 2.6° using a patch-based CPA with fundamental element spacing of only 0.31λ. This is a new result that was not investigated in any of the reviewed work. As the spacing increases, the isotropic RMSE drops. This is expected since higher DOA estimation accuracy is achieved with larger array apertures. Conversely, the RMSE curve of the patch-based array increases with increased spacing up to 0.36λ where it starts decreasing. To investigate this behavior, we look at the phase response of the antenna elements of the array at different spacing. Since the estimation algorithm generally depends on the phase difference of the received signals between antenna pairs, caused by the DOA of the wave and the antenna location, we expect to see higher estimation error when the antennas introduce higher phase shift. Figure 54, Figure 55, and Figure 56 show the phase response of the antenna elements at 0.31λ, 0.36λ, and 0.5λ spacing, respectively. Note that the relative phases (i.e. phase difference between antenna pairs) is higher in Figure 55 with 0.36λ than Figure 54 with 0.31λ. As an example, the average phase difference between antennas 3 and 4 at 0.31λ is 18.8°, while it is 26.5° at 0.36λ and 5.4° at 0.5λ.
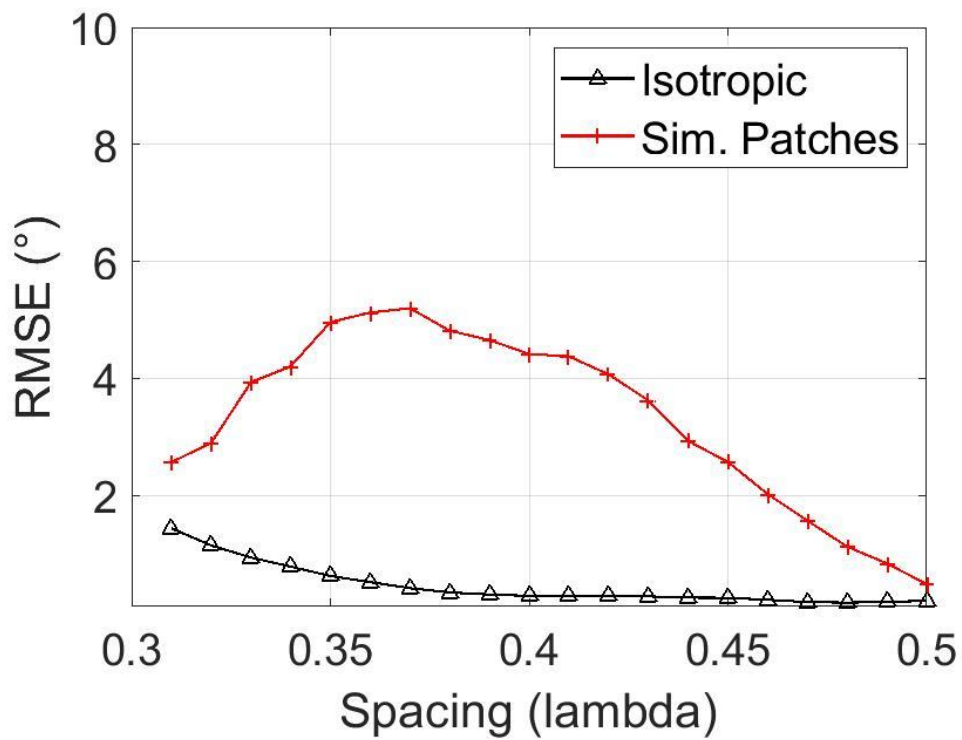
Figure 53 RMSE versus fundamental spacing for CPA of patches.
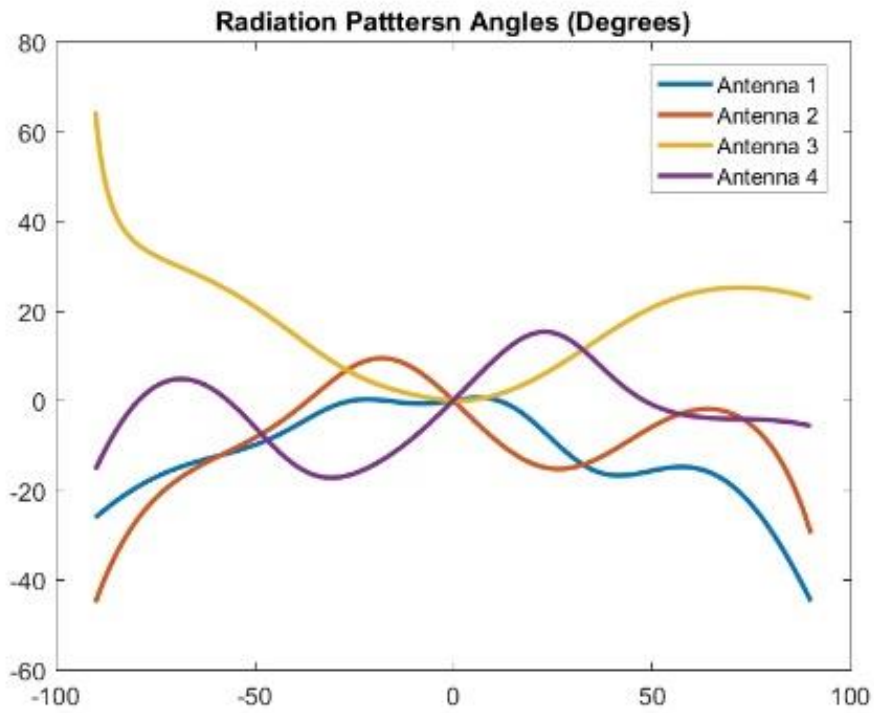

Figure 54 Phase response for the patch-based CPA operating at 5.8 GHz at 0.31λ spacing
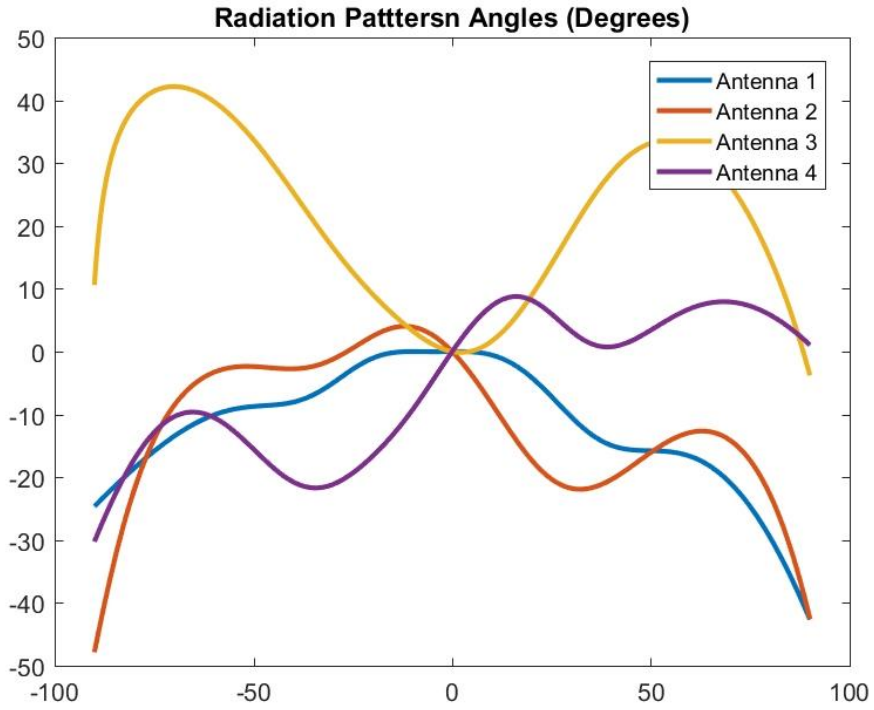
90

Figure 55 Phase response for the patch-based CPA operating at 5.8 GHz at 0.36λ spacing
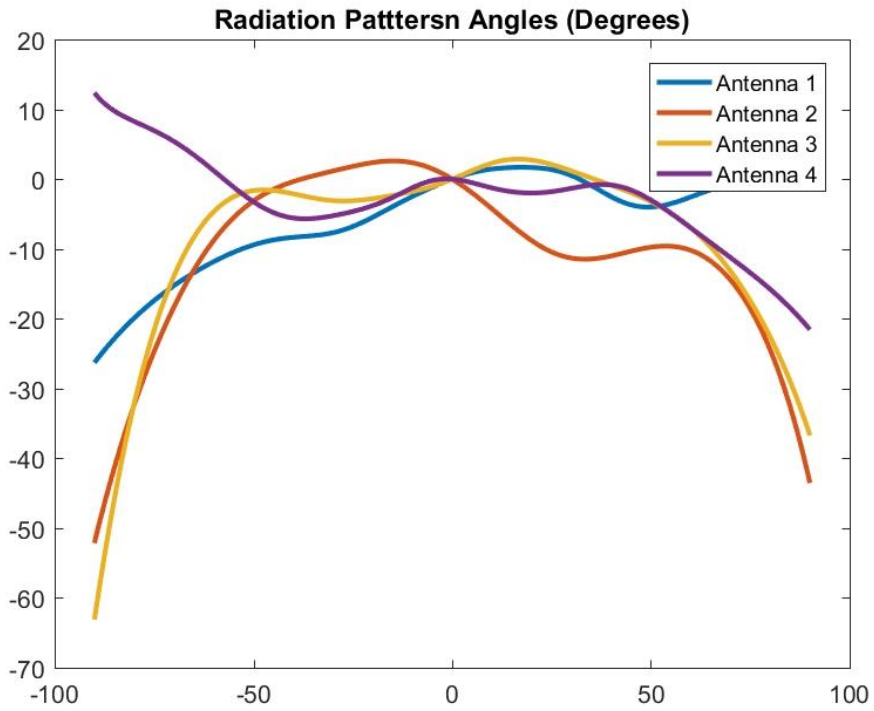

Figure 56 Phase response for the patch-based CPA operating at 5.8 GHz at 0.5λ spacing

5.2 DOA Simulation for Patch-based and Monopole-based Arrays at 2.1 GHz

Similar analysis is performed at 2.1 GHz. The radiation patterns of the six arrays working at 2.1 GHz are extracted and used in DOA estimation simulation. The six arrays are:

1. Patch-based CPA with $M = 2, N = 3$

2. Patch-based 4-element ULA

3. Patch-based 5-element ULA

4. Monopole-based CPA with $M = 2, N = 3$

5. Monopole-based 4-element ULA

6. Monopole-based 5-element ULA

Another simulation set using a CPA of isotropic antennas is also performed to provide a benchmark.

Figure 57 presents the RMSE and missed sources for the CPA and 5-element ULA patch-based arrays, comparing them to the isotropic CPA as a bench mark. The 5-element ULA has the same aperture as the CPA. Below 5 dB SNR, the 5-element ULA shows many missed sources. Above 5 dB, the CPA of patches, with its 4 elements, has less error than the 5 element ULA. At 20 dB SNR, the RMSE for the CPA was 0.75°, compared with 1.08° for the 5-element ULA. This demonstrates the advantage of CPAs where fewer antennas, arranged in a coprime configuration, can achieve more accurate DOA estimation.

The average error introduced due to the utilization of physical antennas rather than isotropic in a CPA is 0.34°.
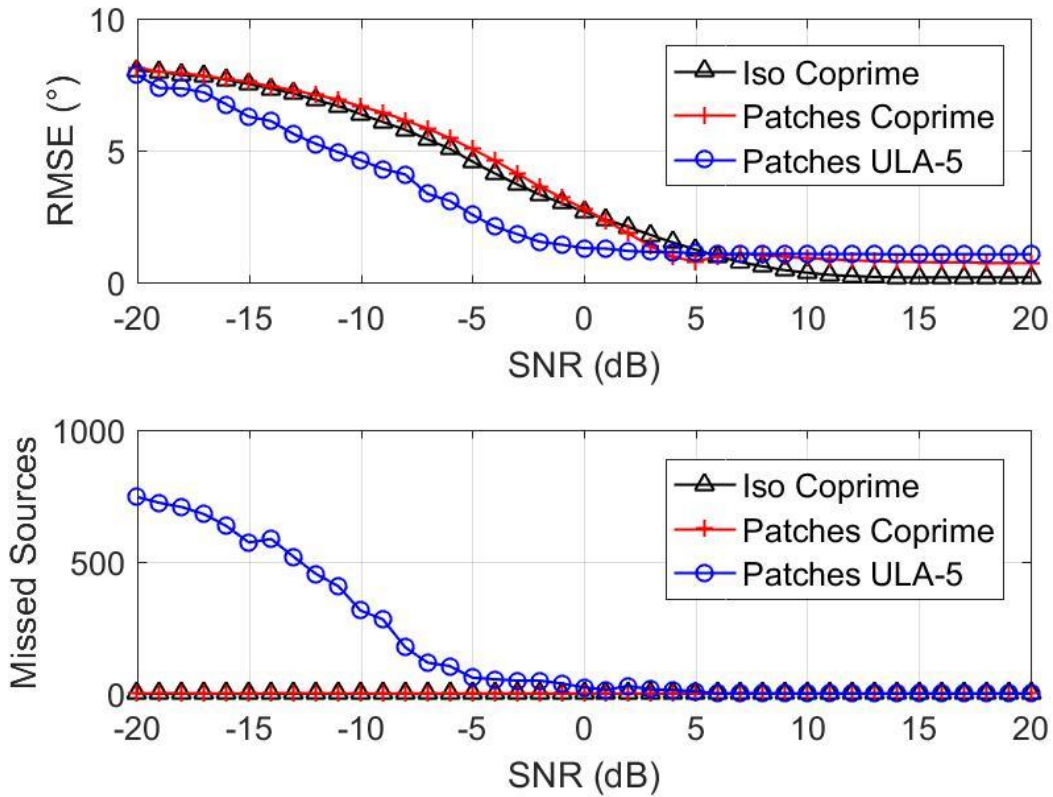
Figure 57 RMSE (°) and missed sources versus SNR for four sources impinging a CPA of isotropic and patch antennas and a 5 element ULA of patch antennas.

Furthermore, using the patch-based arrays, we compare the DOA estimation accuracy between the 4-element CPA and a ULA with the same number of elements. For a 4-element ULA, the maximum number of detectable sources is only 3. Figure 58 shows the comparison in RMSE and missed sources between the 4-element CPA of patches when 4 sources impinge on it versus that of a 4-element ULA when only 3 sources imping on it. Both scenarios have comparable performance at high SNR, with the CPA having an RMSE of 0.75° and the 4-element ULA having an RMSE of 0.79°, confirming the previous

conclusion that simply re-arranging the array elements in a coprime configuration increases the degrees of freedom and hence estimation accuracy.
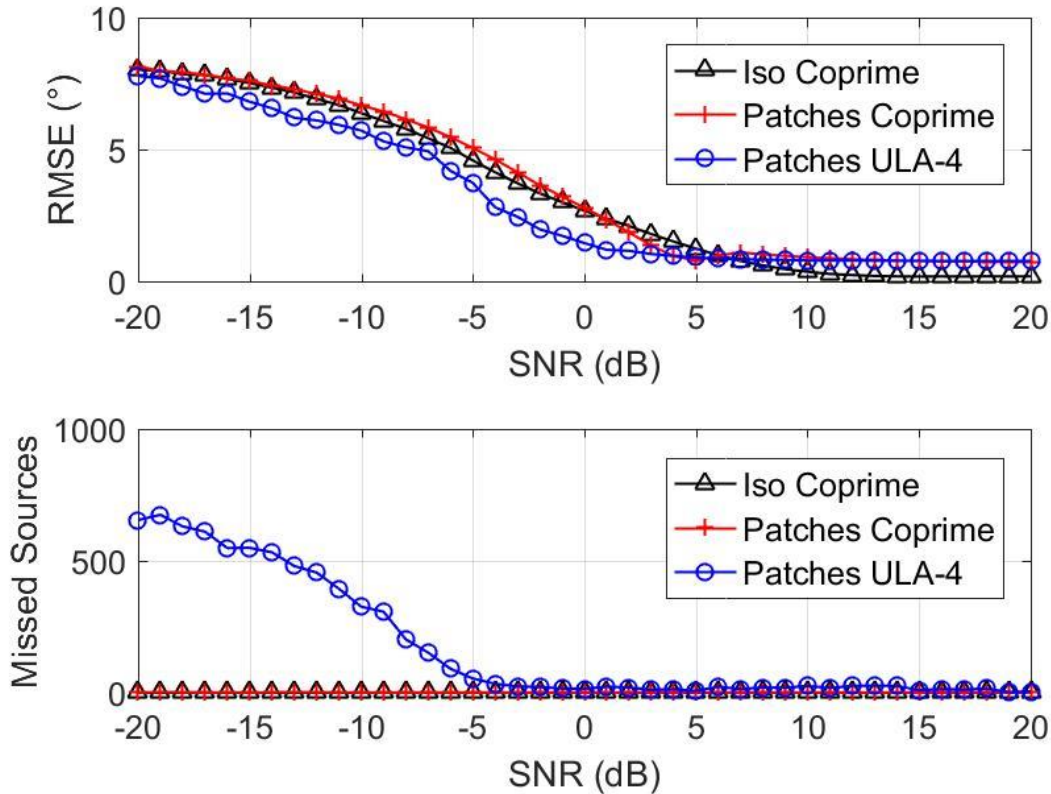
Estimation accuracy versus DOA is examined by running simulations using one impinging source at 20 dB SNR with varying DOA from -90° to 90°. This is presented in Figure 59. The maximum error introduced due to the patch antennas over isotropic is 14.89° at a DOA of -70°. Both 4-element and 5-element ULAs detect all the sources (zero missed sources) between DOAs of -70° and 70°. However, the 4-element CPA has a narrower range of zero missed sources, namely from -60° to 60°. Therefore, while a 4-element CPA has comparable performance versus SNR to the 5-element ULA, ULAs can detect wider ranges of DOAs. Another point to notice here is that while the RMSE in the coprime and 5-element

94

ULA decrease monotonically as the DOA angle approaches zero, the 4-element ULA exhibits a peak in the RMSE around ±50° before it starts to decrease again around zero. This behavior, which is also confirmed in the experiments as will be shown, is most probably due to the phase of the radiation pattern of the array. Looking at Figure 39 which shows the magnitude and phase of the radiation patterns for the array, the maximum separation of the phase curves among the antenna elements occurs around ±50°, supporting this explanation. Since the DOA algorithms depend heavily on the relative phases of the received signals at the individual antennas, and since the phase shift introduced by the physical antennas is not accounted for in the algorithm, the greater the separation in the phase response of the antennas, the greater the introduced error.
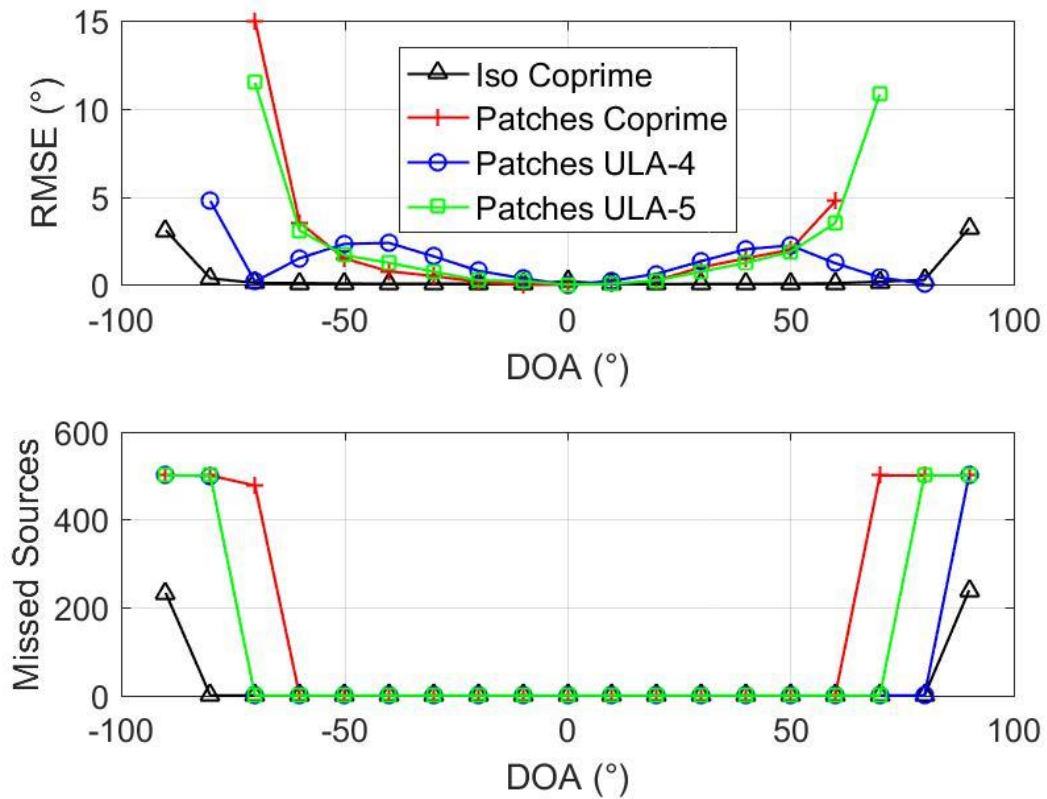
Figure 59 RMSE (°) and missed sources versus DOA for one source at 20 dB SNR impinging a CPA of isotropic and patch antennas, and 4 and 5 element ULA of patch antennas.

95

Figure 60 shows the RMSE and missed sources for the monopole-based arrays. The 5-element ULA misses a large number of sources at low SNR similar to the patches array. Above 8 dB SNR, both arrays have comparable accuracies. An average error of 0.62° is found between the isotropic and the monopole CPAs. At 20 dB SNR, the CPA had an RMSE of 0.64° versus 1.19° for the 5-element ULA. This demonstrates the same conclusion reached with the patch-based arrays: a 4-element CPA has the same or better DOA accuracy than a 5-element ULA regardless of the type of the antenna element.

Similar to what was introduced with patch-based antennas, we can compare the performance of a monopole-based CPA with that of a 4-element ULA of monopoles, comparing coprime with a ULA of the same number of elements. Figure 61 shows that a 4-element ULA of monopoles, impinged by 3 sources, has an minimum RMSE of 7.87° at 20 dB SNR while that of a CPA impinged by 4 sources is around 0.64° only, confirming the previous conclusion that CPAs have better estimation accuracy than their uniform counterparts.

Figure 60 RMSE (°) and missed sources versus SNR for four sources impinging a CPA of isotropic and monopole antennas and a 5 element ULA of monopole antennas.
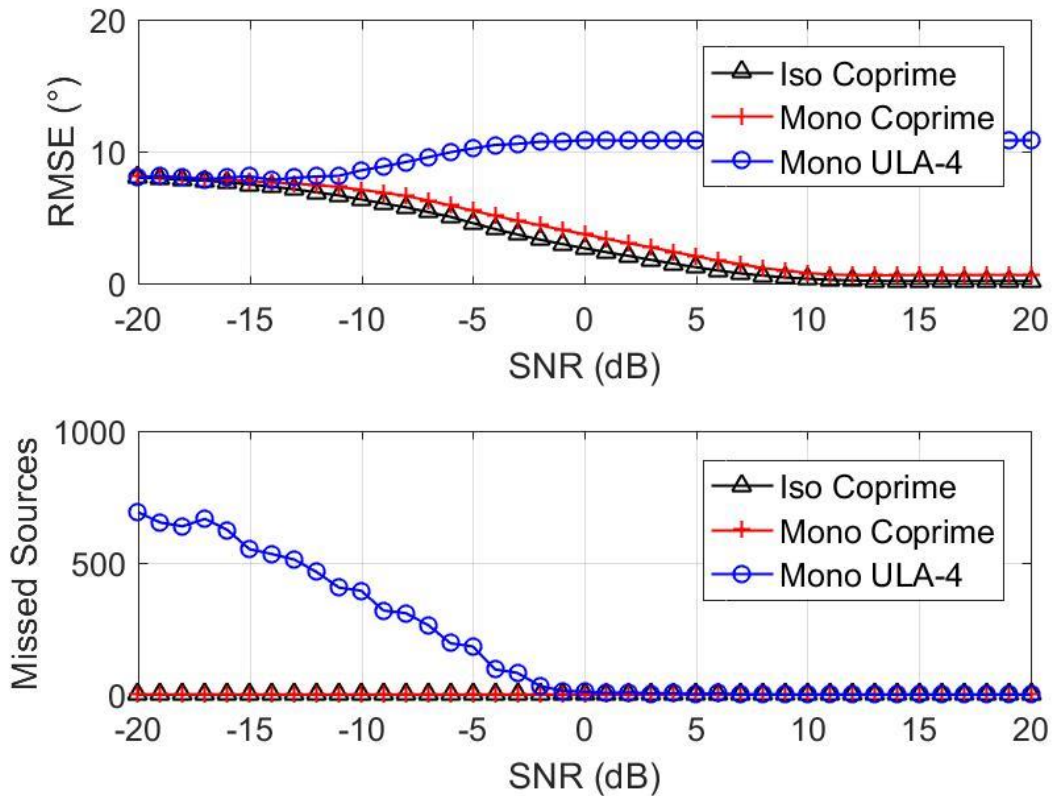
Figure 61 RMSE (°) and missed sources versus SNR for four sources impinging a CPA of isotropic and monopole antennas and three sources impinging a 4 element ULA of monopole antennas.

DOA estimation performance versus DOA angle for monopole-based arrays is introduced in Figure 62. The figure shows that monopole-based arrays, both CPA and ULA, are more sensitive to the DOA than patch-based arrays. This could be a result of the fluctuating phase response of the arrays of monopoles (see Figure 46) compared to that of the patches (see Figure 38). The large difference in phase response among the individual array elements in a monopole array "tricks" the DOA algorithm into detecting the impinging signal at a different angle. The maximum error introduced by the monopole antenna over isotropic is 5.25° occurring around -90° DOA.
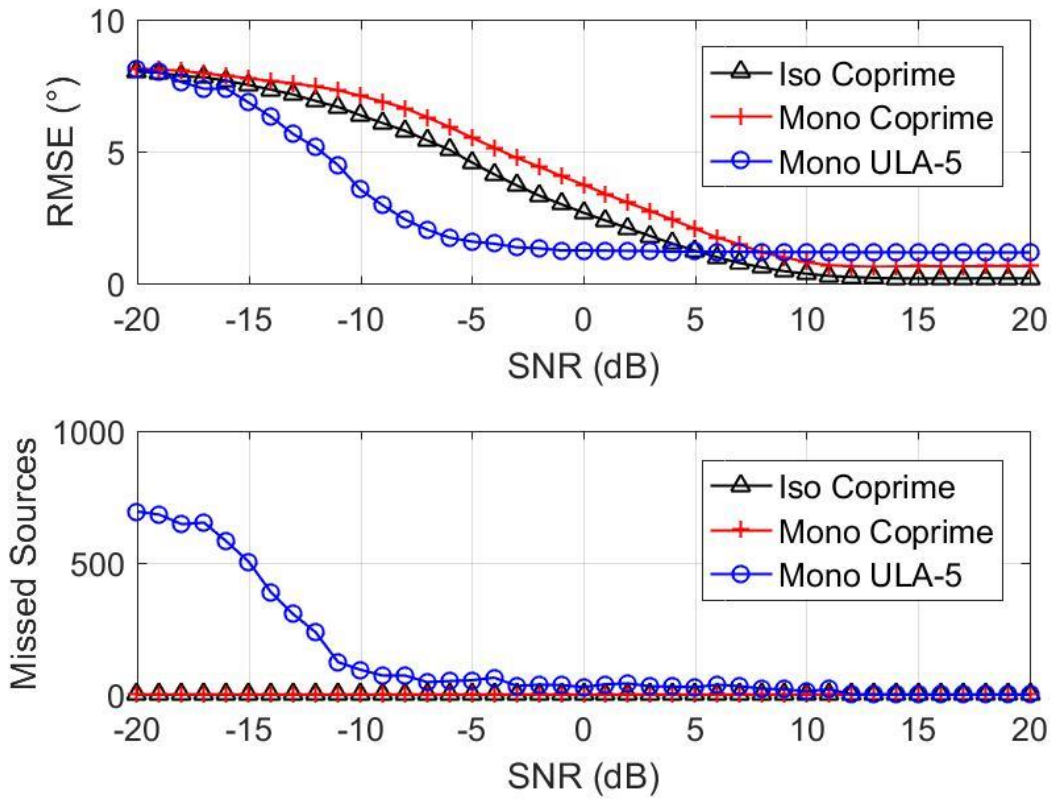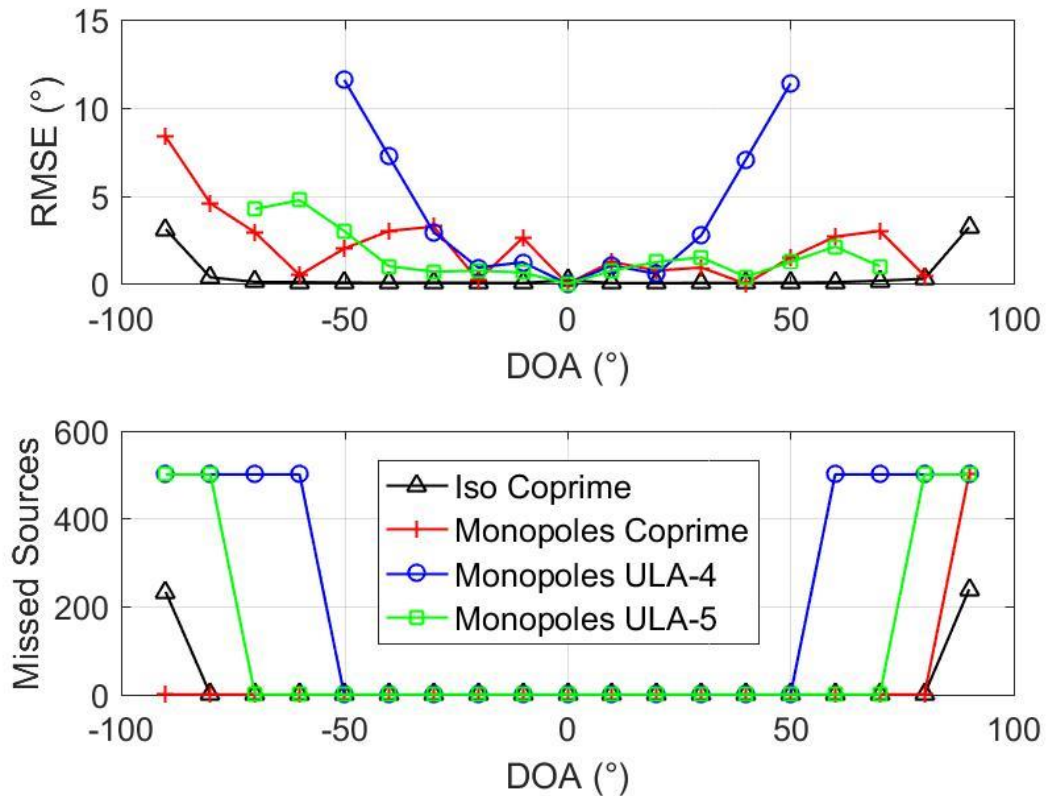
Figure 62 RMSE (°) and missed sources versus DOA for one source at 20 dB SNR impinging a CPA of isotropic and monopole antennas and a 5 element ULA of monopole antennas.

Having demonstrated the advantage of the CPA configuration in DOA applications, it may be of interest to focus on the effect of the antenna elements on the estimation accuracy. For this purpose, we plot the RMSE and missed sources for patch-based and monopole-based CPAs in Figure 63. Both antenna types have virtually zero missed sources throughout the entire SNR range. The patch-based array has better performance at low SNR probably due to the higher directivity of the antennas. At high SNR, both array types have similar performance.
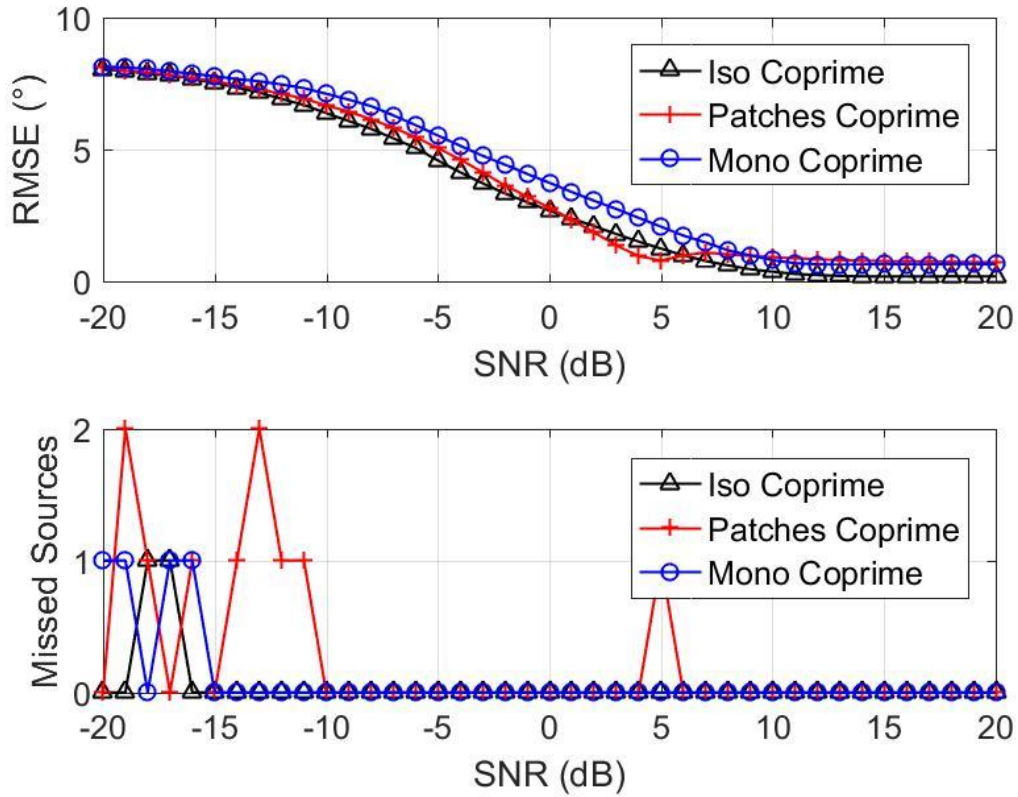
Figure 63 RMSE (°) and missed sources versus SNR for four sources impinging a CPA of isotropic, patch and monopole antennas.

5.3   Experimental Results

Experiments to estimate the DOA using the six arrays operating at 2.1 GHz were carried out at the Telecommunications Research Lab (TRL) at KFUPM using software defined radio (SDR). The setup included multiple universal software radio peripherals (USRP-2950R), each connected to two antenna elements in the array via its receiver ports. A synchronization device, called NI-OctoClock-G CDA-2990, is used to ensure synchronization between the multiple USRPs. The transmitter antennas are connected to the transmitter ports of another USRP, which is in turn connected to the synchronization device. The block diagram of SDR environment setup is depicted in Figure 64.

100
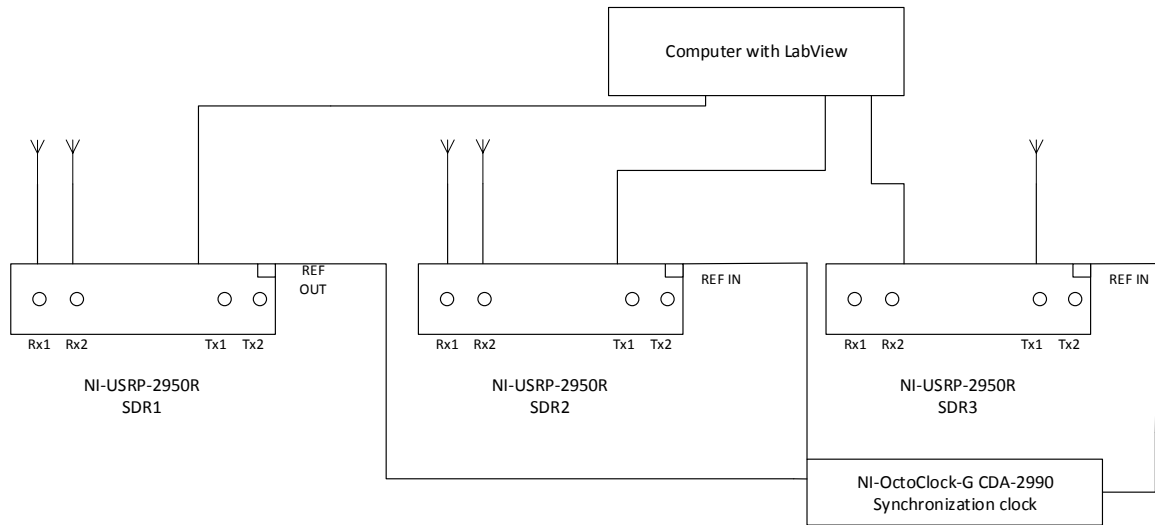
Figure 64 Bock diagram of the SDR experimental setup

The estimation algorithms were implemented in LabView environment; MUSIC was used for ULAs and CS for CPAs. Whenever the system is restarted, the phase of the received signals is calibrated at $0°$ DOA. The distance between the transmitter and receiver antennas was kept above $1.5\ m$ to satisfy the far-field assumption and both receivers and transmitters were $1\ m$ above the ground. Experiments were performed indoor and outdoor to examine the effect of multipath on the detection accuracy. Figure 65 shows the indoor experiment setup and Figure 66 shows the outdoor setup.

In the following sections, the RMSE curves of the experimental results are compared against those of the simulation results. The purpose of this comparison is to verify the utilized simulation model. As will be shown, the experimental results follow the same trend of the simulations with some variations mainly due to multipath.

Figure 65 Indoor experiment setup at TRL in KFUPM.

Figure 66 Outdoor experiment setup.

In the first set of experiments, the six arrays were tested with one transmitter located at various DOA angles ranging between -53° to 53°. At each angle, the RMSE is calculated

from three measurements. The following figures present the experimental results along with the results of the simulations run in the previous section for comparison.

Figure 67, Figure 68, and Figure 69 present the results for the CPA, 4-element ULA and 5-element ULA of patch antennas, respectively. The figures show reasonable match between the simulations and the experiments where the RMSE is high beyond ±50° for the coprime and 5-element ULA. For the 4-element ULA, the experimental results show a peak in RMSE around ±50° due to the phase radiation pattern of the array as mentioned earlier. The maximum difference between simulated and experimental error was 9.75° at -53° DOA for the coprime, 11.08° at -53° DOA for the 4-element ULA, and 9.06° at -53° DOA for the 5-element ULA. The average difference was 2.87°, 2.11°, and 3.15° for the coprime, 4-element ULA, and 5-element ULA, respectively.

Figure 67 Experimental results versus simulation for the CPA of patches using one transmitter at varying DOA.

Figure 68 Experimental results versus simulation for the 4-element ULA of patches using one transmitter at varying DOA.

Figure 69 Experimental results versus simulation for the 5-element ULA of patches using one transmitter at varying DOA.

The results for the monopole arrays are presented in Figure 70, Figure 71, and Figure 72 for the coprime, 4-element ULA and 5-element ULA respectively. Like the patches arrays, there is reasonable match between experimental and simulated estimations. The sensitivity of monopole arrays to DOA that was noticed in the simulations is confirmed experimentally. The maximum difference between simulated and experimental error was 6.06° at -49° DOA for the coprime, 3.37° at -49° DOA for the 4-element ULA, and 7.7° at -53° DOA for the 5-element ULA. The average difference was 1.23°, 1.59°, and 1.39° for the coprime, 4-element ULA, and 5-element ULA, respectively.
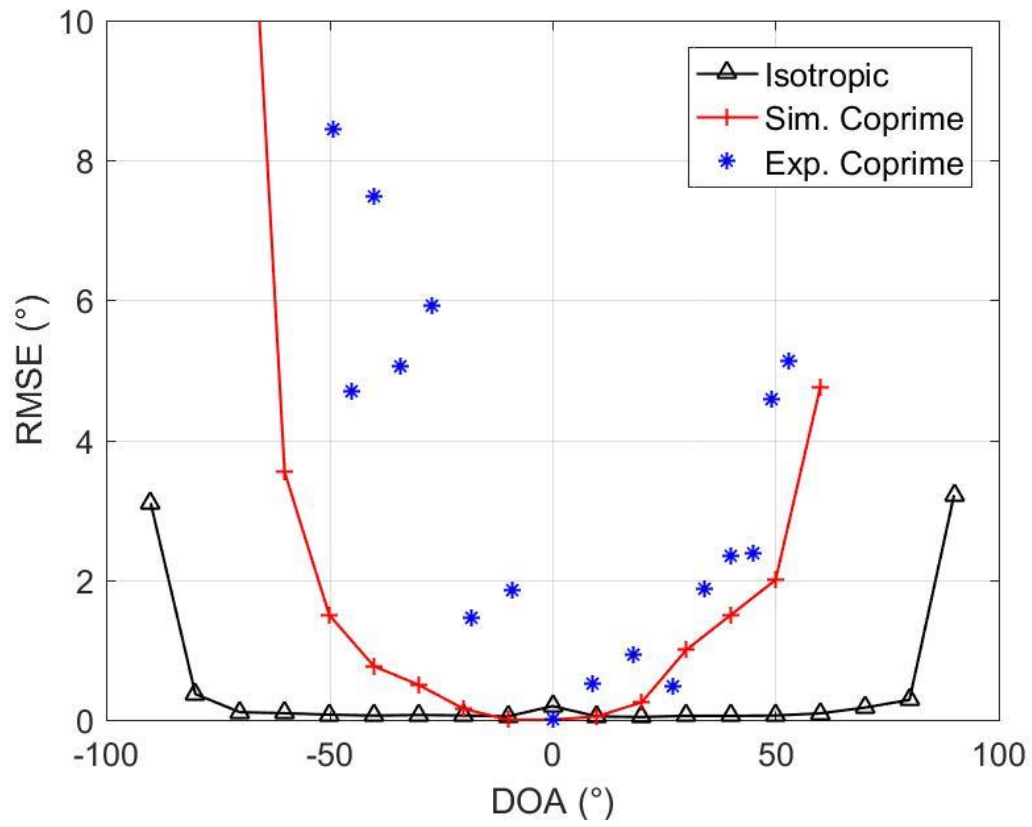
106
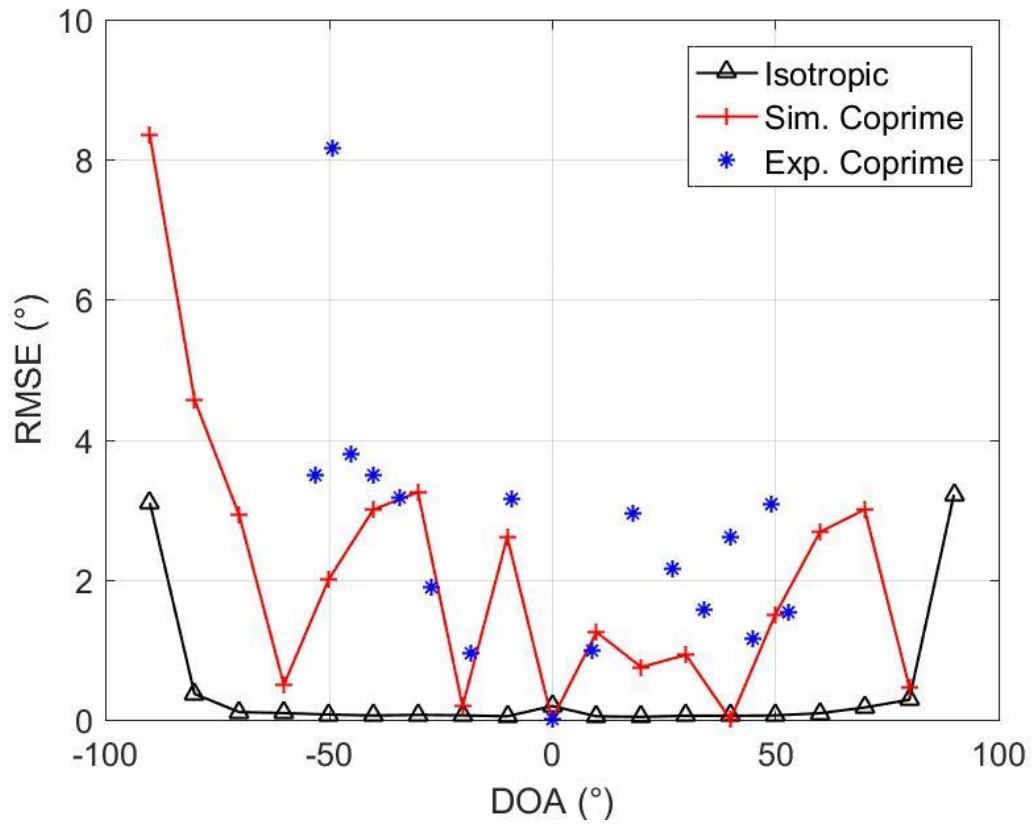
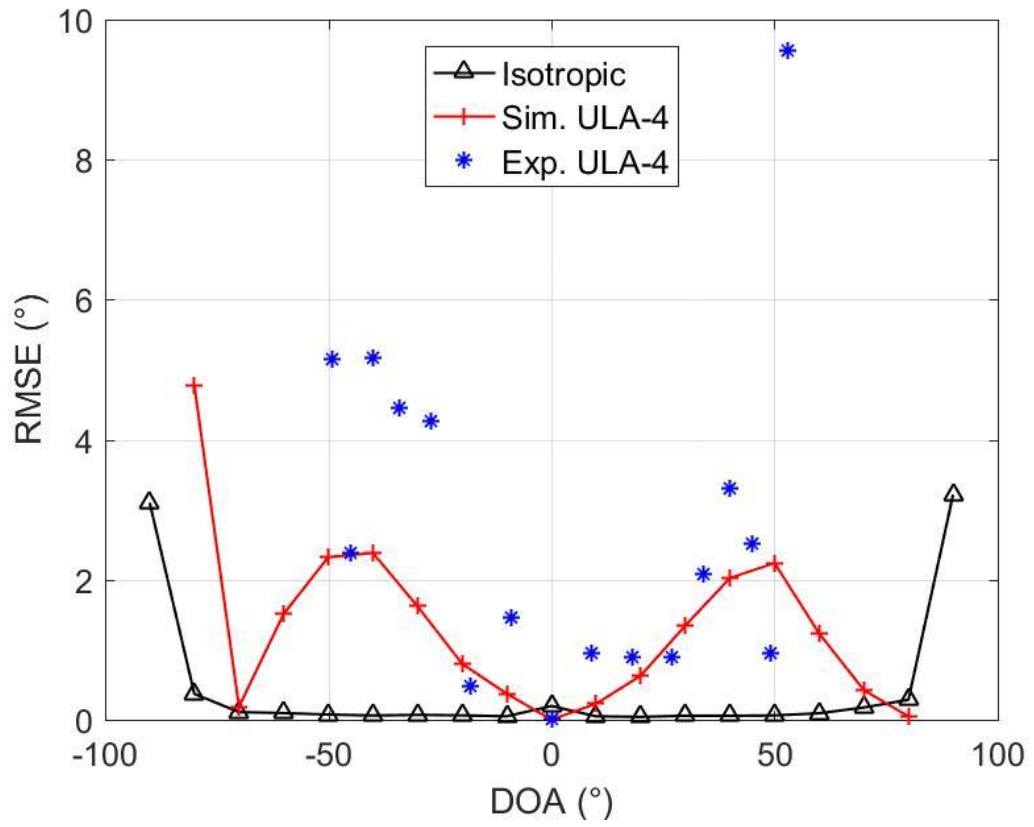**Figure 70 Experimental results versus simulation for the CPA of monopoles using one transmitter at varying DOA.**

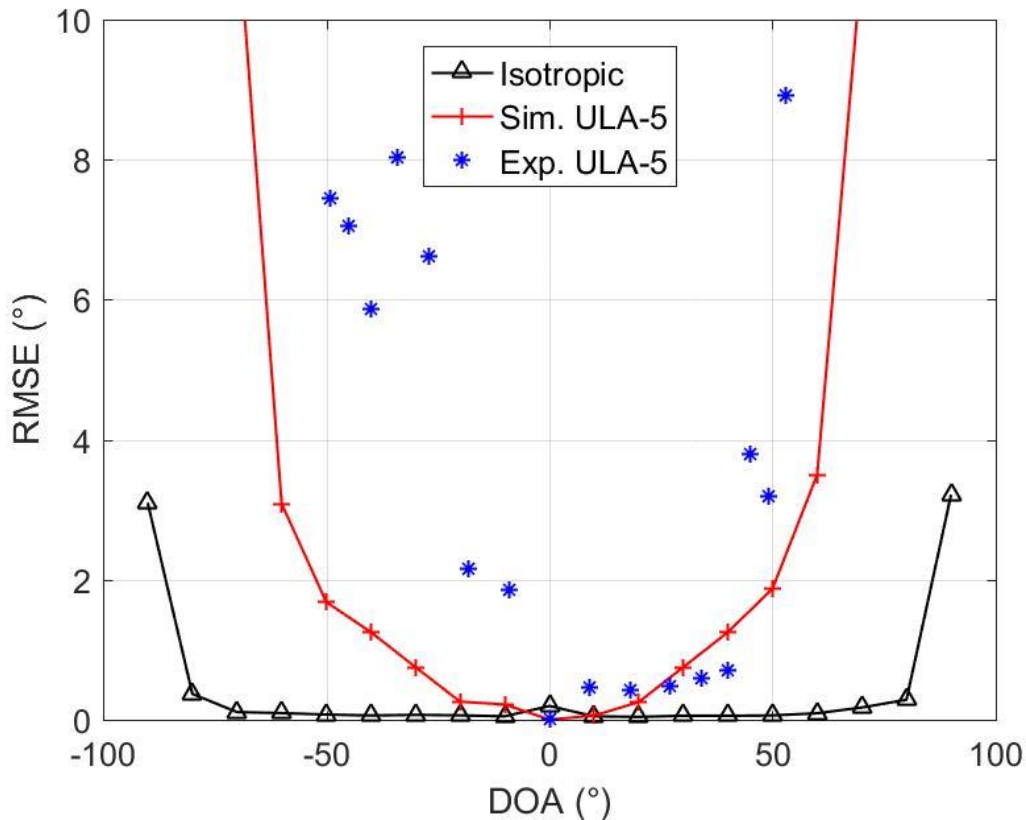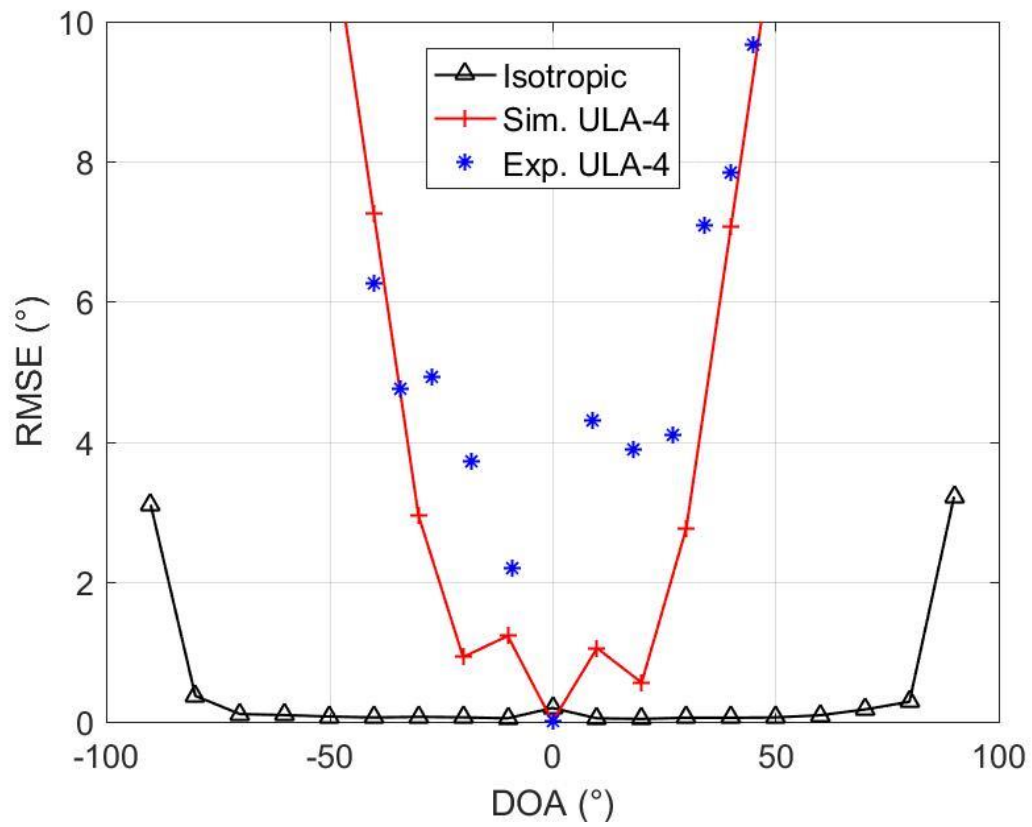**Figure 71 Experimental results versus simulation for the 4-element ULA of monopoles using one transmitter at varying DOA.**
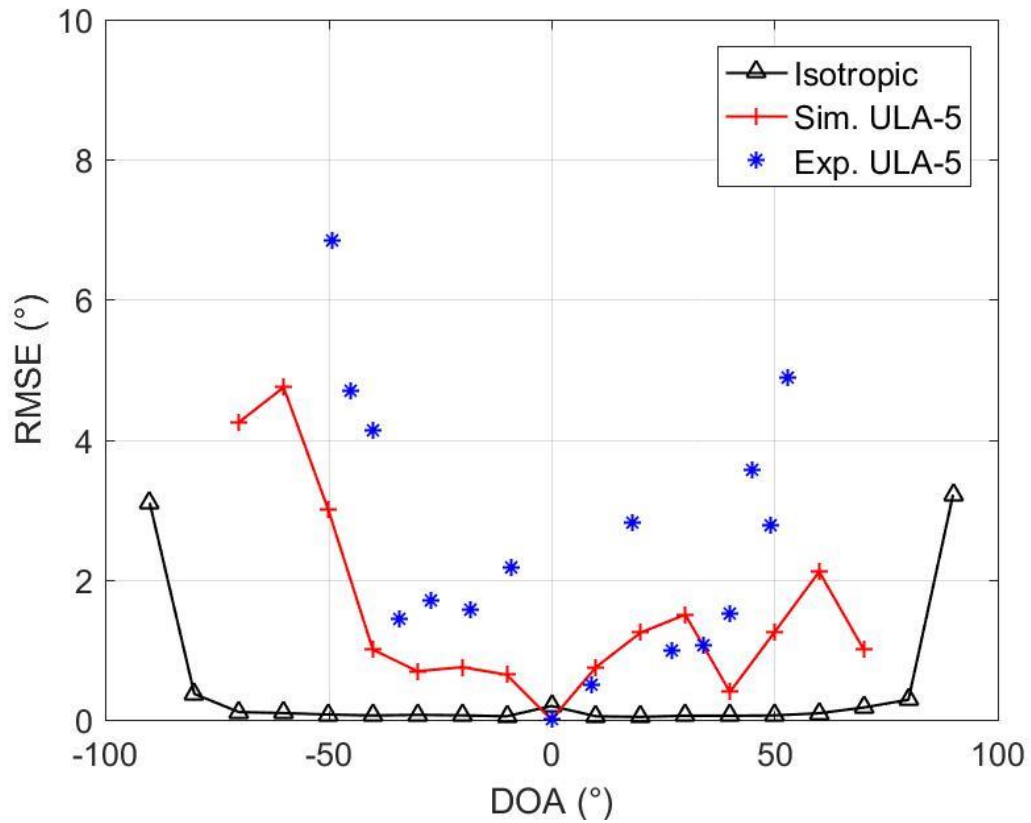
Figure 72 Experimental results versus simulation for the 5-element ULA of Monopoles using one transmitter at varying DOA.

Since the indoor environment suffers more from multipath, experiments were also carried out outdoor using the patch-based CPAs for comparison. Figure 73 presents the results of both indoor and outdoor experiments. The maximum difference between indoor and outdoor RMSE was 7.37° at -53° DOA, and the average difference was 1.54°, suggesting that multipath effect is roughly the same indoor and outdoor.
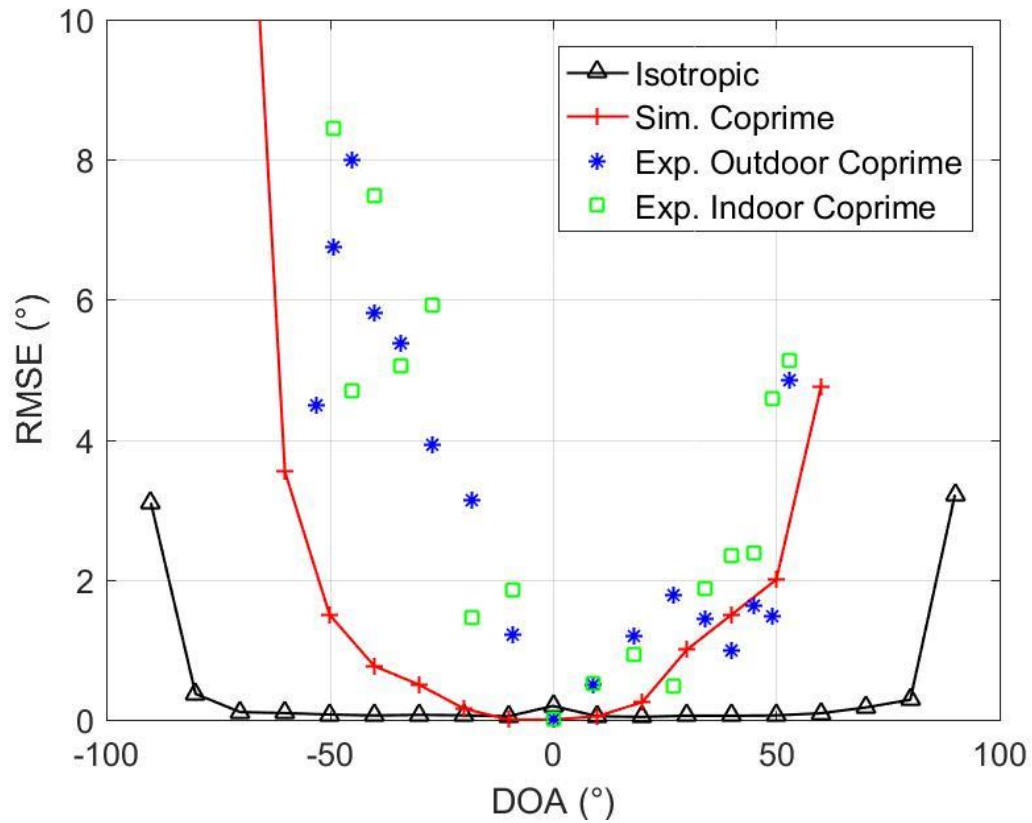
Figure 73 Experimental results versus simulation for the coprime patch arrays indoor and outdoor versus DOA angle.

Another set of experiments were carried out indoor using 2 transmitters simultaneously. The transmitters were placed at 9 different positions as in Table 7. To provide a bench mark for comparison, simulations were run using two transmitters to match the experiment.

110

Position	TX1 Angle (degree)	TX2 Angle (degree)
1	-45	45
2	-40	40
3	-35	35
4	-30	30
5	-25	25
6	-20	20
7	-15	15
8	-10	10
9	-5	5

Figure 74, Figure 75, and Figure 76 show the resulting RMSE using the patch-based coprime, 4-element ULA and 5-element ULA respectively. Notice that each point in the graph represents two DOA angles. For example, the point at $DOA = 25°$ represents the RMSE when the two transmitters are located at $DOA = 25° \ and \ -25°$ and so on. As a general observation, the RMSE reported in the experiments is always larger than expected by the simulations but the general trend versus DOA is similar. The experimental curves follow the general trend of the simulated curves. For the CPA, the maximum and average difference between simulation and experimental data were 2.83° and 1.4°, respectively. For the 4-element ULA, we found 4.81° and 2.06° maximum and average differences, and for the 5-element ULA, the maximum was 4.82° and the average was 2.04°.

Figure 74 Simulation and Experimental RMSE for patch-based CPA with 2 transmitters at varying DOA angles.

Figure 75 Simulation and Experimental RMSE for patch-based 4-element ULA with 2 transmitters at varying DOA angles.

Figure 77, Figure 78, and Figure 79 present the results of the two transmitter experiments using the monopole-based coprime, 4-element ULA and 5-element ULAs respectively. There is less correlation between the experimental and simulation results in the monopole-based arrays compared to the patch-based. For the coprime, the maximum deviation between experimental and simulation was 6.14° and the average was 2.63° (compared to 2.83° and 1.4° for patches). For the 4-element monopole ULA, the maximum deviation was 26.33° and the average was 10.11° (compared to 4.81° and 2.06° for patches). And for the 5-element ULA, the maximum and average deviations were 2.7° and 1.24° (compared to 4.82° and 2.04° for patches). This was expected due to the lower polarization purity of the monopole elements. The cross-polarization component of the monopole elements is

114

significant, but it was ignored in the simulations. In the experiments, the monopole antennas will receive significant portion of power from cross-polarized waves reflected from the surroundings. This effect was ignored in the simulations which explains the greater deviation of the RMSE curves between simulation and experiments in monopoles. Notice that this effect was less visible in the previous experiments using one transmitter.
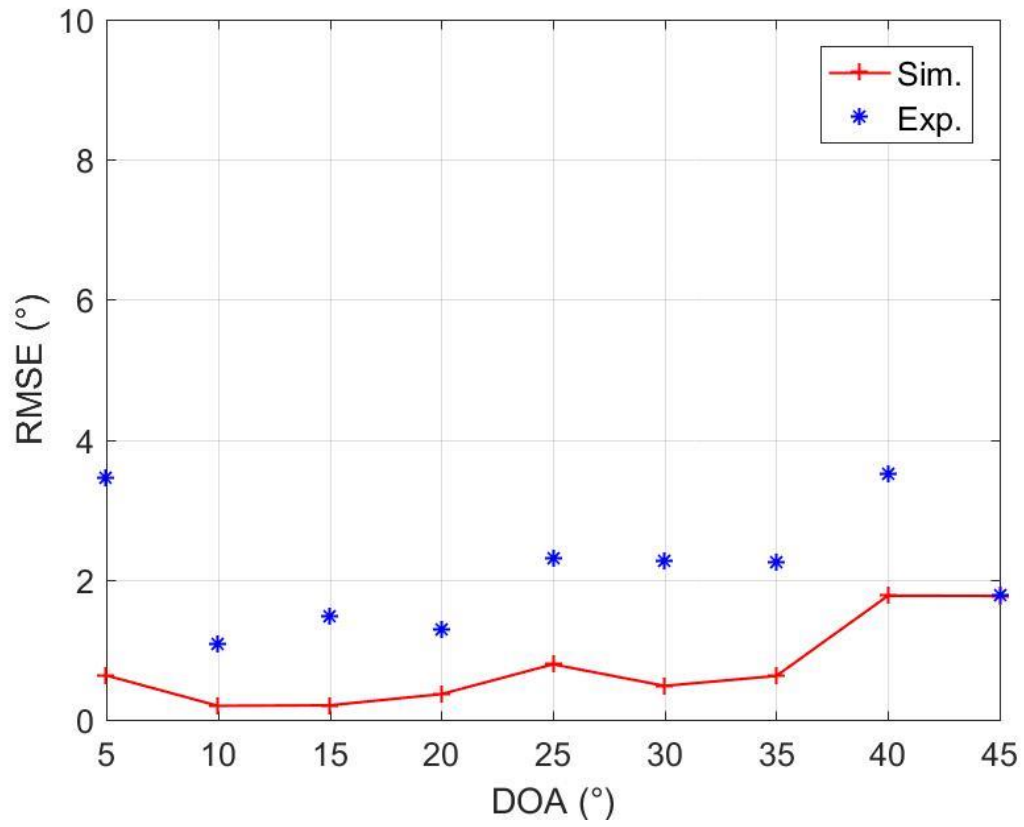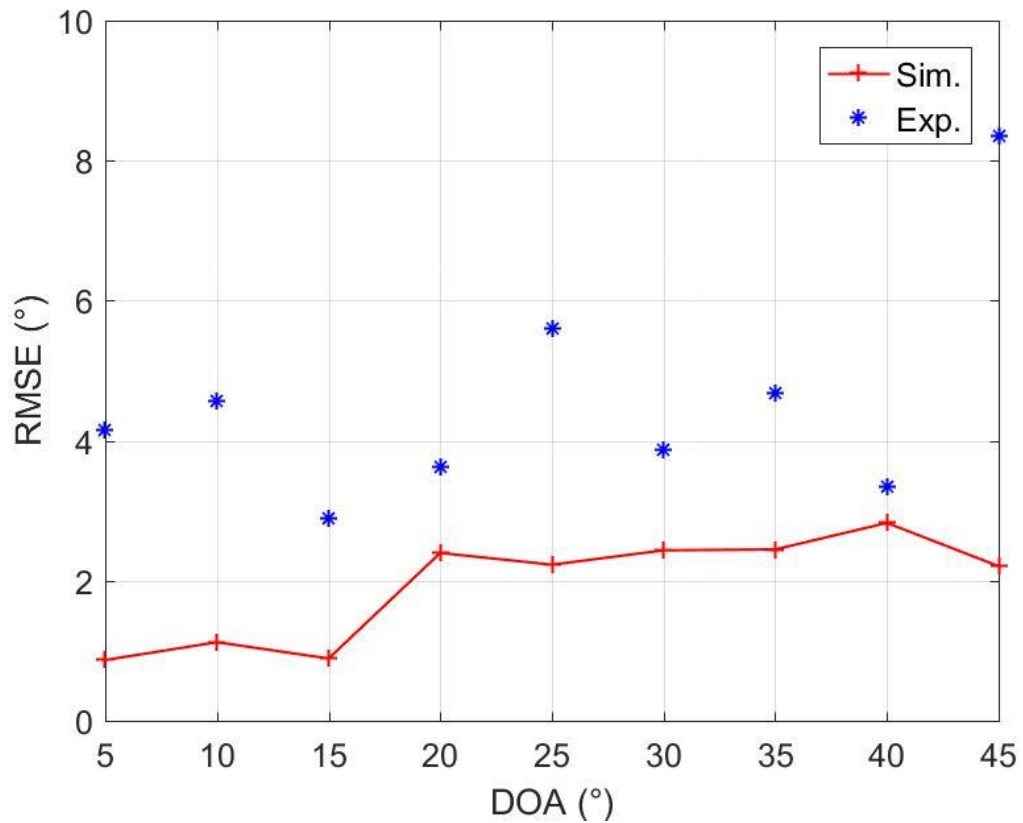

Figure 77 Simulation and Experimental RMSE for Monopole-based CPA with 2 transmitters at varying DOA angles.
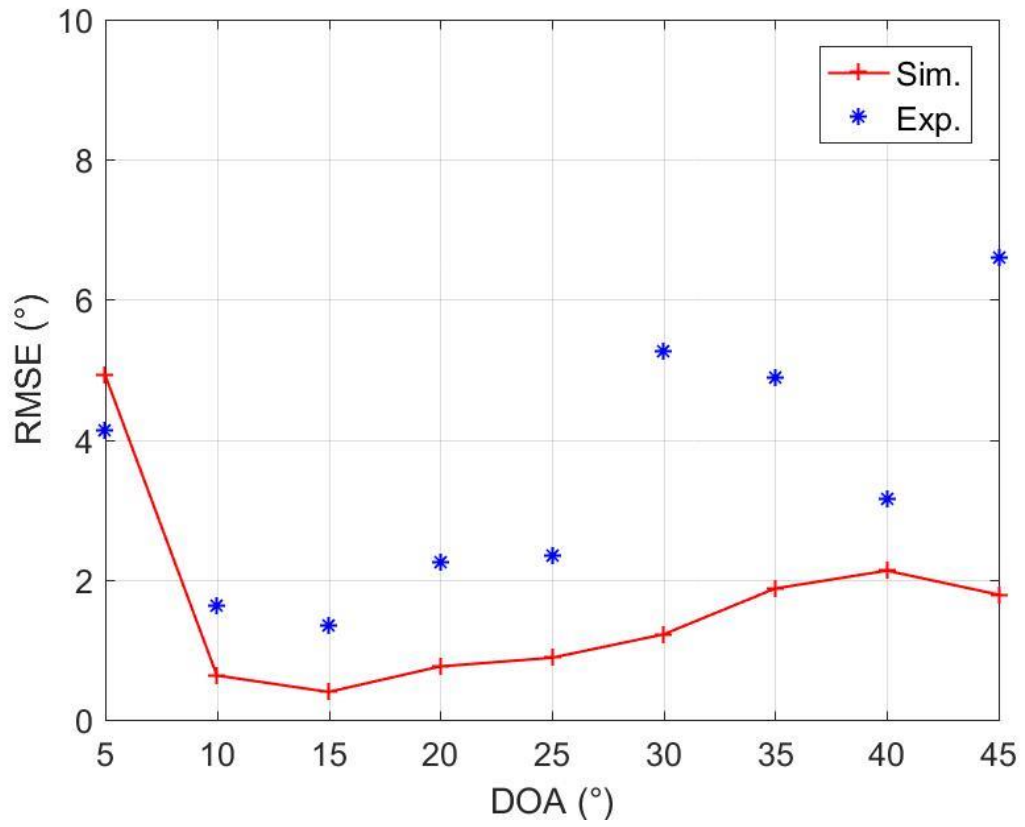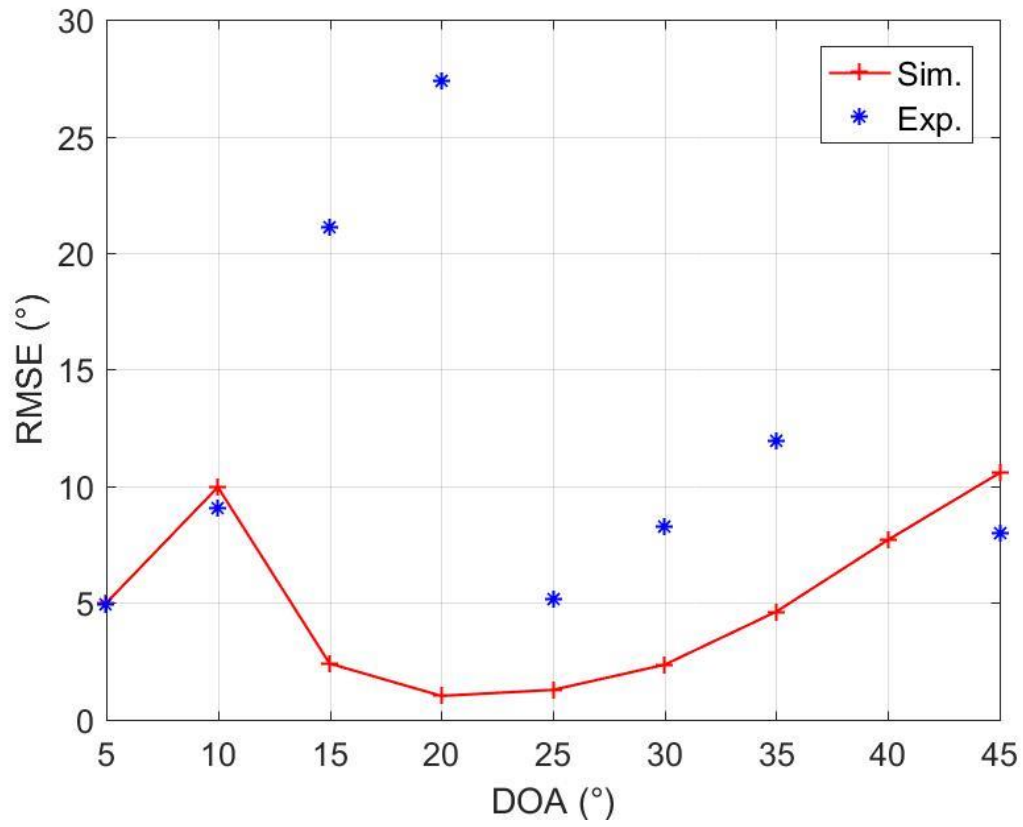
Figure 78 Simulation and Experimental RMSE for Monopole-based 4-element ULA with 2 transmitters at varying DOA angles
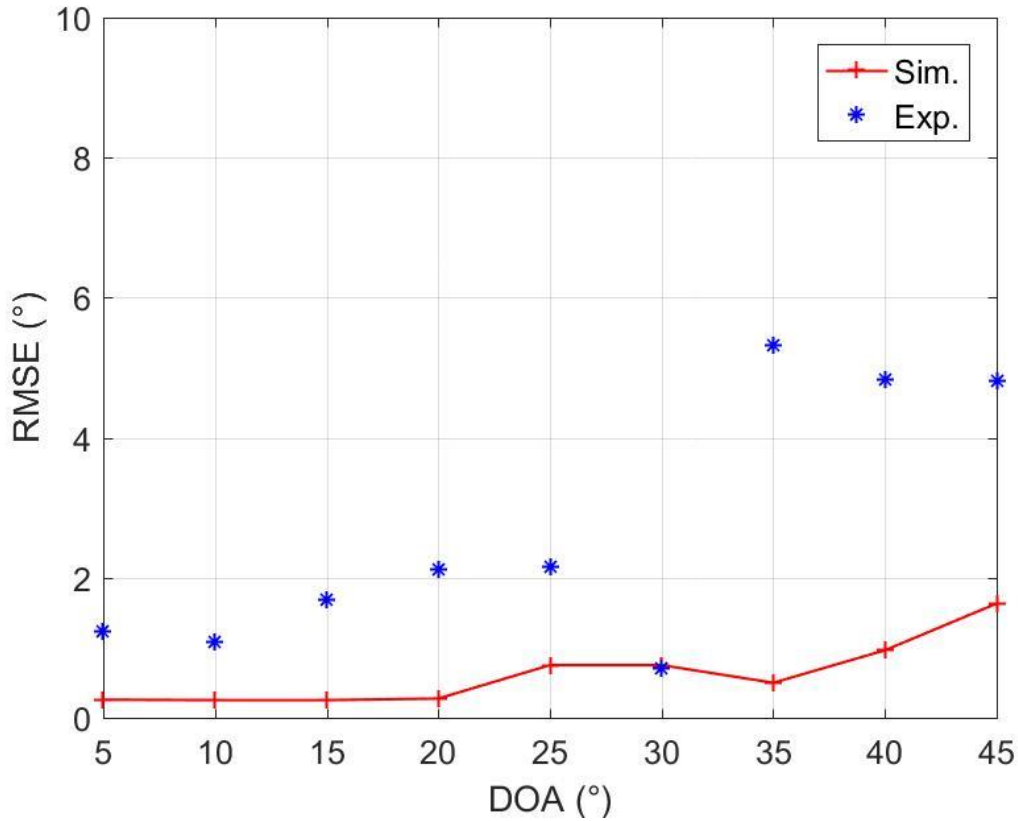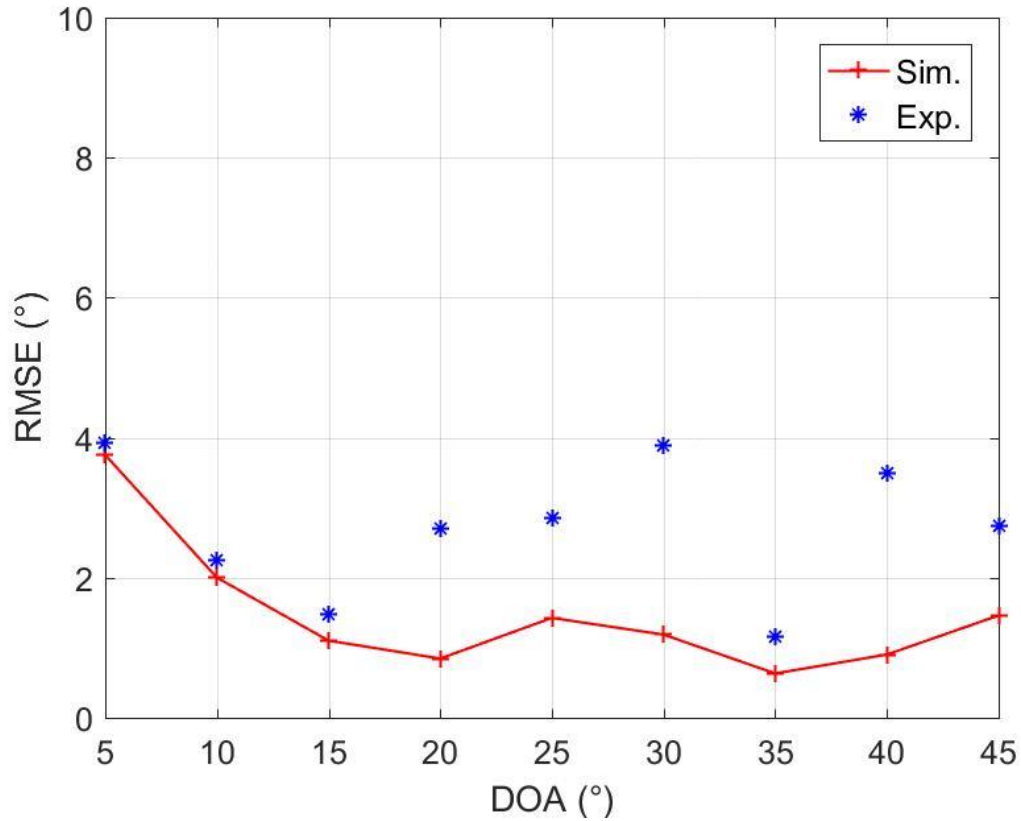
Figure 79 Simulation and Experimental RMSE for Monopole-based 5-element ULA with 2 transmitters at varying DOA angles.

5.4 Summary

In this chapter, we presented the results of the simulations and the experiments performed using the antenna arrays that were modelled and fabricated. Simulations were run for the patch-based arrays operating in the 5.8 GHz band and for the six monopole-based and patch-based arrays operating in the 2.1 GHz band. The simulations were carried out by extracting the radiation patterns of the arrays and incorporating them in the MATLAB code. The output of the simulations consisted of RMSE curves versus SNR and DOA for each array. DOA estimation experiments were performed using SDR for the six arrays working at 2.1 GHz. The experiments were conducted using one and two transmitters both indoor and outdoor to assess the effect of multipath which turned out to be similar in both

cases. The RMSE versus DOA curves in the experiments followed the trend found in the simulations giving confidence to the simulation procedure. The average difference between simulation and experimental RMSE using a CPA impinged by one transmitter was 3.78° for patch-based elements and 2.55° using monopole-based elements. With two transmitters, the average difference between simulation and experiments using a CPA of patches is 1.4° rising to 2.63° with monopoles due to multipath and polarization impurity effects.

CHAPTER 6

Conclusions and Future Work

6.1 Conclusions

The effect of utilizing physical antennas on DOA estimation algorithms in CPAs was investigated in this work. Seven different antenna arrays were designed, modeled and fabricated. The first was a patch-based CPA operating in the 5.8 GHz band, having a 100 MHz bandwidth and with total size of $125 \times 60 \ mm$, targeting handheld wireless devices. Both measured and simulated radiation patterns were incorporated in a MATLAB code to examine their effect on DOA estimation and compared with isotropic antennas. This demonstrated the possibility of using CPAs in small form factors, something that was not investigated before since most work on sparse arrays showed their advantage over ULAs in large arrays only. Using patch elements, the average error introduced by the practical antennas when detecting the DOA of four transmitters located at angles between -50° and 50° was 0.51°. This error goes up to 7.64° when the source is located at 80°. Furthermore, the effect of varying the inter-element spacing of the CPA was also investigated for the first time, opening the door to reducing the size of the arrays to fit smaller applications. A CPA of patch antennas operating at 5.8 GHz with interelement spacing of 0.31λ can be used for DOA estimation with an RMSE of 2.6°.

The effect of using practical antennas in CPAs was also investigated experimentally to confirm their advantages. Six different arrays consisting of patch-based and monopole-

based elements were designed, modeled and fabricated. The patch-based elements provide directional radiation patterns while the monopole-based elements provide omni-directional patterns. The six arrays were designed to operate at 2.1 GHz to match the capability of the available SDR hardware platform, with a minimum bandwidth of 40 MHz for the patch-based elements and 180 MHz for the monopole-based ones. The size of the arrays is suitable for laptops or tablet devices. For each element type (i.e. patch and monopole), three arrays were fabricated: 4-element coprime, 4-element ULA and 5-element ULA. This allowed comparing the performance of the CPA with its ULA counterpart of the same number of element or with the same aperture size. Simulations were also run for the six arrays so that the results can be compared with the experiments.

The average difference in RMSE between simulations and experiments for coprime, 4-element ULA, and 5-element ULA, respectively, was found as follows. Using one transmitter with patch-based arrays, the average difference was 2.87°, 2.11°, and 3.15°, for monopole-based, the average difference was 1.23°, 1.59°, and 1.39°, using two transmitters with patch-based elements, the average difference in RMSE was 1.4°, 2.06°, and 2.04°, and for monopole-based, the average difference was 2.63°, 10.11°, and 1.24°. The effect of cross-polarization was noticed in the experiments performed on monopole-based arrays where the reported estimation error was higher than the simulation suggested, the reason being that the simulations do not account for cross-polarization. This effect was not observed in patch-based antennas due to their low cross-polarization.

It was shown that regardless of the element type, a 4-element CPA performs better that both 4-element and 5-element ULAs in terms of DOA accuracy and DOF. The RMSE when using a patch-based CPA with four sources was 0.75° at 20 dB SNR compared to

1.08° using 5-element ULA, and 0.79° utilizing 4-element ULA with only three sources. For monopole-based, the CPA had an RMSE of 0.64° compared to 1.19° with 5-element ULA and 7.87° with 4-element ULA having three sources only.

Experiments were conducted in indoor and outdoor environments to investigate the multipath effect. Using the patch-based CPA, the maximum difference in RMSE between indoor and outdoor was 7.37° at -53° DOA and the average was 1.54°, suggesting no large difference in the effect of multipath.

The phase component of the radiation pattern was found to have a major impact on the DOA estimation accuracy. The greater the separation in the phase response of the antennas, the greater the introduced error. As a result, monopole-based arrays, with their highly fluctuating phase response versus DOA, are more sensitive to the DOA of the impinging signal than patch-based arrays whose phase patterns are more stable.

As a general conclusion, patch-based arrays provide more accurate DOA estimations compared to monopole-based ones due to their stable phase response and polarization purity.

6.2   Future Work

This work can be extended in the following directions:

1- After assessing the error introduced by physical antennas, it will be helpful to find a way to correct for these errors in the algorithm.

2- Understanding the effect of mutual coupling and properly modeling its effect within actual antennas on the DOA estimation performance is still an open area for further research.

3- In practical situations, the antenna arrays used for DOA estimation will be placed near other metallic objects affecting their radiation patterns and hence their DOA estimation performance. Studying this effect and trying to mitigate it is an important area to study.

4- Using directional antennas can reduce the effect of mutual coupling, allowing the inter-element spacing to be smaller, and probably helping in mitigating the effect of the surrounding metallic objects in practical cases. This can be investigated further using different arrays of highly directive elements at different spacings. The use of reflectors to achieve high directivity is one possibility.

References

[1] "IEEE 5G and Beyond Technology Roadmap White Paper," [Online]. Available: https://5g.ieee.org/images/files/pdf/ieee-5g-roadmap-white-paper.pdf. [Accessed 10 03 2018].

[2] L. C. Godara, Smart Antennas, Boca, Raton: CRC Press, 2004.

[3] C. A. Balanis, Advanced Engineering Electromagnetics Second Edition, Hoboken, NJ: John Wiley & Sons, Inc., 2012.

[4] C. A. Balanis, Antenna Theory Analysis and Design Third Edition, Hoboken, NJ: John Wiley & Sons, Inc., 2005.

[5] M. S. Sharawi, "Use of low-cost patch antennas in modern wireless technology," *IEEE Potentials,* vol. 25, no. 4, pp. 35-47, 2006.

[6] S. Qin, Y. D. Zhange and M. G. Amin, "Generalized Coprime Array Configurations for Direction-of-Arrival Estimation," *IEEE Trans. Signal Process.,* vol. 63, no. 6, pp. 1377-1390, 3 2015.

[7] P. Pal and P. P. Vaidyanathan, "Coprime Sampling and the MUSIC Algorithm," in *2011 Digital Signal Process. and Signal Process. Education Meeting (DSP/SPE)*, Sedona, 2011.

[8] K. Adhikari, J. R. Buck and K. E. Wage, "Beamforming with extended co-prime sensor arrays," in *2013 IEEE Int. Conf. on Acoust., Speech and Signal Process. (ICASSP)*, Vancouver, 2013.

[9] Y. D. Zhang, S. Qin and M. G. Amin, "DOA estimation exploiting coprime arrays with sparse sensor spacing," in *2014 IEEE Int. Conf. on Acoust., Speech and Signal Process. (ICASSP)*, Florence, 2014.

[10] R. O. Schmidt, "Multiple Emitter Location and Signal Parameter Estimation," *IEEE Trans. on Antennas and Propag.,* Vols. AP-34, no. 3, pp. 276-280, 1986.

[11] "girdsystems.com," [Online]. Available: http://www.girdsystems.com/pdf/GIRD_Systems_Intro_to_MUSIC_ESPRIT.pdf. [Accessed 06 2017].

[12] T.-J. Shan, M. Wax and T. Kailath, "On Spatial Smoothing for Direction-of-Arrival Estimation of Coherent Signals," *IEEE Trans. on Acoust., Speech and Signal Process.,* Vols. ASSP-33, no. 4, pp. 806-811, 1985.

[13] Y. D. Zhang, A. G. Moeness and B. Himed, "Sparsity-based DOA estimation using co-prime arrays," in *Acoustics, Speech and Signal Processing (ICASSP), 2013 IEEE International Conference on*, Vancouver, 2013.

[14] R. Roy and T. Kailath, "ESPRIT - Estimation of Signal Parameters Via Rotational Invariance Techniques," *IEEE Trans. on Accoustics, Speech, and Signal Process.,* vol. 37, no. 7, pp. 984-995, 1989.

[15] P. Rocca, M. Abdul Hannan, M. Salucci and A. Massa, "Single-Snapshot DoA Estimation in Array Antennas With Mutual Coupling Through a Multiscaling BCS Strategy," *IEEE Trans. Antennas and Propag.,* vol. 65, no. 6, pp. 3203-3213, 6 2017.

[16] T. E. Tuncer and B. Friedlander, Classic and Modern Direction-of-Arrival Estimation, Academic Press, 2009.

[17] S. A. Alawsh, H. A. Muqaibel and S. M. Sharawi, "DOA estimation in MIMO systems with Compressive Sensing for future handsets," in *2015 IEEE Jordan Conf. on Appl. Elect. Eng. and Computing Technologies (AEECT)*, Amman, 2015.

[18] R. Sanudin, N. H. Noordin, A. O. El-Rayis, N. Haridas, A. T. Erdogan and T. Arslan, "Analysis of DOA estimation for directional and isotropic antenna arrays," in *Antennas and Propagation Conference (LAPC), 2011 Loughborough*, Loughborough, 2011.

[19] Ó. Quevedo-Teruel, M. Sánchez-Fernández, M. L. Pablo-González and E. Rajo-Iglesias, "Alternating Radiation Patterns to Overcome Angle-of-Arrival Uncertainty," *IEEE Antennas and Propag. Magazine,* vol. 52, no. 1, pp. 236-242, 2010.

[20] K. Han, Y. Wang, B. Kou and W. Hong, "Parameters estimation using a random linear array and compressed sensing," in *2010 3rd Int. Congr. on Image and Signal Process.*, Yantai, 2010.

[21] P. Pal and P. P. Vaidyanathan, "Nested Arrays: A Novel Approach to Array Processing With Enhanced Degrees of Freedom," *IEEE Trans. Signal Process.,* vol. 58, no. 8, pp. 4167-4181, 9 2010.

[22] C.-L. Liu and P. P. Vaidyanathan, "Super Nested Arrays: Linear Sparse Arrays With Reduced Mutual Coupling Part I: Fundamentals," *IEEE Trans. Signal Process.,* vol. 64, no. 15, pp. 3997-4012, 8 2016.

[23] C.-L. Liu and P. P. Vaidyanathan, "Hourglass Arrays and Other Novel 2-D Sparse Arrays With Reduced Mutual Coupling," *IEEE Trans. Signal Process.,* vol. 65, no. 13, pp. 3369-3383, 7 2017.

[24] J. Wang, H. Xu, X. Zheng and G. A. E. Vandenbosch, "Tracking more targets with less antenna: An investigation into the co-array concept," in *2015 9th Eur. Conf. on Antennas and Propag. (EuCAP)*, Lisbon, 2015.

[25] E. BouDaher, F. Ahmad, M. Amin and A. Hoorfar, "DOA estimation with co-prime arrays in the presence of mutual coupling," in *Signal Processing Conference (EUSIPCO), 2015 23rd European.*, Nice, 2015.

[26] E. BouDaher, F. Ahmad, M. G. Amin and A. Hoorfar, "Mutual coupling effect and compensation in non-uniform arrays for direction-of-arrival estimation," *Digital Signal Process.,* vol. 61, no. 2, pp. 3-14, 2017.

[27] K. Adhikari, J. R. Buck and K. E. Wage, "Extending coprime sensor arrays to achieve the peak side lobe height of a full uniform linear array," *EURASIP Journal on Advances in Signal Process.,* vol. 2014, no. 1, p. 148, 9 2014.

[28] Y. Liu and R. J. Buck, "Spatial spectral estimation using a coprime sensor array with the min processor," in *Sensor Array and Multichannel Signal Processing Workshop (SAM), 2016 IEEE*, Rio de Janerio, Brazil, 2016.

[29] P. P. Vaidyanathan and P. Pal, "Sparse sensing with coprime arrays," in *2010 Conference Record of the Forty Fourth Asilomar Conference on Signals, Systems and Computers*, Pacific Grove, CA, USA, 2010.

[30] H.-S. Lui, Y. Yu, H. T. Hui and M. S. Leong, "Experimental study of mutual coupling compensation in direction finding using a compact antenna array," in *2010 IEEE Asia-Pacific Symposium on Electromagnetic Compatibility (APEMC)*, Beijing, 2010.

[31] I. Pasya, N. Iwakiri and T. Kobayashi, "Performance of Joint Direction-of-Departure and Direction-of-Arrival Estimation in an Ultra Wideband MIMO RADAR

Depending on Bandwidths," in *Radio and Wireless Symposium (RWS), 2014 IEEE*, Cincinnati, 2014.

[32] B. Sahinbas, L. Weisgerber and M. Schühler, "AoA and source polarization estimation with circularly polarized multibeam antenna using MUSIC algorithm," in *2017 11th Eur. Conf. on Antennas and Propag. (EUCAP)*, Paris, 2017.

[33] H. Paaso, N. Gulati, D. Patron, A. Hakkarainen, J. Werner, K. R. Dandekar, M. Valkamaand and A. Mämmelä, "DoA Estimation Using Compact CRLH Leaky-Wave Antennas: Novel Algorithms and Measured Performance," *IEEE Trans. Antennas and Propag.,* vol. 65, pp. 4836-4849, 9 2017.

[34] S. A. Alawsh, M. T. Alkhodary, A. H. Muqaibel and M. S. Sharawi, "Experimental evaluation of coprime sampler in direction of arrival estimation," in *2016 IEEE Middle East Conference on Antennas and Propagation (MECAP)*, Beirut, 2016.

[35] Q. Shen, W. Liu, W. Cui, S. Wu, Y. D. Zhang and M. G. Amin, "Low Complexity Direction-of-Arrival Estimation Based on Wideband Co-Prime Arrays," *IEEE/ACM Trans. Audio, Speech, Language Process.,* vol. 23, no. 9, pp. 1445-1456, 9 2015.

[36] S. A. Alawsh, O. A. Al Khazragi, A. H. Muqaibel and S. N. Al-Ghadhban, "Sparse Direction of Arrival Estimation Using Sparse Arrays Based on Software-Defined-Radio Platform," in *2017 10th Int. Conf. on Elect. and Electronics Eng. (ELECO)*, Bursa, 2017.

[37] "Microwave Vision Group," 5 12 2017. [Online]. Available: http://www.mvg-world.com/en.

[38] T. S. Rappaport, Wirelss Communications, Prentice Hall PTR, 2013.

[39] M. Agiwal, A. Roy and N. Saxena, "Next Generation 5G Wireless Networks: A Comprehensive Survey," *IEEE Communications Surveys \& Tutorials,* vol. 18, no. 3, pp. 1617-1655, 2016.

Vitae

Name   :Ahmad Ibrahim Oweis

Nationality   :Jordanian

Date of Birth   :11/19/1977

 Email   :oweis@ieee.org

Address   :PO Box 76060, Al Khobar, KSA

Academic Background   :BSc Electrical Engineering, University of Jordan, 2000.

MSc Petroleum Engineering, Heriot-Watt University,

2014

Publications

Journals:

1. **Ahmad Oweis**, Saleh A. Alawsh, Ali H. Muqaibel, and Mohammad S. Sharawi, "A Coprime Array of Patch Antennas for Direction of Arrival Estimation Using Compressed Sensing", submitted in *Microwave and Optical Technology Letters*, Wiley

2. Saleh A. Alawsh, **Ahmad I. Oweis**, Ali H. Muqaibel and Mohammad S. Sharawi, "DOA Estimation Based on Sparse Directional Antenna Arrays", Submitted

Conferences:

1. **Ahmad I. Oweis**, Saleh A. Alawsh, Ali H. Muqaibel, Mohammad S. Sharawi, "A CoPrime Array of Patch Antennas for DOA Estimation in Mobile Handheld Devices," presented in *2018 IEEE International Symposium on Antennas and Propagation and USNC-URSI Radio Science Meeting,* Boston, 2018

2. Saleh A. Alawsh, **Ahmed I. Oweis**, Ali H. Muqaibel, and Mohammed S. Sharawi, "Sparse Direction-of-Arrival Estimation with Directive Coprime Arrays", presented in *2018 IEEE International Symposium on Antennas and Propagation and USNC-URSI Radio Science Meeting,* Boston, 2018